Constraints on Higgs boson production with large transverse momentum using $H \to b\bar{b}$ decays in the ATLAS detector

G. Aad *et al.*[*]
(ATLAS Collaboration)

(Received 17 November 2021; accepted 2 March 2022; published 11 May 2022)

This paper reports constraints on Higgs boson production with transverse momentum above 1 TeV. The analyzed data from proton–proton collisions at a center-of-mass energy of 13 TeV were recorded with the ATLAS detector at the Large Hadron Collider from 2015 to 2018 and correspond to an integrated luminosity of 136 fb^{-1}. Higgs bosons decaying into $b\bar{b}$ are reconstructed as single large-radius jets recoiling against a hadronic system and are identified by the experimental signature of two b-hadron decays. The experimental techniques are validated in the same kinematic regime using the $Z \to b\bar{b}$ process. The 95% confidence-level upper limit on the cross section for Higgs boson production with transverse momentum above 450 GeV is 115 fb, and above 1 TeV it is 9.6 fb. The Standard Model cross section predictions for a Higgs boson with a mass of 125 GeV in the same kinematic regions are 18.4 fb and 0.13 fb, respectively.

DOI: 10.1103/PhysRevD.105.092003

I. INTRODUCTION

The characterization of the Higgs sector has steadily improved since the Higgs boson (H) discovery [1,2] using data from proton–proton (pp) collisions produced by the Large Hadron Collider (LHC) at CERN. Four production modes have been observed, gluon–gluon fusion (ggF), vector-boson fusion (VBF), associated production with a weak vector boson (VH), and associated production with a top quark–antiquark pair ($t\bar{t}H$), along with five decay modes $H \to \gamma\gamma$, ZZ^*, WW^*, $\tau\tau$, $b\bar{b}$ [3,4]. The initial measurements of inclusive cross sections have evolved to include differential cross section measurements, and measurements in the simplified template cross section framework [5–7]. All results agree with the Standard Model (SM) predictions within the current precision, but sizable regions of the Higgs sector remain unexplored. In one such region, where the Higgs boson transverse momentum p_{T}^H reaches the TeV scale, the cross section hierarchy is very different from that in the inclusive cross section, where ggF is nearly 90% of the total. At the TeV scale, the SM predicts the cross sections for the ggF and VH production processes to be roughly equal, while the VBF and $t\bar{t}H$ production cross sections are around 60% and 30% of the ggF process, respectively.

The leading effects of many beyond-the-SM (BSM) scenarios can be parametrized through effective field theories (EFTs), whose operators are suppressed by a new physics scale Λ [8]. Measured observables at the LHC would only be affected through effective interactions among SM particles. For example, the ggF production mode is sensitive to the structure of quasi-point-like couplings within the loop nature of the effective ggH coupling. Studies of Higgs bosons produced with large transverse momentum access regions where some potential BSM effects are enhanced by powers of p_{T}^H/Λ [9–13]. Differential cross section measurements with an extended reach may be more sensitive than higher precision, low energy measurements also because the signal-to-background ratio increases with p_{T}^H.

In the high-p_{T}^H regime, the CMS Collaboration measured a signal yield relative to the SM prediction, or signal strength, of $\mu_{\mathrm{ggF}} = 3.7^{+1.6}_{-1.5}$ in the $H \to b\bar{b}$ decay mode for events containing a large-radius jet with $p_{\mathrm{T}} > 450$ GeV, and presented ggF differential cross sections while considering other Higgs boson production modes as a background [14]. In the $H \to \gamma\gamma$ decay mode, ggF production with $p_{\mathrm{T}}^H > 200$ GeV was measured to a precision of less than 50% relative to the SM prediction [15]. The analysis of VH production with leptonic V decays has achieved considerable sensitivity in the high-p_{T}^H regime [16–18]. The ATLAS Collaboration measured a signal strength of $\mu_{VH} = 0.72^{+0.39}_{-0.36}$ in the $H \to b\bar{b}$ decay mode targeting events with $p_{\mathrm{T}}^H > 250$ GeV, and presented differential cross sections in two exclusive vector-boson transverse momentum regions, 250–400 GeV and above

[*]Full author list given at the end of the article.

400 GeV [17]. However, it is sensitive to different EFT operators than those for ggF and $t\bar{t}H$ production. Recent results on VBF production with Higgs boson decays to photons and leptons also included high-p_{T}^{H} event categories, but have limited reach [19–23]. Similarly, measurements of $t\bar{t}H$ production have yet to reach the high-p_{T}^{H} regime [24,25].

This paper reports the first ATLAS studies of Higgs bosons produced with transverse momentum above 1 TeV. The yield of Higgs bosons decaying into $b\bar{b}$ pairs is determined in several p_{T}^{H} regions. No restrictions are applied to select a particular Higgs boson production mode aside from requiring an energetic hadronic recoil system. The cross section is measured for $p_{\mathrm{T}}^{H} > 450$ GeV, allowing a straightforward comparison with theoretical calculations, such as those reported in Ref. [26]. In addition a differential analysis is performed to extract the cross section in four Higgs boson p_{T} intervals, 300–450 GeV, 450–650 GeV, 650–1000 GeV, and above 1 TeV.

Data used correspond to 136 fb^{-1} of pp collisions at $\sqrt{s} = 13$ TeV and were collected with the ATLAS detector [27] using jet-based trigger requirements during Run 2 (2015–2018) of the LHC. Higgs bosons with a large Lorentz boost are reconstructed as single large-radius jets having a mass compatible with 125 GeV [28]. To populate the signal region, events must have at least two large-radius jets. At least one jet must have $p_{\mathrm{T}} > 450$ GeV to ensure a fully efficient trigger response. Either of the two leading-p_{T} jets in the event must contain evidence of two b-hadron decays. Including the subleading jet as a possible Higgs boson candidate increases the sensitivity for $p_{\mathrm{T}}^{H} > 450$ GeV by 11% and permits a cross section measurement down to $p_{\mathrm{T}}^{H} = 300$ GeV, overlapping with measurements in other decay channels [15,20,22,24,29–31].

For a Higgs boson mass (m_H) of 125 GeV, the SM predicts the ggF production mode contributes nearly half of the Higgs boson events reconstructed near m_H when they are summed over all signal regions. VBF-, VH-, and $t\bar{t}H$-produced events each contribute approximately 15%–20%. Since some of the same dimension-6 EFT operators modify the p_{T}^{H} spectrum in the ggF and $t\bar{t}H$ processes, it could be advantageous to consider $t\bar{t}H$ and ggF production together. These operators can produce enhancements at high p_{T}^{H} that are within the sensitivity of the present analysis without inducing significant deviations from the SM prediction at low p_{T}^{H}. However, the expected yield enhancement differs for the two production modes, with ggF production having a larger increase. While this analysis is primarily sensitive to ggF production, all the main production modes are considered as the signal. This approach enhances the sensitivity to possible BSM effects and minimizes the dependence on theoretical assumptions. Using the $H \to b\bar{b}$ decay, which has the largest branching fraction, mitigates the impact of the smaller absolute cross section in the high-p_{T} regime.

The dominant background process is multijet production, which exhibits a monotonically decreasing jet mass distribution. Hadronically decaying vector bosons, produced in association with jets (V + jets) and events with one or two top quarks (jointly referred to as *Top*) populate the jet mass regions below and above m_H, respectively, as shown in Fig. 1. The Z and H resonance structures are distinct from the smoothly falling multijet background, while the top quark resonance is spread over a large portion of the high-mass region. Therefore, the signal is extracted from the reconstructed jet mass distribution. An analytic function is used to model the multijet background. The jet mass spectra and acceptance for Higgs boson, V + jets, and Top events are estimated from simulation.

A binned maximum-likelihood fit, referred to as the global likelihood fit, is used to measure the signal strength. Unconstrained, or free, parameters for the multijet model's yield and shape, the Z + jets yield, and the Higgs boson yield are determined simultaneously from the signal region

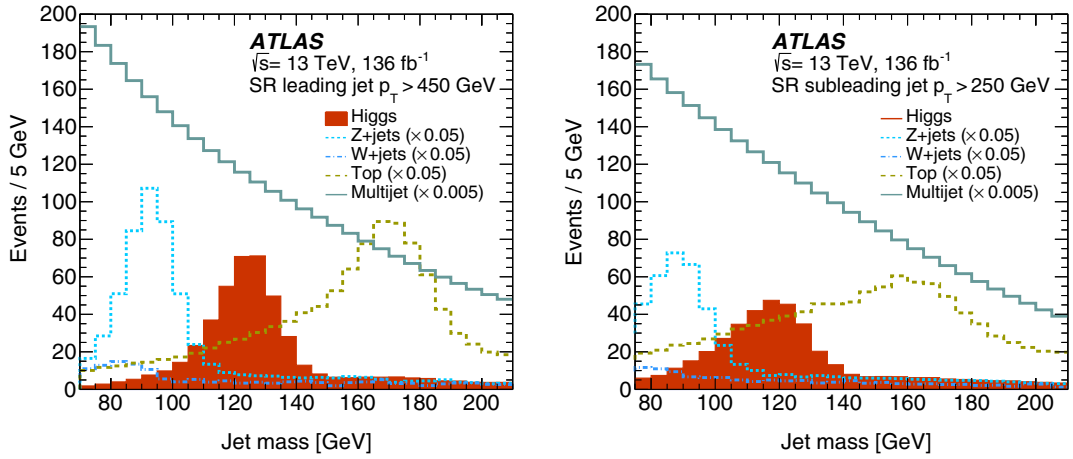

FIG. 1. Jet mass distributions for the Higgs boson, Z + jets, W + jets, and Top contributions from the SM prediction as well as the multijet jet mass distribution extracted from data in the signal region (SR) defined by the leading (left) and subleading (right) jets.

data. Control region data, fit simultaneously with the signal region, determine the unconstrained yield for top quark pair-production ($t\bar{t}$) events. Concurrently, the modeling of the jet mass scale and resolution from V and top quark decays are separately validated in a broad range of jet p_{T}. Validation region data are used to study $V+$ jets events, the parametrization of the multijet model, and the robustness of the global likelihood fit.

II. ATLAS DETECTOR

The ATLAS experiment [27] at the LHC is a multipurpose particle detector with a forward–backward symmetric cylindrical geometry and a near 4π coverage in solid angle.[1] It consists of an inner tracking detector surrounded by a thin superconducting solenoid providing a 2 T axial magnetic field, electromagnetic and hadron calorimeters, and a muon spectrometer. The inner tracking detector covers the pseudorapidity range $|\eta| < 2.5$. It consists of silicon pixel, silicon microstrip, and transition radiation tracking detectors. The Insertable B-Layer, the innermost pixel layer at a mean radius of 3.3 cm, was installed before Run 2 of the LHC [32,33]. Lead/liquid-argon (LAr) sampling calorimeters provide electromagnetic (EM) energy measurements with high granularity. A steel/scintillator-tile hadron calorimeter covers the central pseudorapidity range ($|\eta| < 1.7$). The forward regions are instrumented with LAr calorimeters for EM and hadronic energy measurements up to $|\eta| = 4.9$. The muon spectrometer surrounds the calorimeters and is based on three large air-core toroidal superconducting magnets with eight coils each. The field integral of the toroids ranges between 2.0 and 6.0 T m across most of the detector. The muon spectrometer includes a system of precision chambers for tracking and fast detectors for triggering. A two-level trigger system is used to select events [34]. The first-level trigger is implemented in hardware and uses a subset of the detector information to accept events at a rate below 100 kHz. A software-based trigger reduces the accepted event rate to 1 kHz on average. An extensive software suite [35] is used in the reconstruction and analysis of real and simulated data, in detector operations, and in the trigger and data acquisition systems of the experiment.

III. DATA AND SIMULATED SAMPLES

The data were collected with the ATLAS detector in pp collisions with a center-of-mass energy of 13 TeV during Run 2 (2015–2018) of the LHC [36]. Events must satisfy a set of triggers requiring a jet reconstructed with the anti-k_t algorithm with radius parameter $R = 1.0$ [37]. To adapt to different instantaneous luminosity profiles and the inclusion of pileup suppression techniques within the data acquisition system [38], the jet-p_{T} and mass thresholds differ for each year of data taking. The trigger jet-p_{T} threshold varies from 360 GeV to 420 GeV, and the trigger jet mass threshold is either not applied, 30 GeV, or 35 GeV. Events which pass a trigger requiring a muon with $p_{\mathrm{T}} > 50$ GeV [39] populate a control region for top quark production. The total integrated luminosities are 136 fb^{-1} and 139 fb^{-1} for the jet- and muon-triggered data, respectively, with an uncertainty of 1.7% [40,41].

Monte Carlo (MC) simulated events are used to model the resonant backgrounds ($W+$ jets, $Z+$ jets, and Top production) as well as four Higgs production processes: ggF, VBF, VH, and $t\bar{t}H$. Higgs boson ggF production was simulated at next-to-leading-order (NLO) accuracy in QCD with finite mass effects by using the Hj-MiNLO [42–44] prescription with the POWHEG program [45–47] as discussed in Ref. [48]. NLO accuracy in QCD for VBF and $t\bar{t}H$ production and leading order (LO) accuracy for $gg \to VH$ production was achieved using the POWHEGBOX v2 [45–47,49,50] program. Using the POWHEGBOX v2 program, the improved MINLO [51] calculation, and the GOSAM [52] program, $qq \to VH$ production was also simulated at NLO accuracy in QCD. Corrections for NLO electroweak (EW) effects were applied as a function of the generated Higgs boson transverse momentum for VBF, VH, and $t\bar{t}H$ production. The production cross sections used are compatible with those presented in Ref. [26], except for $t\bar{t}H$ production where a scale factor is applied to match the reported value [26]. The Higgs boson branching fractions were calculated with HDECAY [53–55] and PROPHECY4F [56–58].

Production of $V+$ jets events with hadronic boson decays was simulated with SHERPA to NLO QCD accuracy for one additional parton and LO QCD accuracy for up to four additional partons. Approximate NLO EW corrections [59] were applied as a function of the generated vector-boson momentum p_{T}^{V}. They have a sizable impact on the differential production cross section, reducing the predicted yield by ∼10% at a p_{T}^{V} of 500 GeV and ∼20% above 1 TeV. Calculations of next-to-next-to-leading-order (NNLO) QCD corrections to $V+$ jets production are available [60]. The NNLOJET group performed the calculation for $\sqrt{s} = 8$ TeV [61,62] and has provided custom corrections for the analysis kinematic region for $\sqrt{s} = 13$ TeV as a function p_{T}^{V}. They vary from 1.01 to 1.09 and are applied as a multiplicative factor on top of the NLO EW corrections. Diboson production was found to make a negligible contribution to the present analysis.

The production of top quark pairs, associated production of a top quark with a W boson (tW), and single-top t- and s-channel production were modeled using the

[1] ATLAS uses a right-handed coordinate system with its origin at the nominal interaction point (IP) in the center of the detector and the z-axis along the beam pipe. The x-axis points from the IP to the center of the LHC ring, and the y-axis points upwards. Cylindrical coordinates (r, ϕ) are used in the transverse plane, ϕ being the azimuthal angle around the z-axis. The pseudorapidity is defined in terms of the polar angle θ as $\eta = -\ln\tan(\theta/2)$. Angular distance is measured in units of $\Delta R \equiv \sqrt{(\Delta\eta)^2 + (\Delta\phi)^2}$.

POWHEGBOX v2 [45–47,63–66] generator at NLO in QCD. The diagram subtraction scheme [67] was used in tW events to account for interference and overlap with $t\bar{t}$ production.

The jet mass distribution of nonresonant multijet events is modeled with an analytic function. Simulated events used to study the multijet model were generated using PYTHIA 8.230 [68] with leading-order matrix elements for dijet production and interfaced to a p_{T}-ordered parton shower.

All simulated particles from collisions were processed with the ATLAS detector simulation [69] based on GEANT4 [70]. Pileup, multiple interactions in the same and neighboring bunch crossings, was modeled by overlaying the hard-scatter event with inelastic pp events generated with PYTHIA8.186 [68] using the NNPDF2.3LO set of parton distribution functions (PDFs) [71] and a set of tuned parameters called the A3 tune [72]. For Higgs boson, Top, and dijet production, the EVTGEN1.2.0 program [73] was used to model the decays of bottom and charm hadrons.

For each sample, Table I summarizes the MC generator, parton distribution functions, parton shower and hadronization model, and underlying event tune used, as well as the order of perturbative QCD computations and EW corrections obtained for the cross section. For additional information, see Ref. [74] for V + jets events, Refs. [75–78] for top quark events, and Ref. [79] for multijet events. Systematic uncertainties for process modeling are described in Sec. VII.

TABLE I. The generators used for the simulation of the signal and background processes. The matrix element, parton shower, and underlying event are abbreviated as ME, PS, and UE, respectively. $(*)$ POWHEG was configured to output events with Born k_{T} above 200 GeV using the *bornktmin* setting. $(\bullet)$ Corrections for NLO EW effects computed with HAWK [80,81] are applied as a function of the generated Higgs boson transverse momentum. $(\circ)$ Corrections for NLO EW effects computed with SHERPA+OPENLOOPS [82–84] are applied as a function of the generated Higgs boson transverse momentum and were provided by Ref. [26]. $(\dagger)$ SHERPA provides one additional parton at NLO accuracy and up to four additional partons at LO in QCD and custom NNLO QCD corrections were provided by the NNLOJET group.

Process	ME generator	ME PDF	PS and hadronization	UE model tune	Cross section order
Higgs Boson					
$gg \to H \to b\bar{b}$	POWHEGBOX v2 $^{(*)}$ [45–47] + MINLO [42–44]	NNPDF3.0NNLO [85]	PYTHIA8.212 [68]	AZNLO [86]	NLO(QCD) + LO(EW)
$qq \to H \to q'q'b\bar{b}$	POWHEGBOX v2 [45–47,49]	NNPDF3.0NLO [85]	PYTHIA8.230	AZNLO	NLO(QCD) + NLO(EW)$^{(\bullet)}$
$qq \to WH$					
$\to qq'b\bar{b}$	POWHEGBOX v2 + GOSAM [52] + MINLO [51]	NNPDF3.0NLO	PYTHIA8.240 PYTHIA8.212	AZNLO	NNLO(QCD) + NLO(EW)$^{(\bullet)}$
$\to \ell\nu b\bar{b}$					
$qq \to ZH$					
$\to q\bar{q}b\bar{b}$	POWHEGBOX v2 + GOSAM + MINLO	NNPDF3.0NLO	PYTHIA8.240 PYTHIA8.212	AZNLO	NNLO(QCD) + NLO(EW)$^{(\bullet)}$
$\to \nu\nu b\bar{b}$					
$\to \ell\ell b\bar{b}$					
$gg \to ZH$					
$\to q\bar{q}b\bar{b}$	POWHEGBOX v2 [50]	NNPDF3.0NLO	PYTHIA8.240 PYTHIA8.212	AZNLO	LO + NLL(QCD)
$\to \nu\nu b\bar{b}$					
$\to \ell\ell b\bar{b}$					
$gg \to ttH$					
$tt \to$ all	POWHEGBOX v2	NNPDF3.0NLO	PYTHIA8.230	AZNLO	NLO(QCD) + NLO(EW)$^{(\circ)}$
$H \to$ all					
Vector boson + jets					
$W \to qq$	SHERPA 2.2.8 [83,87,88]	NNPDF3.0NNLO	SHERPA2.2.8 [89,90]	Default	NNLO(QCD) $^{(\dagger)}$ [61,62,91]
$Z \to qq$					approx NLO(EW) [59,92,93]
Top quark, mass set to 172.5 GeV					
$t\bar{t} \to$ all	POWHEGBOX v2 [45–47,63]	NNPDF3.0NLO	PYTHIA8.230	A14 [94]	NNLO + NNLL [95]
tW	POWHEGBOX v2 [45–47,64]	NNPDF3.0NLO	PYTHIA8.230	A14	NLO
t t-channel	POWHEGBOX v2 [45–47,65]	NNPDF3.0NLO	PYTHIA8.230	A14	NLO
t s-channel	POWHEGBOX v2 [45–47,66]	NNPDF3.0NLO	PYTHIA8.230	A14	NLO
Multijet					
Dijets	PYTHIA 8.230	NNPDF2.3LO [71]	PYTHIA8.230	A14	LO

IV. OBJECT SELECTION

For Higgs bosons with a large Lorentz boost, the event topology of $pp \to H(\to b\bar{b}) + J$ is characterized by two jets, one of which contains the decay products of the two b-hadrons.

A. Object reconstruction

Charged-particle tracks [96] are reconstructed in the inner detector and used to form interaction vertices [97]. The primary vertex of the hard interaction is defined as the vertex with the highest sum of squared transverse momenta of associated tracks.

Large-radius ($R = 1.0$) jets are formed by applying the anti-k_t algorithm implemented in FASTJET [98] to topological clusters of noise-suppressed calorimeter energy depositions calibrated to the local hadronic scale [99]. Jet cleaning criteria are applied to identify jets arising from noncollision backgrounds or noise in the calorimeters [100], and events containing such jets are removed. A jet trimming procedure reduces pileup dependence and improves the mass resolution [101]. It produces a collection of subjets by reclustering the constituents of each jet using the k_t algorithm [102] with $R = 0.2$. Subjets with $p_{\mathrm{T}}{}^{\mathrm{subjet}}/p_{\mathrm{T}}{}^{\mathrm{jet}} < 0.05$ are removed and the jet four-momentum is recalculated. The trimmed jet's mass m_J is computed as a weighted combination of the jet mass obtained from the calorimeter measurements and that from the charged component in the inner detector [103]. For jets within $|\eta| < 2$, simulation-based corrections are applied to calibrate p_{T} and m_J, while p_{T} also has corrections based on *in situ* techniques [103].

The anti-k_t algorithm with a variable, p_{T}-dependent radius parameter is used to form track-jets from tracks compatible with the primary vertex [104,105]. The effective jet radius R_{eff} is ρ/p_{T} where the ρ-parameter is set to 30 GeV. The lower and upper bounds on the track-jet radius are 0.02 and 0.4, respectively. Track-jets are matched to large-R jets by ghost association before trimming [106,107]. In simulated events, track-jets are labeled as b-, c- or light-flavor according to which hadrons with $p_{\mathrm{T}} > 5$ GeV are found within $\Delta R = 0.3$ of the jet axis [108].

A multivariate discriminant (denoted MV2 in Ref. [108]) is used to tag track-jets containing a b-hadron decay (b-tagging). Track-jets with $p_{\mathrm{T}} > 10$ GeV, $|\eta| < 2.5$, and at least two tracks are considered. The operating point is tuned to produce an average efficiency of 77% for b-jets in simulated $t\bar{t}$ events, which corresponds to light-flavor jet (u-, d-, s-quark, and gluon) and c-jet misidentification efficiencies of 0.9% and 25%, respectively. If the ΔR between two track-jets with $p_{\mathrm{T}} > 5$ GeV in a large-R jet is smaller than either of their respective variable radii, the jet is not considered for b-tagging [109].

Muons are required to have $|\eta| < 2.5$, $p_{\mathrm{T}}^{\mu} > 10$ GeV, and small impact parameters relative to the primary vertex, as well as to satisfy the "medium" quality criterion [110]. Isolated muons must also satisfy loose track- and calorimeter-based isolation conditions [110].

B. Analysis object definitions

Reconstructed jets possessing properties compatible with an $H \to b\bar{b}$ decay are labeled *candidate jets*. The reconstructed jet containing the Higgs boson decay products, or *H-jet*, is not always the highest-p_{T} jet in the event. The Higgs boson and the hadronic recoil system have equal p_{T}, but the p_{T} ordering of the reconstructed jets is affected by final-state radiation, jet resolution, and activity outside the jet cone. Undetected neutrinos from semileptonic b-hadron decays may also cause the H-jet to be reconstructed as the subleading jet. In around 50% (47%) of selected simulated ggF events, the H-jet is the leading (subleading) jet. Simulated VH events contain similar proportions of leading and subleading H-jets. For $t\bar{t}H$ production, any one of at least three final-state particles can be reconstructed as the leading jet. Therefore, candidate jets are defined as *either* of the two leading-p_{T} jets with $|\eta| < 2$, $p_{\mathrm{T}} > 250$ GeV, $m_J > 60$ GeV, and $2m_J/p_{\mathrm{T}} < 1$. The last requirement selects jets compatible with a boosted decay. Furthermore, they must contain at least two track-jets. A candidate jet is *double-tagged* if its two leading track-jets are b-tagged and *antitagged* if neither are b-tagged. Each signal region requires a double-tagged candidate jet, as discussed in Sec. VA.

A "muon-in-jet" correction is applied to candidate jets to account for the presence of semileptonic b-hadron decays. It utilizes the leading-p_{T} muon passing a minimum set of quality criteria and found within $\Delta R = \min(0.4, 0.04 + 10/p_{\mathrm{T}}^{\mu})$ of a b-tagged track-jet. The muon four-momentum is added to the trimmed jet while the energy deposited by the muon in the calorimeter is removed. After correcting 13% (33%) of leading (subleading) H-jets in simulated ggF events, the m_J width is reduced by 5% (12%). Henceforth, p_{T} and m_J refer to the muon-corrected jet transverse momentum and mass, respectively, and $p_{\mathrm{T}}^{\mathrm{u}}$ and m_J^{u} represent the corresponding uncorrected versions.

C. Reconstructed object systematic uncertainties

The most important experimental uncertainties originate from the jet mass resolution (JMR) modeling and jet mass scale (JMS) calibration. Uncertainties in b-tagging efficiency scaling factors and the jet energy scale are found to play a minor role. The remaining uncertainties, including those arising from muon trigger, reconstruction, identification, and isolation rate modeling [111], are negligible.

With appreciable reconstructed V and top quark resonance peaks, adjustments of the JMS and JMR central values and uncertainties are possible. Considerations about the validity of transferring these improvements between processes, or along jet p_{T}, inform the correlation scheme described below. It was verified that the chosen configuration is conservative

in terms of the expected sensitivity to the $V+$jets and H signal strengths. Jet observables in the simulation are smeared to assess the impact of scale and resolution uncertainties. A ratio of calorimeter-based to track-based measurements in dijet data and simulation defines the uncertainties in the jet energy (relative 1%–2%) and mass scales (relative 2%–10%) [103]. Jet energy scale and mass scale uncertainties are divided into 23 and 6 separate components, respectively, to account for different sources of uncertainty. The level of JMS agreement between data and simulation, while within the systematic uncertainties, displays a process and jet-p_{T} dependence. Therefore, JMS uncertainties for $t\bar{t}$ events are separated from those for $V+$jets and H events within the global likelihood, discussed in Sec. VIII. The dominant component in terms of reconstructed mass scale is further separated so as to act independently on all processes ($t\bar{t}$, $V+$jets, and H) and in all analysis jet-p_{T} bins. Consistent with previous studies of trimmed jets [112,113], the energy resolution has an absolute 2% uncertainty, while the mass resolution has a relative 20% uncertainty. JMR uncertainties act independently on each process ($t\bar{t}$, $V+$jets, and H) and in each analysis jet-p_{T} bin to account for generator, process, and p_{T} dependence. The $V+$jets JMR uncertainty is reduced using independent measurements as described in Sec. VII B.

The impact of uncertainties in b-tagging rates for b-, c-, and light-flavor jets is determined separately in various kinematic regions [108,114,115]. Each flavor category uncertainty is decomposed into independent components. A specific component for each jet flavor, based on the impact of experimental and theoretical uncertainties, accounts for an extrapolation of the scaling factors to jets with p_{T} beyond the calibration dataset's kinematic reach [116]. The thresholds are 250 GeV, 140 GeV, and 300 GeV for b-, c-, and light-flavor track-jets, respectively.

V. EVENT SELECTION AND CATEGORIZATION

Events are classified into three orthogonal regions: a signal region (SR) used to extract the signal strength, a control region used to study top quark events ($\mathrm{CR}_{t\bar{t}}$), and a validation region (VR) used to study the multijet and $V+$jets background models. Each region is further configured depending on jet p_{T} to determine the various signal strengths as described below.

A. Signal and validation regions

A uniform requirement for both the VR and SR in all data-taking years of at least one jet with $p_{\mathrm{T}}^{\mathrm{u}} > 450$ GeV and $m_J^{\mathrm{u}} > 60$ GeV removes the kinematic regime biased by the trigger requirements. A second jet with $p_{\mathrm{T}}^{\mathrm{u}} > 200$ GeV is required. At least one of the two leading-p_{T} jets must satisfy the candidate jet criteria.

The event categorization first considers the leading jet. If it is a double-tagged candidate jet, the event populates the leading-jet signal region (SRL). Only if the leading jet is not a double-tagged candidate jet, and the subleading jet is, the event is categorized into the subleading-jet signal region (SRS). Approximately 40% of the H events surviving the kinematic cuts pass the b-tagging requirement [117]. In simulated multijet events satisfying the SR requirements, roughly 70% of the candidate jets with mass close to m_H contain two b-hadrons and less than 5% of candidate jets do not contain any heavy-flavor hadrons. The SRS has a sensitivity approximately 50% lower than that of the SRL, due in part to inferior mass resolution.

Both the leading and subleading jets are always considered when creating the validation regions. The leading-jet validation region (VRL) includes events where the leading jet is an antitagged candidate jet, and the subleading jet either has the same distinction or is not a candidate jet. An analogous definition defines the subleading-jet validation region (VRS). Figure 2 summarizes the event categorization.

The signal strength is extracted in an inclusive signal region containing candidate jets with $p_{\mathrm{T}} > 250$ GeV. For the cross section measurements, the signal region is further configured into a fiducial signal region containing candidate jets with $p_{\mathrm{T}} > 450$ GeV and four differential signal regions defined by requiring the candidate jet p_{T} to be in the ranges 250–450 GeV, 450–650 GeV, 650–1000 GeV, or above 1 TeV. Only the leading-jet SR is used for the highest-p_{T} differential SR, $p_{\mathrm{T}} > 1$ TeV. Only the subleading-jet SR is populated for regions with $p_{\mathrm{T}} < 450$ GeV. The VRs follow the same definition. Table II summarizes the analysis signal regions. For measurements within the fiducial and differential regions, the signal yields within *volumes* defined by requirements on the generator's event "truth" record are extracted as described in Sec. IX C.

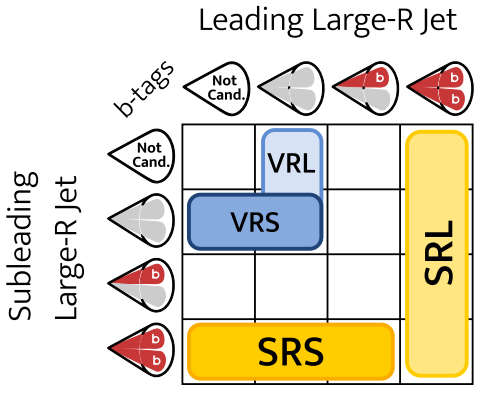

FIG. 2. Diagram showing the event categorization criteria. The columns (rows) divide events into categories based on when the leading(subleading)-p_{T} jet is not a candidate jet, when neither of the two leading-p_{T} track-jets are b-tagged, when one of the track-jets is b-tagged, and when both track-jets are b-tagged. SRL and SRS denote the leading-jet and subleading-jet signal regions. VRL and VRS denote the leading-jet and subleading-jet validation regions.

TABLE II. A summary of the candidate jet p_{T} requirements is given for the three analysis SR configurations. Each SR has an associated $\mathrm{CR}_{t\bar{t}}$ and VR with the same jet p_{T} requirements.

	Candidate jet p_{T} (GeV)	
Region	SRL	SRS
Inclusive	>450	>250
Fiducial	>450	>450
Differential	450–650, 650–1000, >1000	250–450, 450–650, 650–1000

Within each region, the discriminating variable, m_J, is studied in 5 GeV bins. As a simple analytic function is used to model the multijet background, m_J is studied in a restricted range where this background decreases monotonically. The combination of the $m_J^{\mathrm{u}} > 60$ GeV selection and the presence of a muon and neutrino from semileptonic b-hadron decays reduces the acceptance for m_J values near the selection threshold. Since the b-tagging efficiency diminishes with decreasing angular distance to another hadronic object [118], the low m_J region in the signal region is further sculpted. The prevalence of each effect determines the minimum m_J requirement. The SR mass range in each region is either 70 GeV to 210 GeV or 75 GeV to 210 GeV, depending on the jet being leading or subleading and the p_{T} range. The VRs use the same p_{T} bins and m_J ranges.

B. $t\bar{t}$ control region

A dedicated $t\bar{t}$ control region, $\mathrm{CR}_{t\bar{t}}$, using muon-trigger events, provides data with a high purity of top quark pair events to determine the $t\bar{t}$ yield in conditions equivalent to those of the SRs. The reconstructed final state is a top quark and a top antiquark with one semileptonic decay and one hadronic decay, with a minimum angular separation in the transverse plane. An isolated muon, with $p_{\mathrm{T}}^{\mu} > 52.5$ GeV, close to a jet J_b containing at least one track-jet defines the former, and a jet J_t with at least three track-jets defines the latter. Both jets are required to have $p_{\mathrm{T}} > 250$ GeV and exactly one of the leading two (three) track-jets in J_b (J_t) must be b-tagged. Considering multiple track-jets within J_b improves the identification efficiency of a b-quark reconstructed as a large-R jet by 7.5%.

To ensure the kinematics of top quarks reconstructed in the $\mathrm{CR}_{t\bar{t}}$ resemble those in the SR, only events with $140 < m_{J_t} < 200$ GeV are considered, removing those where J_t does not contain all the top quark decay products. Residual differences between the $\mathrm{CR}_{t\bar{t}}$ J_t and SRS candidate jet p_{T} spectra below 450 GeV originate from the different trigger requirements. The ratio of the jet p_{T} spectrum in simulated $t\bar{t}$ events in the $\mathrm{CR}_{t\bar{t}}$ to the jet p_{T} spectrum in the SRS reproduces the difference. It is used to adjust the simulated $t\bar{t}$ event weights and remove data events in the $\mathrm{CR}_{t\bar{t}}$ with $p_{\mathrm{T}}^{J_t} < 450$ GeV.

The same p_{T} boundaries used in the SR are also applied to $p_{\mathrm{T}}^{J_t}$ to define the inclusive and differential $\mathrm{CR}_{t\bar{t}}$ regions. The selection criteria, summarized in Table III, achieve over 95% purity in $t\bar{t}$ events for each $\mathrm{CR}_{t\bar{t}}$ p_{T} bin.

VI. HIGGS BOSON MODELING

The limited number of event selection criteria pertaining to properties of the recoil system or other activity in the event result in an inclusive analysis in terms of the Higgs boson production modes. Table IV shows the relative contributions of the four main production modes as a function of Higgs boson candidate p_{T}, according to SM predictions and within the Higgs boson window ($105 < m_J < 140$ GeV). In both the SRL and SRS, ggF production contributes the most for $p_{\mathrm{T}}^{\mathrm{jet}} > 450$ GeV. For $p_{\mathrm{T}}^{\mathrm{jet}} < 450$ GeV, $t\bar{t}H$ accounts for around 40% of the selected Higgs boson events. A hadronically decaying top quark can satisfy the jet trigger requirements without a high p_{T}^{H} value, thus resulting in a significant contribution of $t\bar{t}H$ events with relatively low Higgs boson p_{T}. Almost 90% of $t\bar{t}H$ events in the Higgs boson window arise from $H \to b\bar{b}$ decays. The majority of the remainder are $H \to W^{\pm}W^{\mp}$ events and these climb to almost 15% for larger m_J values.

The uncertainty on the cross section and acceptance for ggF-produced events is 20%. It includes variations of the factorization and renormalization scales, the PDF, and the parton shower model to account for their respective uncertainties. Reference [119] demonstrates that the NLO correction is nearly the same in the infinite top-mass approximation and full SM calculation, so no additional systematic uncertainty is assigned. Uncertainties on the cross section and acceptance for the VBF, VH, and $t\bar{t}H$ processes are taken to be 0.5%, 5%, and 13%, respectively [26]. Systematic uncertainties in the EW corrections (expressed as $1 + \delta_{\mathrm{EW}}$) are taken as δ_{EW}^2 following the recommendations in Ref. [5].

TABLE III. A summary of the $\mathrm{CR}_{t\bar{t}}$ selection criteria.

Jet	N track-jets	N b-tags	Angular selection	Jet mass (GeV)
J_b	≥1	1	$0.04 + 10/p_{\mathrm{T}}^{\mu} < \Delta R(\mu, J^b) < 1.5$	⋯
J_t	≥3	1	$\Delta\phi(J^b, J^t) > \frac{2\pi}{3}$	140–200

TABLE IV. The fractional contribution of each production mode to a given analysis region around the Higgs boson mass peak, defined as $105 < m_J < 140$ GeV. The fraction is given relative to the total signal yield in the analysis region in question.

	Jet p_T range (GeV)			
Process	250–450	450–650	650–1000	>1000
		SRL		
ggF	···	0.56	0.50	0.39
VBF	···	0.17	0.16	0.17
VH	···	0.14	0.18	0.25
$t\bar{t}H$	···	0.13	0.16	0.19
		SRS		
ggF	0.28	0.46	0.43	···
VBF	0.07	0.19	0.21	···
VH	0.26	0.24	0.26	···
$t\bar{t}H$	0.39	0.11	0.10	···

VII. BACKGROUND PROCESS MODELING

Multijet production is the dominant background process. The $V+$jets and top quark resonance peaks flank the Higgs boson signal in low- and high-mass sidebands, respectively, but also leak into the Higgs boson signal window. Within $105 < m_J < 140$ GeV, $V+$jets accounts for about 1% of the total background, top quarks for about 3%, and multijets provide the rest. The expected Higgs boson signal contribution corresponds to 0.2% of the background for jet $p_T > 450$ GeV in the mass window and 20%–80% of the data statistical precision in the analysis jet-p_T bins.

Therefore, an accurate and precise determination of the background is paramount and is achieved starting with the determination of the $V+$jets and top quark backgrounds. These backgrounds are determined by maximizing a binned likelihood function defined as the product of Poisson probability terms for each bin of the m_J distributions in the SRL, SRS, and $\mathrm{CR}_{t\bar{t}}$. Unconstrained normalization parameters are common to the signal and control regions within each jet p_T range. Systematic uncertainties are included as constrained nuisance parameters. Details are given in Sec. VIII.

A. Top quark production

The candidate jet in SR top quark events usually contains the remnants of a b-quark and the two hadronic decay products of a W boson. As discussed above, the $\mathrm{CR}_{t\bar{t}}$ design ensures the same physics processes also populate the control region. The simulated jet mass distributions in the CR and SR are similar in shape and peak near the top quark mass because both regions probe a comparable top quark momentum range. Therefore, any adjustment of the simulated top quark events made to improve their agreement with data in the $\mathrm{CR}_{t\bar{t}}$ can be directly applied to the SR. This is achieved by including the $\mathrm{CR}_{t\bar{t}}$ in the global likelihood described in Sec. VIII. The inclusive $\mathrm{CR}_{t\bar{t}}$ has a $t\bar{t}$ purity of 97% with similar levels found in the fiducial and differential region configurations. With such high purity, the $t\bar{t}$ normalization is determined directly from data with better than 10% precision in most regions.

In the SR, tW-produced events where a top quark is matched to a candidate jet contribute 2%–3% relative to the $t\bar{t}$ yield. For t-channel production, the ratio to $t\bar{t}$ is 1%–5%. Both have a candidate jet mass distribution similar to that in $t\bar{t}$ production. To reduce effects due to limited MC sample size, the mass spectrum's shape for events with one top quark used in the likelihood described in Sec. VIII is obtained by scaling the $t\bar{t}$ MC sample to the number of events predicted by the dedicated tW and t-channel MC samples within each jet p_T bin. The contribution from s-channel production is negligible.

For $t\bar{t}$ production, comparisons between nominal and alternative simulated samples provide systematic uncertainty estimates for the parton shower model (HERWIG 7 replaces PYTHIA8) and the matrix element calculation (MADGRAPH5_AMC@NLO replaces POWHEGBOX v2). The comparisons show a 6%–20% and 1%–19% difference in yield in the various analysis regions, respectively. Within the nominal sample, variations of internal weights are used to estimate the systematic uncertainties associated with initial- and final-state radiation (1%–7%), as well as the renormalization and factorization scales (negligible). All experimental uncertainties described in Sec. IV C are utilized. Uncertainties in the b-tagging efficiency for b-jets and the JMS have the largest impact on the $t\bar{t}$ normalization. A 50% normalization uncertainty is applied to the estimated number of events with a single-top quark, mainly driven by the comparison between the diagram subtraction and diagram removal schemes [67] in tW events.

Figure 3 shows the jet mass distribution for each analysis p_T bin in the $\mathrm{CR}_{t\bar{t}}$ after the global likelihood fit described in Sec. VIII in the differential configuration. The simulation, shown with a 68% confidence level (CL) uncertainty band, agrees well with the data.

B. $V+$jets production

With a decay structure and relative experimental resolution similar to that of the Higgs boson, the vector-boson mass peaks offer a unique opportunity to validate the experimental performance. Events with Z bosons in the signal region outnumber H events by over a factor of 20. Experimental effects that are challenging to discern in a statistically limited H production measurement will be evident in the Z observation. A well-understood Z measurement is therefore a precursor to a robust H measurement. Furthermore, the validation region offers a sample with a topology similar to the SR with which to study $V+$jets production with a larger event sample but a lower signal-to-background ratio.

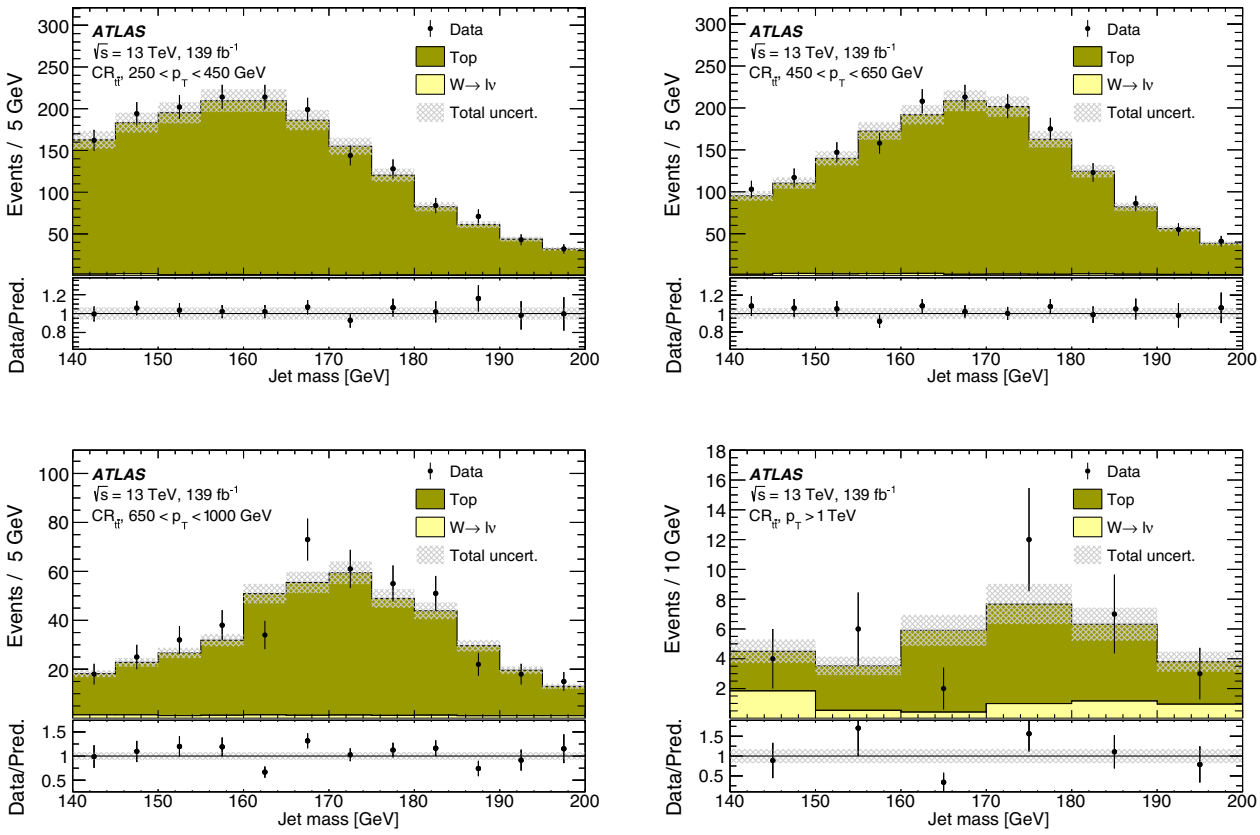

FIG. 3. The post-fit $\mathrm{CR}_{t\bar{t}}$ J_t mass distribution in the four p_{T} regions used in the global likelihood of the differential fit (Sec. IX C). The $W(\ell\nu)$ contribution is flat in jet mass and for events with $p_{\mathrm{T}} < 1$ TeV it is estimated to be 1–3% of the total. The $p_{\mathrm{T}} > 1$ TeV region is shown in 10 GeV jet mass bins. The ratio of the data to the background prediction is shown in the lower panel. The shaded areas indicate the 68% CL for all background processes.

In the VR, $W+$jets events outnumber Z events nearly three to one due to the larger cross section and comparable acceptance. The decay products of the vector boson are reconstructed within the selected candidate jet in over 60% of events. In the remainder, the selected candidate jet is created by the recoil hadronic system, resulting in a nonresonant mass distribution, similar in shape to the multijet background, that enhances the high-mass tail. In the SR, the $Z+$jets event contribution is dominant and exceeds that of $W+$jets events by more than a factor of three, because of the sizable $Z \to b\bar{b}$ branching fraction and the flavor-tagging requirements. About 90% of the candidate jets in $Z+$jets events contain the decay products of a vector boson. Due to the low misidentification rate for b-tagging, only 40% of candidate jets in $W+$jets events are from the boson decay. The prevalence of candidate jets from the recoil system in $W+$jets events leads to a broad m_J distribution in the SR.

The $Z+$jets normalization is determined directly from the data with the global likelihood described in Sec. VIII. Therefore, the impact of the considered systematic uncertainties in the modeling is limited to relative changes in acceptance across regions and the m_J distribution shape. The $W+$jets cross section is assigned a 10% uncertainty in the signal region [120]. For both processes, the largest effect from seven independent pairs of renormalization and factorization scale variations by factors of 0.5 and 2 corresponds to a 3%–20% error in the expected relative acceptance across regions. An alternative PDF set (MMHT2014NLO), α_{s} variations within the nominal PDF set, and changing the cluster fragmentation model to the Lund string model [121] does not lead to a significant change in the acceptance estimate relative to the nominal model. In the $\mathrm{CR}_{t\bar{t}}$, the minor $W+$jets contribution, referred to as $W(\ell\nu)$, has a total uncertainty of 30%.

All experimental uncertainties described in Sec. IV C are applied. Uncertainties in the JMR and JMS have the largest impact on the $V+$jets normalization. Using the multijet model described in Sec. VII C and the likelihood described in Sec. VIII, the jet mass distribution in the leading-jet validation region is described to the level of agreement between simulation and data shown in Fig. 4.

1. Jet mass resolution uncertainty

The fitted $Z+$jets normalization in the SR had a significant correlation with the reconstructed m_J resolution as the flexibility of the $Z+$jets template and the multijet

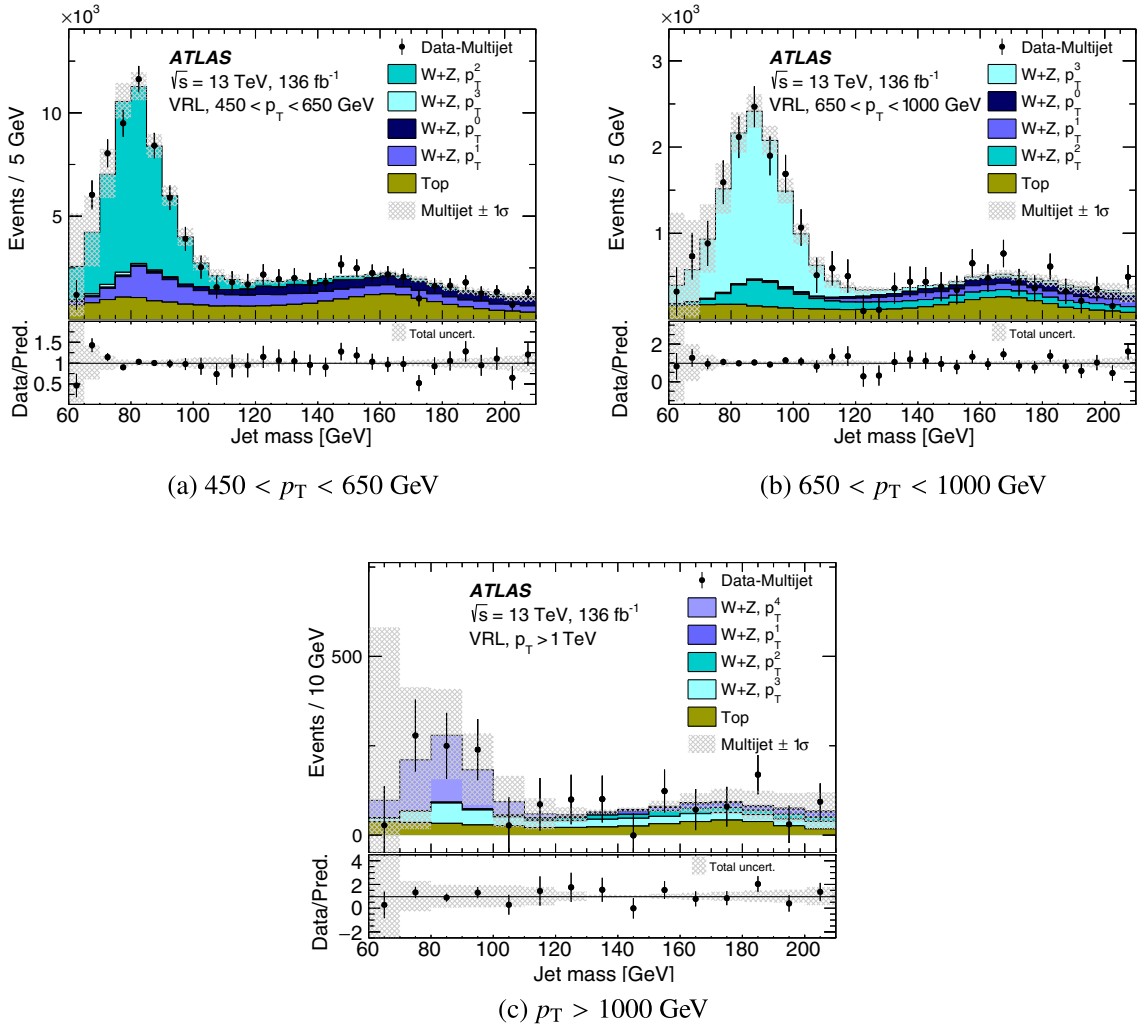

(a) $450 < p_{\mathrm{T}} < 650$ GeV

(b) $650 < p_{\mathrm{T}} < 1000$ GeV

(c) $p_{\mathrm{T}} > 1000$ GeV

FIG. 4. Post-fit leading-jet invariant mass distributions after the multijet background was subtracted in the validation region for data (points with error bars) and the $V+$jets ($W+Z$) and Top components (histograms) for (a) $450 < p_{\mathrm{T}} < 650$ GeV, (b) $650 < p_{\mathrm{T}} < 1000$ GeV, and (c) $p_{\mathrm{T}} > 1$ TeV shown in wider 10 GeV jet mass bins. The $V+$jets contribution is split into five generator "truth" p_{T}^{V} volumes labeled p_{T}^{0}–p_{T}^{4} for $p_{\mathrm{T}}^{V} < 300$ GeV, 300–450 GeV, 450–650 GeV, 650–1000 GeV, and > 1000 GeV, respectively. The $t\bar{t}$ normalization and its uncertainty are set to the corresponding values from the $\mathrm{CR}_{t\bar{t}}$. The m_J range has been extended down to 60 GeV for only this fit to show the level of agreement along the rising edge of the $V+$jets m_J distribution. The ratio of the data to the background prediction is shown in the lower panel. The shaded areas indicate the 68% CL for all background processes.

model could open a local minimum in the likelihood fit minimization procedure. Tests using subsets of a hybrid validation region, constructed to have a known amount of each process and discussed in the next section, highlighted this feature. In some instances, the best-fit value of the JMR parameter broadened the $Z+$jets peak, corresponding to an increase of the $Z+$jets normalization and a decrease of the multijet contribution compared to the expected values.

To stabilize the fit response, the Z and W resonance jet mass width is measured directly in two data samples as a function of p_{T} and used to create additional constraints on the $V+$jets JMR parameter in the global likelihood (see Sec. VIII). The two data samples are an alternative $t\bar{t}$ CR ($\mathrm{WCR}_{t\bar{t}}$) and the VRL. The $\mathrm{WCR}_{t\bar{t}}$ consists of selected semileptonic $t\bar{t}$ events having a resolved Wb pair from a hadronically decaying top quark, providing a high-purity reconstructed W peak with jet p_{T} from 200 GeV up to about 600 GeV. The VRL covers the entire jet-p_{T} range above 450 GeV, providing a clear V peak but with considerably more multijet background.

The measured jet mass width of the W and Z resonances shows a smooth evolution from low p_{T} in the $\mathrm{WCR}_{t\bar{t}}$ to high p_{T} in the VRL (see Fig. 5). These results differ from the nominal simulated m_J resolution by less than 2.5% and have a precision that is around one fifth of the original JMR uncertainty after systematic uncertainties are incorporated to transfer the result to the $Z \to b\bar{b}$-dominated $V+$jets sample in the SR. When included in the global likelihood, the correlation between the $Z+$jets normalization and the JMR is reduced compared to when the auxiliary mass

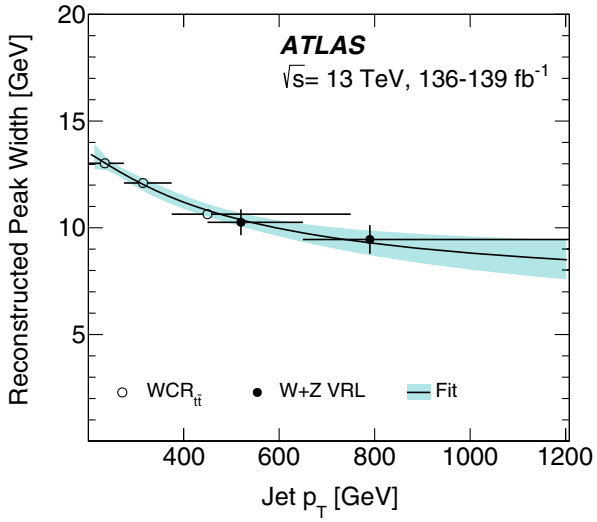

FIG. 5. A summary of the Z and W resonance peak reconstructed-width measurements as a function of the jet p_{T} using a resolved W boson in top quark decays in the $\mathrm{WCR}_{t\bar{t}}$ region and the combined W and Z boson mass distribution in the validation region. The horizontal bars cover the jet p_{T} range used for the corresponding point and the points are centered at the average jet p_{T} in the same range. The continuous black curve is a fit to the measurements with resultant errors shown as a cyan band.

measurement is not considered. For example, in the inclusive signal region it decreases from ∼90% to ∼30%.

C. Multijet production

The monotonically decreasing jet mass spectrum of the multijet background is modeled with an exponential function of a polynomial:

$$f_N(x|\vec{\Theta}) = \Theta_0 \exp\left(\sum_{i=1}^{N} \Theta_i x^i\right), \tag{1}$$

where $x = (m_J - 140\ \mathrm{GeV})/70\ \mathrm{GeV}$ and Θ_i are the parameters of the fit. Parameter values are determined independently in each region simultaneously with the signal extraction. The optimal degree of the polynomial, N in Eq. (1), depends on the mass spectrum's shape and the number of events analyzed. Values of N which are too large increase correlations between the multijet and resonant process models, decreasing their statistical significance. Values of N which are too small induce biases in the resonant process yields because the function is too rigid. These effects are studied in the VRL (VRS), which contains 58 (51) times the amount of SRL (SRS) data. To determine N, statistical tests are performed on modified VR subsets, referred to as hybrid VR *slices*, with roughly the same number of events as the corresponding SR.

The hybrid VR is the best available proxy for the SR. The slices are generated from the VR subsets by replacing the VR resonance peaks with the corresponding SM prediction in the SR and correcting the underlying multijet mass spectrum shape to match that of the SR. The multijet shape difference between the SR and the VR is defined as the ratio of the SR multijet model ($\mathrm{MJ_{SR}}$) to the VR multijet model ($\mathrm{MJ_{VR}}$) (see Fig. 6). The $\mathrm{MJ_{SR}}$ is obtained from a global likelihood fit to the SRs and $\mathrm{CR}_{t\bar{t}}$, including all experimental and modeling systematic uncertainties. The Higgs boson signal normalization parameter is blinded and common unconstrained normalization parameters are used within each jet p_{T} region for the $V+$jets and $t\bar{t}$ templates separately. The $\mathrm{MJ_{VR}}$ is created from the average of the multijet model parameter values obtained from likelihood fits to ten[2] random, orthogonal subsets of the VR including the full set of systematic uncertainties. The input $t\bar{t}$ normalization and associated uncertainty are set to representative values from the $\mathrm{CR}_{t\bar{t}}$. The VR $V+$jets and Top estimates (V_{VR} and $\mathrm{Top_{VR}}$) are created from the average post-fit contributions from the same ten fits to the VR. Each slice of the hybrid VR, $\mathrm{VR}^i_{\mathrm{hyb}}$, is built as

$$\mathrm{VR}^i_{\mathrm{hyb}} = (\mathrm{VR}^i - V_{\mathrm{VR}} - \mathrm{Top_{VR}}) \times \left(\frac{\mathrm{MJ_{SR}}}{\mathrm{MJ_{VR}}}\right) + V_{\mathrm{SR}} + t\bar{t}_{\mathrm{SR}} + H_{\mathrm{SR}},$$

where VR^i is the jet mass distribution of the data events in the ith VR slice and V_{SR}, $t\bar{t}_{\mathrm{SR}}$, and H_{SR} are the nominal MC predictions for $V+$jets, $t\bar{t}$, and H production in the SR, respectively. The ratio of $\mathrm{MJ_{SR}}$ over $\mathrm{MJ_{VR}}$ is stable versus N.

The optimal N for each region is chosen by considering three metrics evaluated with the $\mathrm{VR_{hyb}}$ collection. First, a log-likelihood ratio (LLR) test compares the result of an N-parameter fit (null hypothesis) with the result of an $(N+1)$-parameter fit (alternative hypothesis) in each $\mathrm{VR_{hyb}}$ slice without any injected SM resonances. By Wilks' theorem, the likelihood ratio follows an asymptotic χ^2 distribution with one degree of freedom when the data corresponds to the null hypothesis. The corresponding distribution of p-values is flat. The smallest N that yields a uniform distribution of p-values is selected.

The LLR test ensures a good description of the data over the full mass range, but resonance measurements are sensitive to local effects. Two rate tests sensitive to local effects rely on the fit result for a free normalization parameter and its associated error (generalized as $\mu^{\mathrm{VR}} \pm \sigma^{\mathrm{VR}}_{\mathrm{stat}}$) for either the $Z+$jets process or the Higgs boson process. Both utilize $\mathrm{VR_{hyb}}$ slices with all SR resonances injected at the SM rates. The fraction of results $F_{2\sigma}$ where $|\mu^{\mathrm{VR}} - 1|$ is beyond twice its error $\sigma^{\mathrm{VR}}_{\mathrm{stat}}$ gives an estimate of the probability that the multijet model allows a substantial artificial excess or deficit. A 2σ threshold

[2]Ten subsets balance the statistical precision with the need to use greater values of N to model a larger dataset.

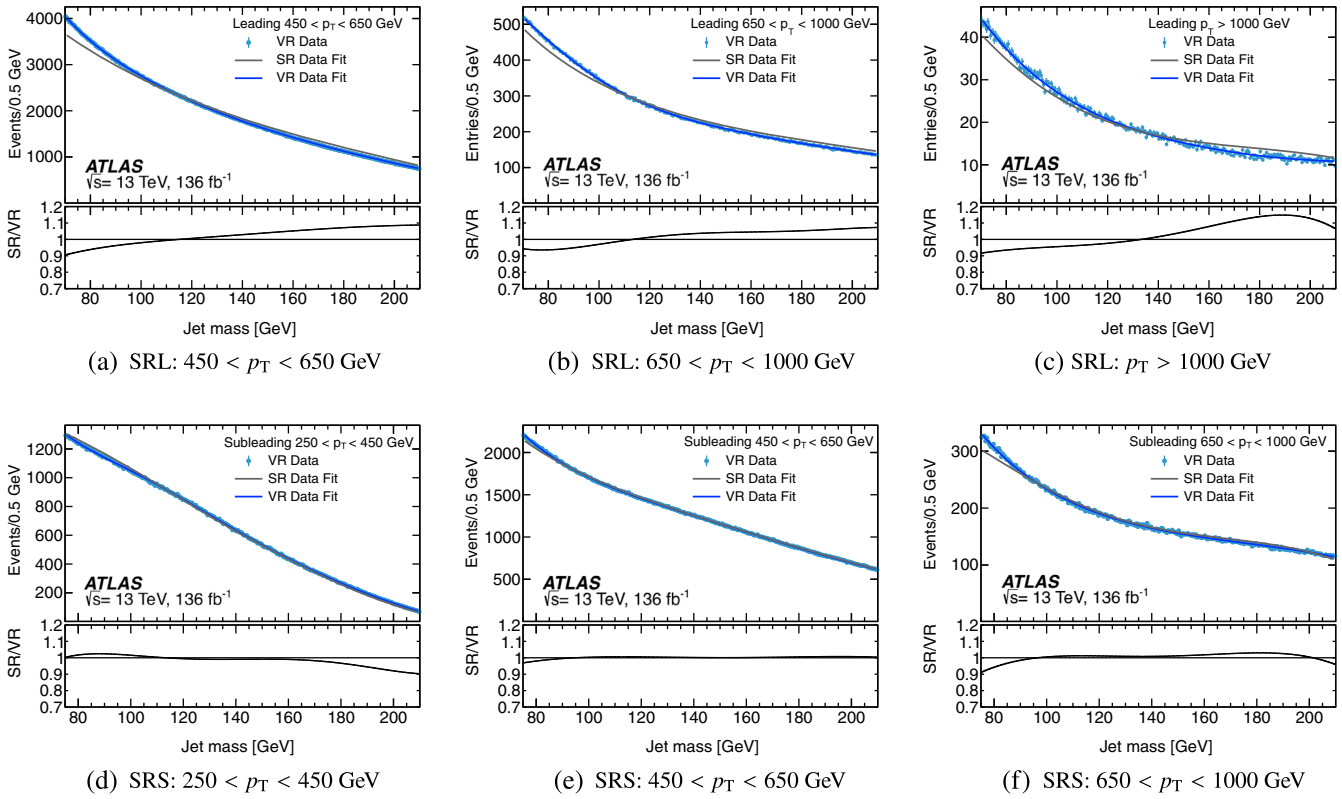

(a) SRL: $450 < p_{\mathrm{T}} < 650$ GeV (b) SRL: $650 < p_{\mathrm{T}} < 1000$ GeV (c) SRL: $p_{\mathrm{T}} > 1000$ GeV

(d) SRS: $250 < p_{\mathrm{T}} < 450$ GeV (e) SRS: $450 < p_{\mathrm{T}} < 650$ GeV (f) SRS: $650 < p_{\mathrm{T}} < 1000$ GeV

FIG. 6. Comparison of the multijet jet mass distribution shapes from the different p_{T}-binned analysis regions. The solid lines show the multijet function shape after a fit to the SR data (gray) and VR data (blue). The solid points are the data from VR slices with the same number of events as the SR after the SM resonances are subtracted. The bottom panel shows the ratio of the SR data fit to the VR data fit. The $250 < p_{\mathrm{T}} < 450$ GeV region is only populated in the subleading-jet SR and events with $p_{\mathrm{T}} > 1$ TeV are only considered in the leading-jet SR.

ensures some results from the full set of VR slices cross the boundary. The average value of $(\mu^{\mathrm{VR}} - 1)/\sigma^{\mathrm{VR}}_{\mathrm{stat}}$ is denoted by $\overline{\mu/\sigma}$ and indicates a bias in determining the signal strength. The value of N chosen by the LLR test is incremented until $F_{2\sigma}$ is compatible with 0.05, and $\overline{\mu/\sigma}$ stabilizes for both $Z+$jets and H production. The chosen values of N do not change when including systematic uncertainties and when not injecting the $Z+$jets and H processes into the $\mathrm{VR}_{\mathrm{hyb}}$ slices (with appropriate changes to the definition of $F_{2\sigma}$ and $\overline{\mu/\sigma}$). A fifth-degree polynomial is used in both inclusive regions, while either a fourth- or fifth-degree polynomial is used in the analysis p_{T} bins.

A nonzero value of $\overline{\mu/\sigma}$ for the N chosen in each region indicates a bias in the background model. It defines the spurious-signal systematic uncertainty and is in the range 0.01–0.33 for H and 0.15–0.65 for $Z+$jets production. A compatible estimate of the spurious-signal systematic uncertainty is found when not injecting the $Z+$jets or H processes into the $\mathrm{VR}_{\mathrm{hyb}}$ slices. In all cases, the spurious-signal systematic uncertainty has an insignificant impact on the sensitivity.

Above 1 TeV, the $V+$jets yield extracted from the VR has a sizable statistical uncertainty, necessitating a change in the above procedure (see Fig. 4). Comparisons of fit quality and $\overline{\mu/\sigma}$ for both $Z+$jets and the Higgs boson in the hybrid VR for an N of 4, 5, and 6 show no improvement in modeling from the higher-order functions. The $\overline{\mu/\sigma}$ is calculated in two ways to estimate the spurious-signal systematic uncertainty for the chosen value of $N = 4$. The V_{VR} subtracted from each VR^i slice is taken from the average post-fit contributions to five subsets of the VR or the SM prediction. The spurious-signal systematic uncertainty is found to be 0.5 and 0.3 for $Z+$jets and H, respectively, and has an insignificant impact on the sensitivity.

Finally, an alternative function for the multijet background modeling, the Laurent series, was tested. It provides a similar level of agreement with the multijet background in the $\mathrm{VR}_{\mathrm{hyb}}$ collection. The differences between the two models are much smaller than the data statistical uncertainty and the expected Higgs boson yield. Therefore, the model choice does not motivate an additional systematic uncertainty.

VIII. STATISTICAL ANALYSIS

Signal yields are extracted by minimizing the negative logarithm of a likelihood function $\mathcal{L}(\mu, \vec{\theta})$ with the

TABLE V. A summary of the systematic uncertainties included within the profile likelihood for the H and Z signal strength extraction. For a given uncertainty, the second column lists each process which has independent nuisance parameters within the likelihood. The third column describes how the systematic uncertainty is correlated across regions: "all" indicates a fully correlated parameter, "p_{T} bins" indicates a decorrelation between the analysis p_{T} bins, and "LS" means it is decorrelated between the SRL and SRS. For the inclusive and fiducial analysis configurations, "bins" does not apply, and should be understood to mean the same as "all." The fourth column describes the change induced by the parameter. "S" means the m_J shape will change while "N" denotes parameters which change the normalization and can result in a migration of events between regions. $(*)$ Two minor components separately apply to $t\bar{t}$ and $V+$jets events. $(\bullet)$ For cross section limits and measurements, this uncertainty covers relative acceptance across regions instead of the absolute cross section uncertainty. $(\circ)$ The spurious-signal uncertainty is only applied to $Z+$jets when the procedure to extract signal strengths in "truth"-based volumes is tested using $Z+$jets events in the SR.

Description	Processes	Category	Effect
Reconstructed object systematic uncertainties			
JMR	$t\bar{t}$, $V+$jets, H	p_{T} bins	N + S
JMS (dominant)	$t\bar{t}$, $V+$jets, H	p_{T} bins	N + S
JMS (rest)	$t\bar{t}$, $V+$jets $+H$	All	N + S
Jet energy scale	all$^{(*)}$	All	N + S
Jet energy resolution	All	All	N + S
b-tag efficiency for b-jets	All	All	N + S
b-tag efficiency for c-jets	All	All	N + S
b-tag efficiency for light-flavor jets Process modeling systematic uncertainties	All	All	N + S
Process modeling systematic uncertainties			
Renormalization and factorization scale	$V+$jets	All	N + S
Cross section	$W+$jets	All	N
Cross section and acceptance	$W(\ell\nu)$	All	N
Parton shower model	$t\bar{t}$	All	N + S
Matrix element calculation	$t\bar{t}$	All	N + S
Initial- and final-state radiation	$t\bar{t}$	All	N + S
Cross section and acceptance	t	All	N
Cross section and acceptance$^{(\bullet)}$	H	All	N
NLO EW corrections	VBF $+VH+t\bar{t}H$	All	N
Spurious signal	H	p_{T}^{H} bins $\times$ LS	N
	$Z+$jets $^{(\circ)}$	p_{T}^{Z} bins $\times$ LS	N

ROOSTATS framework [122,123]. The likelihood function is defined as the product of Poisson probability terms, one for each bin of the m_J distribution of the SRL, SRS, and CR$_{t\bar{t}}$. Bin widths are set to 5 GeV, necessitating technical advancements within RooStats to fit an analytic function to a wide-binned dataset [124]. Systematic uncertainties enter the likelihood as nuisance parameters, $\vec{\theta}$, constrained with Gaussian or log-normal probability density function priors. The JMR constraints obtained from the WCR$_{t\bar{t}}$ and VRL regions are included as Gaussian probability density function priors. Unconstrained, or *free*, parameters control the normalization of the MC templates within each jet p_{T} region or within a given "truth"-based volume and are common to the SRL, SRS, and CR$_{t\bar{t}}$. For the multijet model, the function normalization and its polynomial coefficients are free parameters and independent for each jet mass distribution. Signal yields are expressed as signal strengths, μ, obtained by normalizing the fitted number of signal events to the corresponding SM predictions. Upper limits on the Higgs boson signal strengths and production cross section are derived using the CL$_{\mathrm{s}}$ method [125,126]. The expected limits assume no Higgs boson contribution.

Table V summarizes the systematic uncertainties considered in the likelihood fit. In addition, uncertainties due to the limited number of events in the simulated samples used for the background predictions are parametrized using the Beeston–Barlow "lite" technique [127]. Systematic variations yielding large statistical fluctuations are smoothed using custom algorithms which also remove variations resulting in effects below 2% within a given region.

IX. RESULTS

The three analysis configurations designed to probe Higgs boson production with considerable transverse momentum are summarized in Table II. The inclusive region provides a measure of the H signal strength, the fiducial region allows a measurement of the fiducial cross section, and the differential regions are used to measure the cross section in four p_{T} bins. All H production modes are considered for the signal strength extraction. Signal

TABLE VI. A summary of the fiducial and STXS volumes used to determine which signal events are considered for the signal strength measurement in the fiducial and differential regions, respectively. Signal cross sections outside of these volumes are constrained to their SM prediction.

Volume	p_{T}^{H} (GeV)	$\lvert y_H \rvert$
Fiducial	>450	<2
STXS	300–450, 450–650, 650–1000, >1000	<2

strengths within the fiducial region consider events within a fiducial *volume* defined by requirements on the generator's event "truth" record, the Higgs boson transverse momentum (p_{T}^{H}), and rapidity (y_H). Using the same "truth" information within the differential regions, *volumes* like the bins used in the simplified template cross section (STXS) framework and simply referred to as STXS volumes, are considered; the p_{T}^{H} requirements match those for ggF production in the STXS scheme [5–7], but the y_H requirement is more stringent and all production modes are included. The analysis jet-p_{T} bins align well with the p_{T}^{H}-defined volumes. The yield of signal events outside the targeted volume(s) are constrained to their SM prediction within the theoretical and experimental uncertainties. The cross sections are obtained from the fitted signal yields divided by the integrated luminosity, corrected by the product of the estimated selection efficiency and fiducial or STXS volume acceptance. Using the same p_{T} boundaries, cross section measurements of $V+$jets production in the VRL and of $Z+$jets production in the SR validate the method. For these tests, the fiducial and STXS volumes are defined by the generator "truth" vector-boson transverse momentum (p_{T}^{V}). Table VI summarizes the fiducial and STXS volumes and the SM predicted cross sections are in the HEPData repository [128].

A. Inclusive region

The inclusive region yields a Higgs boson signal strength of $\mu_H = 0.8 \pm 3.2$ for the combination of SRL, SRS and $\mathrm{CR}_{t\bar{t}}$. The results are summarized in Table VII and the yields in Table VIII. The post-fit SRL and SRS jet mass distributions are shown in Fig. 7. The Higgs boson signal sensitivity is limited by the size of the data sample. The leading sources of systematic uncertainty are the jet mass resolution and mass scale. The $\mu_{t\bar{t}}$ value is compatible with $t\bar{t}$ event measurements in a similar kinematic phase-space [129]. With nearly 99% purity in top-jet events, the $\mathrm{CR}_{t\bar{t}}$ data reduces the top quark jet JMR uncertainty to a relative 7% (from 20%). For $V+$jets (Top) events, the JMS uncertainty's nuisance parameter is pulled by −80% (20%) of its original width, and its width is reduced by 50% (50%). The $V+$jets resonance peak position moves by about 2 GeV from the MC prediction. No other nuisance parameters are significantly modified.

TABLE VII. Expected and observed values of the signal strengths for the H, Z and $t\bar{t}$ components in the inclusive fit. Absolute cross section uncertainties are not included in the reported μ_Z and $\mu_{t\bar{t}}$ values.

Result	μ_H	μ_Z	$\mu_{t\bar{t}}$
Expected	1.0 ± 3.2	1.00 ± 0.17	1.00 ± 0.07
Observed	0.8 ± 3.2	1.29 ± 0.22	0.80 ± 0.06

TABLE VIII. Event yields and associated uncertainties after the global likelihood fit in the inclusive region. The total background yield can differ from the sum of the individual components due to rounding.

Process	SRL	SRS	$\mathrm{CR}_{t\bar{t}}$
Multijet	$590\,700 \pm 4200$	$529\,300 \pm 3500$	···
$Z+$jets	$16\,100 \pm 2800$	$12\,000 \pm 2100$	···
$W+$jets	3050 ± 720	2510 ± 500	···
Top	$16\,300 \pm 1900$	$15\,900 \pm 2000$	3737 ± 68
$W(\ell\nu)$	···	···	53 ± 16
H	400 ± 1500	300 ± 1300	···
Total	$626\,530 \pm 820$	$560\,090 \pm 770$	3790 ± 66
Data	626 532	560 083	3791

B. Fiducial region

In the fiducial region, the Higgs boson yield and cross section are determined within the fiducial volume defined by the Higgs boson transverse momentum $p_{\mathrm{T}}^{H} > 450$ GeV and rapidity $\lvert y_H \rvert < 2.0$. Compared to the inclusive measurement discussed above, the fiducial region does not include the SRS region below 450 GeV. The acceptance times efficiency values for the different SM Higgs boson production processes are given in Table IX.

Two Higgs boson mass templates are used in each SR. The first describes the jet mass distribution of events within the fiducial volume; the second includes events outside the fiducial volume, i.e. those with p_{T}^{H} below 450 GeV. The first component accounts for more than 80% of the Higgs boson signal selected and has a free normalization parameter common to the SRL and SRS. The second component is constrained to the SM value within the theoretical and experimental uncertainties and also tends to have a broader mass spectrum shifted to higher values.

This procedure is first tested with $W \to qq'$ and $Z \to qq'$ in the VR and $Z \to b\bar{b}$ in the SR. For these tests, the V and Z mass templates are structured similarly to those of the Higgs boson described above. The Higgs boson yields are kept fixed to the SM expectations in the fit and the result is insensitive to this choice. The fitted signal strength for $V+$jets with $p_{\mathrm{T}}^{V} > 450$ GeV is 1.01 ± 0.09. In the SR, the

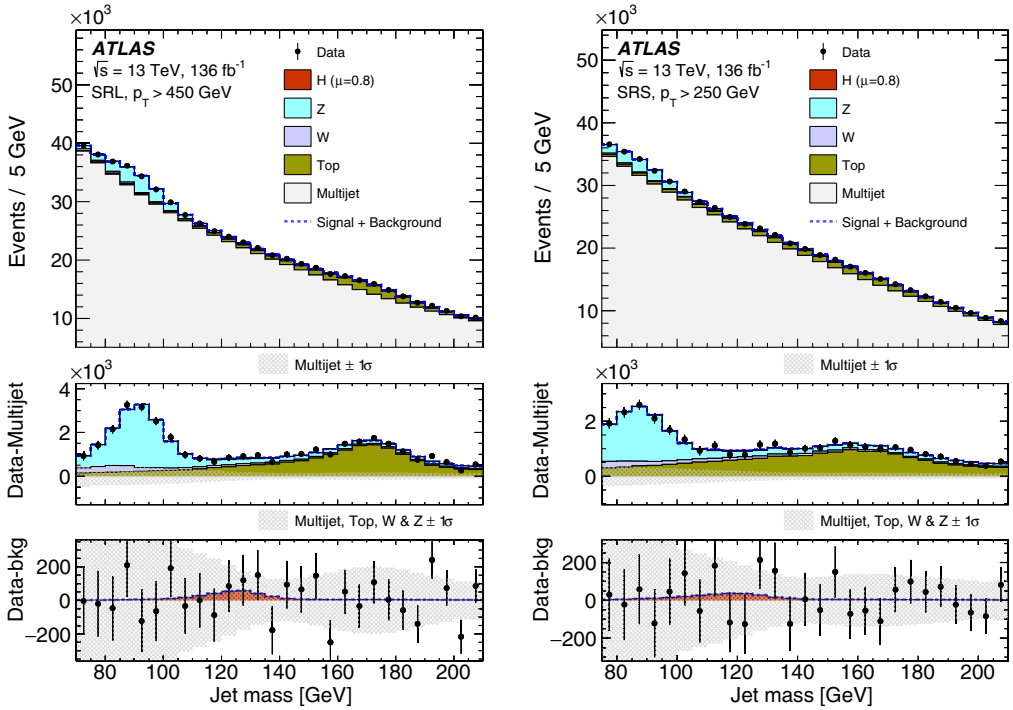

FIG. 7. Post-fit jet mass distributions for the various components in the inclusive SRL (left) and SRS (right) regions. The middle panels show the distributions after subtraction of the multijet distribution. The shaded areas indicate the 68% CL for the multijet background from the fitted parameters and normalizations of the exponentiated polynomials. The lower panels show the distributions after subtraction of all the fitted background processes: multijet, $V+$ jets, and Top. The shaded areas indicate the 68% CL for all background processes.

signal strength for Z events with $p_{\mathrm{T}}^{V} > 450$ GeV is 1.35 ± 0.25. These results are in agreement with the SM.

When extracting the Higgs boson signal strength, the likelihood fit result for $p_{\mathrm{T}}^{H} > 450$ GeV provides a signal strength of $\mu_H = -0.1 \pm 3.5$. The corresponding observed (expected) 95% CL upper limit on the Higgs boson production cross section is

$$\sigma_H(p_{\mathrm{T}}^{H} > 450\ \mathrm{GeV}) < 115(128)\ \mathrm{fb}$$

and the SM prediction is 18.4 fb.

The results are summarized in Table X. The $\mu_{t\bar{t}}$ value is compatible with $t\bar{t}$ event measurements in a similar kinematic phase-space [129]. The Higgs boson signal strength sensitivity is limited by the data sample size, and the impact from the main sources of uncertainty is given in Table XI. The jet uncertainties give the largest contribution of systematic uncertainty, driven by JMS

TABLE IX. Signal acceptance times efficiency within the fiducial volume used in the fiducial region.

Process	$p_{\mathrm{T}}^{H} > 450$ GeV, $\lvert y_H \rvert < 2$
All	0.24
ggF	0.26
VBF	0.22
VH	0.27
$t\bar{t}H$	0.20

TABLE X. Expected and observed values of the signal strengths for the H, Z, and $t\bar{t}$ components in the fiducial fits. The value for μ_H refers to the fiducial volume $|y_H| < 2.0$ and $p_{\mathrm{T}}^{H} > 450$ GeV, while those for μ_Z and $\mu_{t\bar{t}}$ pertain to regions of jet p_{T} above 450 GeV. Absolute cross section uncertainties are not included in the reported μ_Z and $\mu_{t\bar{t}}$ values.

Result	μ_H	μ_Z	$\mu_{t\bar{t}}$
Expected	1.0 ± 3.4	1.00 ± 0.18	1.00 ± 0.08
Observed	-0.1 ± 3.5	1.30 ± 0.22	0.75 ± 0.06

TABLE XI. Contributions to the systematic uncertainties for the measurement of the fiducial volume signal strength, defined as the signal yield relative to the SM prediction. The total uncertainty is also given for comparison.

Uncertainty Contribution	$p_{\mathrm{T}}^{H} > 450$ GeV
Total	3.5
Statistical	2.6
Systematic	2.3
Jet systematic uncertainties	2.2
Modeling and theory systems	0.8
Flavor-tagging systems	0.2

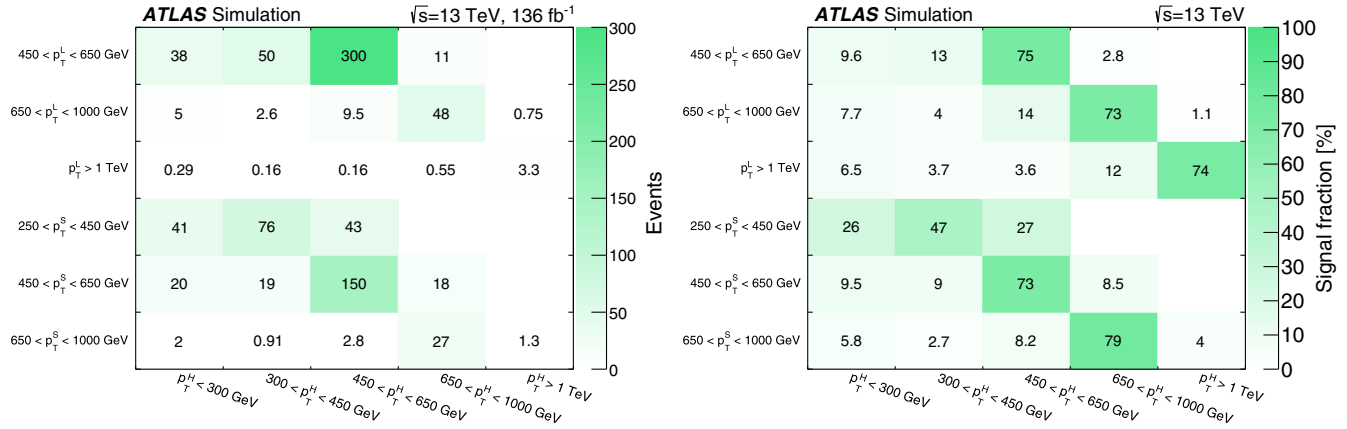

FIG. 8. For each of the p_{T}^{H} differential volumes (x-axis), the expected signal event yield for all Higgs boson events (left) and the fraction of signal in percent (right) in each reconstructed jet p_{T} region (y-axis) is shown. The leading jet's p_{T} in the SRL is denoted by $p_{\mathrm{T}}^{\mathrm{L}}$ and the subleading jet's p_{T} in the SRS is denoted by $p_{\mathrm{T}}^{\mathrm{S}}$.

effects. Half of the JMS contribution comes from the JMS uncertainty for both the $V+\mathrm{jets}$ and $t\bar{t}$ events, while the other half corresponds to the uncertainty in the JMS of reconstructed Higgs bosons. With nearly 99% purity in top-jet events, the $\mathrm{CR}_{t\bar{t}}$ data reduces the top quark jet JMR uncertainty to a relative 5%, one quarter of the original size. In $V+\mathrm{jets}$ events, the dominant JMS uncertainty's nuisance parameter is pulled by -80% of its original width, and its width is reduced by 50%. This moves the $V+\mathrm{jets}$ resonance peak position about 2 GeV. For Top events, the corresponding parameter is also constrained to 50% of its original value. No other nuisance parameters are modified significantly.

C. Differential regions

Possible deviations from the SM predictions could manifest with an amplitude increasing with p_{T}^{H}. The differential regions aim to measure the Higgs boson transverse momentum spectrum in four p_{T}^{H} volumes 300–450 GeV, 450–650 GeV, 650–1000 GeV, and greater than 1 TeV using four signal regions requiring the candidate jet p_{T} to be in the range 250–450 GeV, 450–650 GeV, 650–1000 GeV, or above 1 TeV (see Table II). Extending the procedure adopted for the fiducial region measurement, a Higgs boson mass template for each p_{T}^{H} volume is used within each jet p_{T} region in the global likelihood. The $p_{\mathrm{T}}^{H}>1$ TeV volume probes a new domain of highly boosted Z and Higgs boson reconstruction. The expected sensitivity in the SRS with jet p_{T} above 1 TeV is marginal because the muon-in-jet correction and b-tagging turn-on effects are more significant than in the SRL. Therefore, only the SRL and $\mathrm{CR}_{t\bar{t}}$ regions are included for measurements above 1 TeV. Figure 8 presents the expected signal yield in each candidate jet p_{T} region for each STXS volume and the corresponding fraction of signal events. The acceptance times efficiency values for the different Higgs boson production processes are given in Table XII.

Again, the procedure is tested with $W\to qq'$ and $Z\to qq'$ in the VR and $Z\to b\bar{b}$ in the SR with the V and Z mass templates structured similarly to those of the Higgs boson described above. Due to the larger sample size, the VRL is divided into five slices, the fit is performed independently on each slice, and the results are averaged. In the SR, the Z fit is performed in

TABLE XII. Signal acceptance times efficiency for the STXS volumes in the differential measurement. Along with the p_{T}^{H} requirements shown, $|y_H|<2$ is required. For events with $p_{\mathrm{T}}^{H}<300$ GeV, the acceptance times efficiency is less than 0.1×10^{-2}.

Process	$300<p_{\mathrm{T}}^{H}<450$ GeV	$450<p_{\mathrm{T}}^{H}<650$ GeV	$650<p_{\mathrm{T}}^{H}<1000$ GeV	$p_{\mathrm{T}}^{H}>1$ TeV
All	1.3×10^{-2}	0.23	0.31	0.23
ggF	0.7×10^{-2}	0.25	0.35	0.28
VBF	0.4×10^{-2}	0.21	0.32	0.25
VH	1.7×10^{-2}	0.26	0.30	0.20
$t\bar{t}H$	4.7×10^{-2}	0.19	0.24	0.19

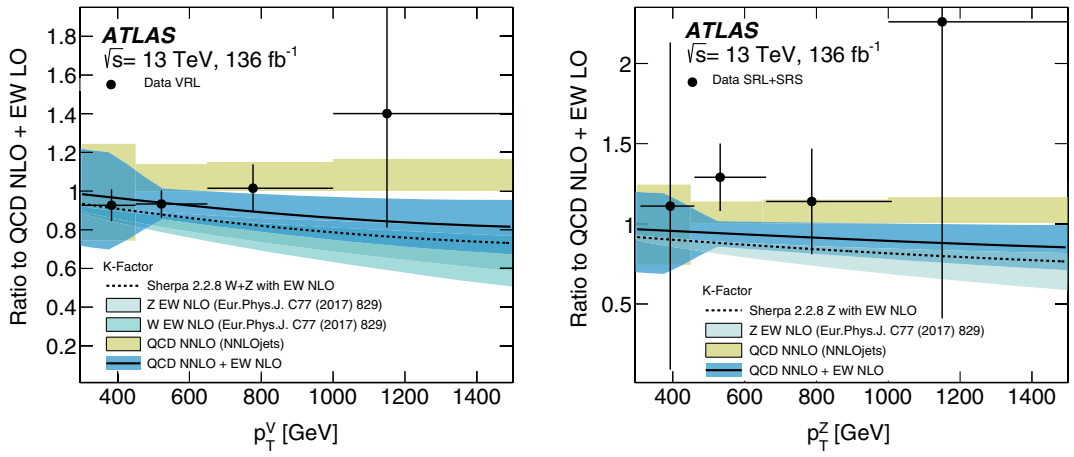

(a) V+jets in VRL (b) Z+jets in SR

FIG. 9. Comparison of differential fit signal strengths for (a) V + jets in the VRL and (b) Z + jets in the SR. The signal strength within the STXS volumes is calculated relative to the prediction at NLO QCD and LO EW accuracy. They are compared with the NLO EW correction provided by SHERPA, the NNLO QCD correction provided by the NNLOJET group, and their product. The Higgs boson yields are kept fixed to the SM expectation when extracting the Z + jets signal strength within the STXS volumes. The points are located at the weighted center of the bin considering the underlying p_{T}^{V} or p_{T}^{H} spectrum.

the SRL, SRS, and $\mathrm{CR}_{t\bar{t}}$ regions with the Higgs boson contribution fixed to the SM prediction. Again, the results do not change when using a freely floating Higgs boson normalization. Results of the two differential fits are shown in Fig. 9, where they are compared with the predictions for the EW NLO and QCD NNLO corrections as a function of reconstructed p_{T}^{V}. Both results agree with SM expectations.

To extract the four Higgs boson signal strengths within the STXS volumes, ten differential SR and CR regions defined in Table II are fitted simultaneously, exploiting the corresponding systematic uncertainty configurations shown in Table V. The results are summarized in Table XIII and Fig. 10. The $t\bar{t}$ normalization corrections determined from the data in each jet p_{T} region are compatible with $t\bar{t}$ event measurements in a similar kinematic phase-space [129]. The four Higgs boson signal strengths are compatible, with a p-value of 0.53. Post-fit jet mass distributions from the SRL are shown in Fig. 11.

The resulting Higgs boson production cross section for $p_{\mathrm{T}}^{H} > 1$ TeV is

TABLE XIII. Expected and observed values of the signal strengths for the H, Z, and $t\bar{t}$ components in the differential fits. The value for μ_H refers to a STXS volume, while those for μ_Z and $\mu_{t\bar{t}}$ pertain to the corresponding jet p_{T} regions. Absolute cross section uncertainties are not included in the reported μ_Z and $\mu_{t\bar{t}}$ values.

	μ_H	
p_{T}^{H} (GeV)	Expected	Observed
300–450	1 ± 18	-6 ± 18
450–650	1.0 ± 3.3	-3 ± 5
650–1000	1 ± 6	5 ± 7
>1000	1 ± 30	18 ± 32

	μ_Z		$\mu_{t\bar{t}}$	
Jet p_{T} (GeV)	Expected	Observed	Expected	Observed
250–450	1.0 ± 1.1	1.8 ± 1.1	1.00 ± 0.07	0.85 ± 0.06
450–650	1.00 ± 0.17	1.28 ± 0.22	1.00 ± 0.07	0.76 ± 0.06
650–1000	1.00 ± 0.33	1.4 ± 0.4	1.00 ± 0.09	0.74 ± 0.08
>1000	1.0 ± 1.6	2.4 ± 1.7	1.00 ± 0.22	0.57 ± 0.18

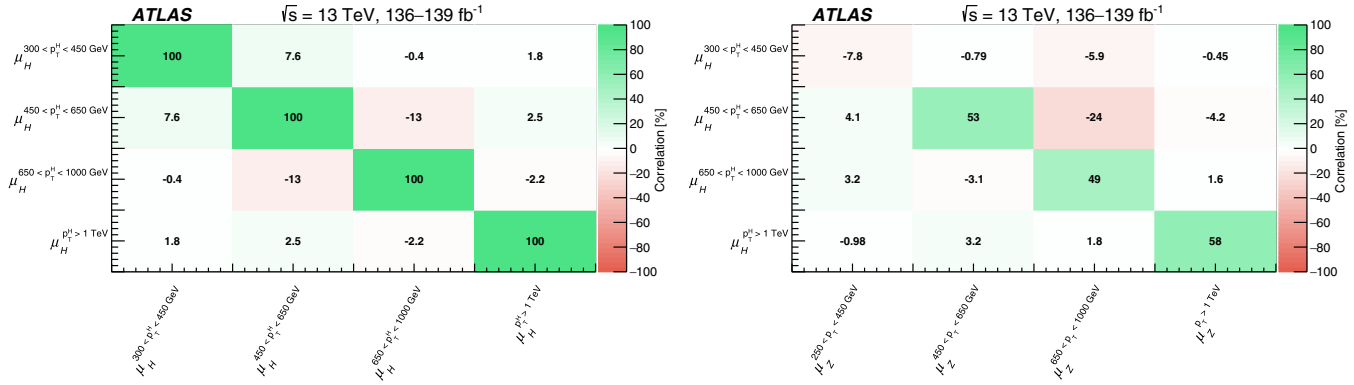

FIG. 10. Correlations among the four Higgs boson signal strengths, and between the four Higgs boson and $Z+$ jets signal strengths. The Higgs boson signal strengths μ_H are labeled with the corresponding p_{T}^H range as a superscript. The $Z+$ jets signal strengths μ_Z are labeled with the corresponding jet p_{T} range as a superscript.

$$\sigma_H(p_{\mathrm{T}}^H > 1\ \mathrm{TeV}) = 2.3 \pm 3.9(\mathrm{stat}) \pm 1.3(\mathrm{syst}) \pm 0.5(\mathrm{theory})\ \mathrm{fb}$$

and the SM prediction is 0.13 fb. The differential results correspond to the following observed (expected) 95% CL upper limits on the Higgs boson differential production cross sections:

$$\sigma_H(300 < p_{\mathrm{T}}^H < 450\ \mathrm{GeV}) < 2.9(3.1)\ \mathrm{pb},$$
$$\sigma_H(450 < p_{\mathrm{T}}^H < 650\ \mathrm{GeV}) < 89(102)\ \mathrm{fb},$$
$$\sigma_H(650 < p_{\mathrm{T}}^H < 1000\ \mathrm{GeV}) < 39(34)\ \mathrm{fb},$$
$$\sigma_H(p_{\mathrm{T}}^H > 1000\ \mathrm{GeV}) < 9.6(7.4)\ \mathrm{fb}.$$

The fitted values and upper limits of the Higgs boson signal strengths in four p_{T}^H intervals are shown in Fig. 12.

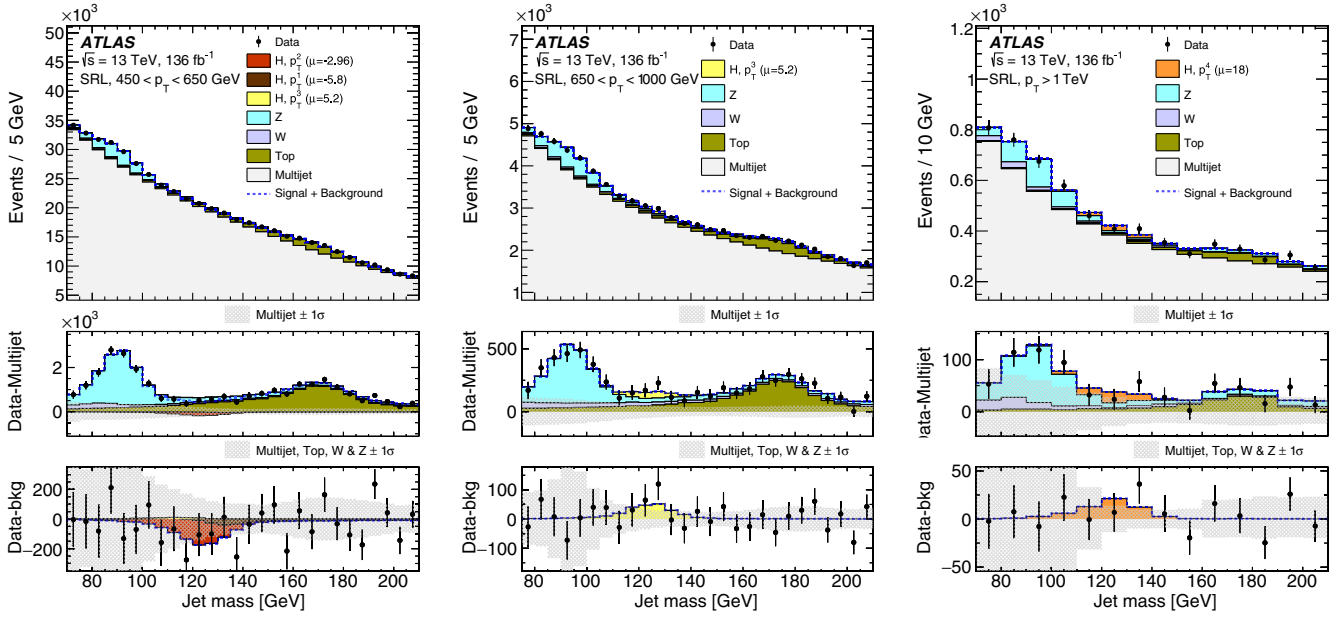

FIG. 11. Post-fit jet mass distributions of the various components in the differential leading-jet signal region defined by the selected candidate jet with $450 < p_{\mathrm{T}} < 650$ GeV (left), $650 < p_{\mathrm{T}} < 1000$ GeV (middle), and $p_{\mathrm{T}} > 1000$ GeV (right) shown in wider 10 GeV bins. The middle panels show the distributions after subtraction of the multijet distribution. The shaded areas indicate the 68% CL for the multijet background from the fitted parameters and normalizations of the exponentiated polynomials. The lower panels show the distributions after subtraction of all the fitted background processes: multijet, $V+$ jets, and Top. The shaded areas indicate the 68% CL for all background processes. The five STXS volumes are labeled p_{T}^0–p_{T}^4 corresponding to $p_{\mathrm{T}}^H < 300$ GeV, 300–450 GeV, 450–650 GeV, 650–1000 GeV, and >1000 GeV, respectively. The p_{T}^0 event yield is constrained to its SM value within the theoretical and experimental uncertainties and free parameters act independently on the remaining four volumes. Contributions below 0.5 per mille of the total yield are not shown.

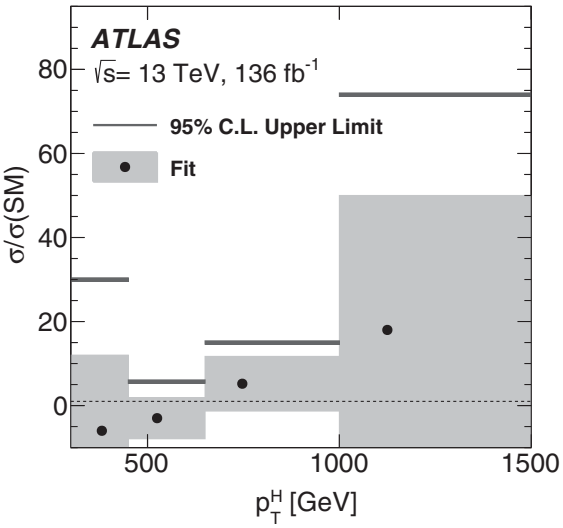

FIG. 12. Summary of the STXS volume signal strengths measured using the differential signal regions. Within the same kinematic regimes, measurements of the $Z \to b\bar{b}$ process agree with the Standard Model predictions, validating the methods. The points are located at the weighted center of the bin considering the underlying p_{T}^{H} spectrum.

The largest source of uncertainty is the data sample size. The contributions from the main sources of uncertainty are summarized in Table XIV. The jet uncertainties tend to give the largest contribution of systematic uncertainty, driven by JMS effects. The dominant JMS uncertainty component in $V+$jets events is reduced by 30%–40% separately in the three SRs with jet $p_{\mathrm{T}} > 450$ GeV. The same component is reduced by 20%–65% for Top events over the full jet p_{T} range. The JMS nuisance parameter receives small pulls that differ between $V+$jets and Top events and with p_{T}. The impact of JMR increases above 1 TeV, where the JMR measurement constraints on $V+$jets are looser due to the extrapolation uncertainties (see Fig. 5). The JMR uncertainty for jets in Top events is constrained to a relative 6%–9% (from 20%) below 1 TeV but is 18% above 1 TeV. Similarly, the flavor-tagging uncertainties increase above 1 TeV due to the extrapolation from the p_{T} range of the calibration regions. The $t\bar{t}$ modeling systematic uncertainties are more relevant in the first jet-p_{T} bin and decrease above 450 GeV, where the top quark decay products become more collimated, thus reducing the contamination around the Higgs boson mass peak. The fit reduces these systematic uncertainties by 20%–30%, driven by the purity of the $\mathrm{CR}_{t\bar{t}}$. Other than the few mentioned, no other nuisance parameter has a posterior probability very different from the prior.

X. CONCLUSIONS

High-p_{T} Higgs boson production is studied in the $b\bar{b}$ decay channel probing a new highly Lorentz-boosted boson reconstruction domain with transverse momentum above 1 TeV. The results are based on pp collision data collected at $\sqrt{s} = 13$ TeV with the ATLAS detector during Run 2 of the LHC, corresponding to an integrated luminosity of 136 fb^{-1}. The Higgs boson is reconstructed as a single large-R jet and identified with b-tagging techniques. The measured signal strengths of $W \to qq'$ and $Z \to qq'$ in the validation region and $Z \to b\bar{b}$ in the signal region agree with the SM predictions and validate the experimental techniques.

The observed (expected) 95% CL limit on the Higgs boson production cross section for $p_{\mathrm{T}}^{H} > 450$ GeV obtained from the fiducial signal region is 115 (128) fb. From the four differential signal regions, the observed (expected) 95% CL limits on the Higgs boson production cross section are:

$$\begin{aligned}
\sigma_H(300 < p_{\mathrm{T}}^{H} < 450\ \mathrm{GeV}) &< 2.9(3.1)\ \mathrm{pb},\\
\sigma_H(450 < p_{\mathrm{T}}^{H} < 650\ \mathrm{GeV}) &< 89(102)\ \mathrm{fb},\\
\sigma_H(650 < p_{\mathrm{T}}^{H} < 1000\ \mathrm{GeV}) &< 39(34)\ \mathrm{fb},\\
\sigma_H(p_{\mathrm{T}}^{H} > 1000\ \mathrm{GeV}) &< 9.6(7.4)\ \mathrm{fb}. \qquad (2)
\end{aligned}$$

The Higgs boson production cross section for $p_{\mathrm{T}}^{H} > 1$ TeV is found to be

$$\begin{aligned}
&\sigma_H(p_{\mathrm{T}}^{H} > 1\ \mathrm{TeV})\\
&\quad = 2.3 \pm 3.9(\mathrm{stat}) \pm 1.3(\mathrm{syst}) \pm 0.5(\mathrm{theory})\ \mathrm{fb}.
\end{aligned}$$

All of the Higgs boson results are consistent with the Standard Model predictions.

TABLE XIV. Contributions to the systematic uncertainties for the differential measurements of the signal strength, defined as the signal yield relative to the SM prediction within STXS volumes. The total uncertainty is also given for comparison.

Uncertainty Contribution	$300 < p_{\mathrm{T}}^{H} < 450$ GeV	$450 < p_{\mathrm{T}}^{H} < 650$ GeV	$650 < p_{\mathrm{T}}^{H} < 1000$ GeV	$p_{\mathrm{T}}^{H} > 1$ TeV
Total	18	5.0	6.5	32
Statistical	16	3.0	5.5	30
Systematic	7	3.9	3.4	10
Jet systematic uncertainties	6	3.8	3.4	9.5
Modeling and theory systs.	4	0.7	0.7	2
Flavor-tagging systs.	0.2	0.4	0.4	2

ACKNOWLEDGMENTS

We thank CERN for the very successful operation of the LHC, as well as the support staff from our institutions without whom ATLAS could not be operated efficiently. We acknowledge the support of ANPCyT, Argentina; YerPhI, Armenia; ARC, Australia; BMWFW and FWF, Austria; ANAS, Azerbaijan; SSTC, Belarus; CNPq and FAPESP, Brazil; NSERC, NRC and CFI, Canada; CERN; ANID, Chile; CAS, MOST and NSFC, China; Minciencias, Colombia; MEYS CR, Czech Republic; DNRF and DNSRC, Denmark; IN2P3-CNRS and CEA-DRF/IRFU, France; SRNSFG, Georgia; BMBF, HGF and MPG, Germany; GSRI, Greece; RGC and Hong Kong SAR, China; ISF and Benoziyo Center, Israel; INFN, Italy; MEXT and JSPS, Japan; CNRST, Morocco; NWO, Netherlands; RCN, Norway; MEiN, Poland; FCT, Portugal; MNE/IFA, Romania; JINR; MES of Russia and NRC KI, Russian Federation; MESTD, Serbia; MSSR, Slovakia; ARRS and MIZŠ, Slovenia; DSI/NRF, South Africa; MICINN, Spain; SRC and Wallenberg Foundation, Sweden; SERI, SNSF and Cantons of Bern and Geneva, Switzerland; MOST, Taiwan; TAEK, Turkey; STFC, United Kingdom; DOE and NSF, United States of America. In addition, individual groups and members have received support from BCKDF, CANARIE, Compute Canada and CRC, Canada; COST, ERC, ERDF, Horizon 2020 and Marie Skłodowska-Curie Actions, European Union; Investissements d'Avenir Labex, Investissements d'Avenir Idex and ANR, France; DFG and AvH Foundation, Germany; Herakleitos, Thales and Aristeia programmes co-financed by EU-ESF and the Greek NSRF, Greece; BSF-NSF and GIF, Israel; Norwegian Financial Mechanism 2014-2021, Norway; NCN and NAWA, Poland; La Caixa Banking Foundation, CERCA Programme Generalitat de Catalunya and PROMETEO and GenT Programmes Generalitat Valenciana, Spain; Göran Gustafssons Stiftelse, Sweden; The Royal Society and Leverhulme Trust, United Kingdom. The crucial computing support from all WLCG partners is acknowledged gratefully, in particular from CERN, the ATLAS Tier-1 facilities at TRIUMF (Canada), NDGF (Denmark, Norway, Sweden), CC-IN2P3 (France), KIT/GridKA (Germany), INFN-CNAF (Italy), NL-T1 (Netherlands), PIC (Spain), ASGC (Taiwan), RAL (UK) and BNL (USA), the Tier-2 facilities worldwide and large non-WLCG resource providers. Major contributors of computing resources are listed in Ref. [130].

[1] ATLAS Collaboration, Observation of a new particle in the search for the Standard Model Higgs boson with the ATLAS detector at the LHC, Phys. Lett. B **716**, 1 (2012).

[2] CMS Collaboration, Observation of a new boson at a mass of 125 GeV with the CMS experiment at the LHC, Phys. Lett. B **716**, 30 (2012).

[3] ATLAS Collaboration, Combined measurements of Higgs boson production and decay using up to 80 fb^{-1} of proton-proton collision data at $\sqrt{s} = 13$ TeV collected with the ATLAS experiment, Phys. Rev. D **101**, 012002 (2020).

[4] CMS Collaboration, Combined measurements of Higgs boson couplings in proton-proton collisions at $\sqrt{s} = 13$ TeV, Eur. Phys. J. C **79**, 421 (2019).

[5] D. de Florian *et al.*, Handbook of LHC Higgs cross sections: 4. Deciphering the nature of the Higgs sector, arXiv:1610.07922.

[6] J. R. Andersen *et al.*, Les Houches 2015: Physics at TeV colliders standard model working group report, *9th Les Houches Workshop on Physics at TeV Colliders (PhysTeV 2015) Les Houches, France, 2015* (2016), http://lss.fnal.gov/archive/2016/conf/fermilab-conf-16-175-ppd-t.pdf.

[7] S. Amoroso *et al.*, Les Houches 2019: Physics at TeV colliders: Standard model working group report, *11th Les Houches Workshop on Physics at TeV Colliders: PhysTeV Les Houches*, 2020, arXiv:2003.01700.

[8] R. Contino, M. Ghezzi, C. Grojean, M. Muhlleitner, and M. Spira, Effective Lagrangian for a light Higgs-like scalar, J. High Energy Phys. 07 (2013) 035.

[9] C. Grojean, E. Salvioni, M. Schlaffer, and A. Weiler, Very boosted Higgs in gluon fusion, J. High Energy Phys. 05 (2014) 022.

[10] A. Biekötter, A. Knochel, M. Krämer, D. Liu, and F. Riva, Vices and virtues of Higgs effective field theories at large energy, Phys. Rev. D **91**, 055029 (2015).

[11] K. Mimasu, V. Sanz, and C. Williams, Higher order QCD predictions for associated Higgs production with anomalous couplings to gauge bosons, J. High Energy Phys. 08 (2016) 039.

[12] M. Grazzini, A. Ilnicka, M. Spira, and M. Wiesemann, Modeling BSM effects on the Higgs transverse-momentum spectrum in an EFT approach, J. High Energy Phys. 03 (2017) 115.

[13] A. Banfi, A. Bond, A. Martin, and V. Sanz, Digging for top squarks from Higgs data: From signal strengths to differential distributions, J. High Energy Phys. 11 (2018) 171.

[14] CMS Collaboration, Inclusive search for highly boosted Higgs bosons decaying to bottom quark-antiquark pairs in proton-proton collisions at $\sqrt{s} = 13$ TeV, J. High Energy Phys. 12 (2020) 085.

[15] CMS Collaboration, Measurements of Higgs boson production cross sections and couplings in the diphoton decay channel at $\sqrt{s} = 13$ TeV, J. High Energy Phys. 07 (2021) 027.

[16] ATLAS Collaboration, Measurements of WH and ZH production in the $H \to b\bar{b}$ decay channel in pp collisions at 13 TeV with the ATLAS detector, Eur. Phys. J. C **81**, 178 (2021).
[17] ATLAS Collaboration, Measurement of the associated production of a Higgs boson decaying into b-quarks with a vector boson at high transverse momentum in pp collisions at $\sqrt{s} = 13$ TeV with the ATLAS detector, Phys. Lett. B **816**, 136204 (2021).
[18] CMS Collaboration, Observation of Higgs Boson Decay to Bottom Quarks, Phys. Rev. Lett. **121**, 121801 (2018).
[19] ATLAS Collaboration, Cross-section measurements of the Higgs boson decaying into a pair of τ-leptons in proton-proton collisions at $\sqrt{s} = 13$ TeV with the ATLAS detector, Phys. Rev. D **99**, 072001 (2019).
[20] ATLAS Collaboration, Higgs boson production cross-section measurements and their EFT interpretation in the 4ℓ decay channel at $\sqrt{s} = 13$ TeV with the ATLAS detector, Eur. Phys. J. C **80**, 957 (2020); **81**, 29(E) (2021).
[21] ATLAS Collaboration, Measurements of Higgs bosons decaying to bottom quarks from vector boson fusion production with the ATLAS experiment at $\sqrt{s} = 13$ TeV, Eur. Phys. J. C **81**, 537 (2021).
[22] CMS Collaboration, Measurements of production cross sections of the Higgs boson in the four-lepton final state in proton-proton collisions at $\sqrt{s} = 13$ TeV, Eur. Phys. J. C **81**, 488 (2021).
[23] CMS Collaboration, Search for the standard model Higgs boson produced through vector boson fusion and decaying to $b\bar{b}$, Phys. Rev. D **92**, 032008 (2015).
[24] ATLAS Collaboration, Observation of Higgs boson production in association with a top quark pair at the LHC with the ATLAS detector, Phys. Lett. B **784**, 173 (2018).
[25] CMS Collaboration, Measurement of the Higgs boson production rate in association with top quarks in final states with electrons, muons, and hadronically decaying tau leptons at $\sqrt{s} = 13$ TeV, Eur. Phys. J. C **81**, 378 (2020).
[26] K. Becker *et al.*, Precise predictions for boosted Higgs production, arXiv:2005.07762.
[27] ATLAS Collaboration, The ATLAS experiment at the CERN large hadron collider, J. Instrum. **3**, S08003 (2008).
[28] J. M. Butterworth, A. R. Davison, M. Rubin, and G. P. Salam, Jet Substructure as a New Higgs-Search Channel at the LHC, Phys. Rev. Lett. **100**, 242001 (2008).
[29] ATLAS Collaboration, Measurements of Higgs boson properties in the diphoton decay channel with 36 fb^{-1} of pp collision data at $\sqrt{s} = 13$ TeV with the ATLAS detector, Phys. Rev. D **98**, 052005 (2018).
[30] ATLAS Collaboration, Measurements of the Higgs boson inclusive and differential fiducial cross sections in the 4ℓ decay channel at $\sqrt{s} = 13$ TeV, Eur. Phys. J. C **80**, 942 (2020).
[31] CMS Collaboration, Measurement of the Higgs boson production rate in association with top quarks in final states with electrons, muons, and hadronically decaying tau leptons at $\sqrt{s} = 13$ TeV, Eur. Phys. J. C **81**, 378 (2021).
[32] ATLAS Collaboration, ATLAS insertable B-layer technical design report, Report No. ATLAS-TDR-19; Report No. CERN-LHCC-2010-013, 2010, https://cds.cern.ch/record/1291633; Addendum: Report No. ATLAS-TDR-19-ADD-1; Report No. CERN-LHCC-2012-009, 2012, https://cds.cern.ch/record/1451888.
[33] B. Abbott *et al.*, Production and integration of the ATLAS Insertable B-Layer, J. Instrum. **13**, T05008 (2018).
[34] ATLAS Collaboration, Operation of the ATLAS trigger system in Run 2, J. Instrum. **15**, P10004 (2020).
[35] ATLAS Collaboration, The ATLAS Collaboration software and firmware, Report No. ATL-SOFT-PUB-2021-001, 2021, https://cds.cern.ch/record/2767187.
[36] ATLAS Collaboration, Performance of the ATLAS trigger system in 2015, Eur. Phys. J. C **77**, 317 (2017).
[37] M. Cacciari, G. P. Salam, and G. Soyez, The anti-k_t jet clustering algorithm, J. High Energy Phys. 04 (2008) 063.
[38] ATLAS Collaboration, Performance of pile-up mitigation techniques for jets in pp collisions at $\sqrt{s} = 8$ TeV using the ATLAS detector, Eur. Phys. J. C **76**, 581 (2016).
[39] ATLAS Collaboration, Performance of the ATLAS muon triggers in Run 2, J. Instrum. **15**, P09015 (2020).
[40] ATLAS Collaboration, Luminosity determination in pp collisions at $\sqrt{s} = 13$ TeV using the ATLAS detector at the LHC, Report No. ATLAS-CONF-2019-021, 2019, https://cds.cern.ch/record/2677054.
[41] G. Avoni *et al.*, The new LUCID-2 detector for luminosity measurement and monitoring in ATLAS, J. Instrum. **13**, P07017 (2018).
[42] K. Hamilton, P. Nason, and G. Zanderighi, MINLO: Multi-scale improved NLO, J. High Energy Phys. 10 (2012) 155.
[43] J. M. Campbell, R. K. Ellis, R. Frederix, P. Nason, C. Oleari, and C. Williams, NLO Higgs boson production plus one and two jets using the POWHEG BOX, MadGraph4 and MCFM, J. High Energy Phys. 07 (2012) 092.
[44] K. Hamilton, P. Nason, C. Oleari, and G. Zanderighi, Merging $H/W/Z + 0$ and 1 jet at NLO with no merging scale: A path to parton shower + NNLO matching, J. High Energy Phys. 05 (2013) 082.
[45] S. Alioli, P. Nason, C. Oleari, and E. Re, A general framework for implementing NLO calculations in shower Monte Carlo programs: the POWHEG BOX, J. High Energy Phys. 06 (2010) 043.
[46] P. Nason, A new method for combining NLO QCD with shower Monte Carlo algorithms, J. High Energy Phys. 11 (2004) 040.
[47] S. Frixione, P. Nason, and C. Oleari, Matching NLO QCD computations with Parton Shower simulations: The POWHEG method, J. High Energy Phys. 11 (2007) 070.
[48] K. Hamilton, P. Nason, and G. Zanderighi, Finite quark-mass effects in the NNLOPS POWHEG + MiNLO Higgs generator, J. High Energy Phys. 05 (2015) 140.
[49] P. Nason and C. Oleari, NLO Higgs boson production via vector-boson fusion matched with shower in POWHEG, J. High Energy Phys. 02 (2010) 037.
[50] H. B. Hartanto, B. Jäger, L. Reina, and D. Wackeroth, Higgs boson production in association with top quarks in the POWHEG BOX, Phys. Rev. D **91**, 094003 (2015).
[51] G. Luisoni, P. Nason, C. Oleari, and F. Tramontano, $HW^{\pm}/HZ + 0$ and 1 jet at NLO with the POWHEG BOX interfaced to GoSam and their merging within MiNLO, J. High Energy Phys. 10 (2013) 083.

[52] G.Cullen, N. Greiner, G. Heinrich, G. Luisoni, P. Mastrolia, G. Ossola, T. Reiter, and F. Tramontano, Automated one-loop calculations with GoSam, Eur. Phys. J. C **72**, 1889 (2012).

[53] A. Djouadi, J. Kalinowski, and M. Spira, HDECAY: A program for Higgs boson decays in the Standard Model and its supersymmetric extension, Comput. Phys. Commun. **108**, 56 (1998).

[54] M. Spira, QCD Effects in Higgs Physics, Fortschr. Phys. **46**, 203 (1998).

[55] A. Djouadi, M. M. Mühlleitner, and M. Spira, Decays of supersymmetric particles: The program SUSY-HIT (SUspect-SdecaY-Hdecay-InTerface), Acta Phys. Pol. B **38**, 635 (2007).

[56] A. Bredenstein, A. Denner, S. Dittmaier, and M. M. Weber, Radiative corrections to the semileptonic and hadronic Higgs-boson decays $H \to WW/ZZ \to 4$ fermions, J. High Energy Phys. 02 (2007) 080.

[57] A. Bredenstein, A. Denner, S. Dittmaier, and M. M. Weber, Precise predictions for the Higgs-boson decay $H \to WW/ZZ \to 4$ leptons, Phys. Rev. D **74**, 013004 (2006).

[58] A. Bredenstein, A. Denner, S. Dittmaier, and M. M. Weber, Precision calculations for the Higgs decays $H \to ZZ/WW \to 4$ leptons, Nucl. Phys. B, Proc. Suppl. **160**, 131 (2006).

[59] E. Bothmann *et al.*, Event generation with Sherpa 2.2, SciPost Phys. **7**, 034 (2019).

[60] U. Blumenschein *et al.*, Pushing the precision frontier at the LHC with V + jets, arXiv:1802.02100.

[61] A. Gehrmann-De Ridder, T. Gehrmann, E. W. N. Glover, A. Huss, and T. A. Morgan, Precise QCD Predictions for the Production of a Z Boson in Association with a Hadronic Jet, Phys. Rev. Lett. **117**, 022001 (2016).

[62] A. Gehrmann-De Ridder, T. Gehrmann, E. W. N. Glover, A. Huss, and T. A. Morgan, The NNLO QCD corrections to Z boson production at large transverse momentum, J. High Energy Phys. 07 (2016) 133, We thank Nigel Glover and Alexander Huss for providing $\sqrt{s} = 13$ TeV corrections for the analysis fiducial volume.

[63] S. Frixione, P. Nason, and G. Ridolfi, A Positive-weight next-to-leading-order Monte Carlo for heavy flavour hadroproduction, J. High Energy Phys. 09 (2007) 126.

[64] E. Re, Single-top Wt-channel production matched with parton showers using the POWHEG method, Eur. Phys. J. C **71**, 1547 (2011).

[65] R. Frederix, E. Re, and P. Torrielli, Single-top t-channel hadroproduction in the four-flavour scheme with POWHEG and aMC@NLO, J. High Energy Phys. 09 (2012) 130.

[66] S. Alioli, P. Nason, C. Oleari, and E. Re, NLO single-top production matched with shower in POWHEG: s- and t-channel contributions, J. High Energy Phys. 09 (2009) 111; 02 (2010) 011(E).

[67] S. Frixione, E. Laenen, P. Motylinski, C. White, and B. R. Webber, Single-top hadroproduction in association with a W boson, J. High Energy Phys. 07 (2008) 029.

[68] T. Sjöstrand, S. Ask, J. R. Christiansen, R. Corke, N. Desai, P. Ilten, S. Mrenna, S. Prestel, C. O. Rasmussen, and P. Z. Skands, An introduction to PYTHIA 8.2, Comput. Phys. Commun. **191**, 159 (2015).

[69] ATLAS Collaboration, The ATLAS simulation infrastructure, Eur. Phys. J. C **70**, 823 (2010).

[70] S. Agostinelli *et al.* (GEANT4 Collaboration), Geant4—a simulation toolkit, Nucl. Instrum. Methods Phys. Res., Sect. A **506**, 250 (2003).

[71] R. D. Ball, V. Bertone, S. Carrazza, C. S. Deans, L. D. Debbio, S. Forte, A. Guffanti, N. P. Hartland, J. I. Latorre, J. Rojo, and M. Ubiali, Parton distributions with LHC data, Nucl. Phys. **B867**, 244 (2013).

[72] ATLAS Collaboration, The Pythia 8 A3 tune description of ATLAS minimum bias and inelastic measurements incorporating the Donnachie-Landshoff diffractive model, Report No. ATL-PHYS-PUB-2016-017, 2016, https://cds.cern.ch/record/2206965.

[73] D. J. Lange, The EvtGen particle decay simulation package, Nucl. Instrum. Methods Phys. Res., Sect. A **462**, 152 (2001).

[74] ATLAS Collaboration, ATLAS simulation of boson plus jets processes in Run 2, Report No. ATL-PHYS-PUB-2017-006, 2017, https://cds.cern.ch/record/2261937.

[75] ATLAS Collaboration, Studies on top-quark Monte Carlo modelling for Top2016, Report No. ATL-PHYS-PUB-2016-020, 2016, https://cds.cern.ch/record/2216168.

[76] ATLAS Collaboration, Simulation of top-quark production for the ATLAS experiment at $\sqrt{s} = 13$ TeV, Report No. ATL-PHYS-PUB-2016-004, 2016, https://cds.cern.ch/record/2120417.

[77] ATLAS Collaboration, Studies on top-quark Monte Carlo modelling with Sherpa and MG5_aMC@NLO, Report No. ATL-PHYS-PUB-2017-007, 2017, https://cds.cern.ch/record/2261938.

[78] ATLAS Collaboration, Improvements in $t\bar{t}$ modelling using NLO + PS Monte Carlo generators for Run 2, Report No. ATL-PHYS-PUB-2018-009, 2018, https://cds.cern.ch/record/2630327.

[79] ATLAS Collaboration, Multijet simulation for 13 TeV ATLAS analyses, Report No. ATL-PHYS-PUB-2019-017, 2019, https://cds.cern.ch/record/2672252.

[80] A. Denner, S. Dittmaier, S. Kallweit, and A. Muck, Electroweak corrections to Higgs-strahlung off W/Z bosons at the Tevatron and the LHC with HAWK, J. High Energy Phys. 03 (2012) 075.

[81] A. Denner, S. Dittmaier, S. Kallweit, and A. Mück, HAWK 2.0: A Monte Carlo program for Higgs production in vector-boson fusion and Higgs strahlung at hadron colliders, Comput. Phys. Commun. **195**, 161 (2015).

[82] F. Buccioni, J.-N. Lang, J. M. Lindert, P. Maierhöfer, S. Pozzorini, H. Zhang, and M. F. Zoller, OpenLoops 2, Eur. Phys. J. C **79**, 866 (2019).

[83] F. Cascioli, P. Maierhöfer, and S. Pozzorini, Scattering Amplitudes with Open Loops, Phys. Rev. Lett. **108**, 111601 (2012).

[84] A. Denner, S. Dittmaier, and L. Hofer, Collier: A fortran-based complex one-loop library in extended regularizations, Comput. Phys. Commun. **212**, 220 (2017).

[85] R. D. Ball, V. Bertone, S. Carrazza, C. S. Deans, L. D. Debbio, S. Forte, A. Guffanti, N. P. Hartland, J. I. Latorre, J. Rojo, and M. Ubiali, Parton distributions for the LHC run II, J. High Energy Phys. 04 (2015) 040.

[86] ATLAS Collaboration, Measurement of the Z/γ^* boson transverse momentum distribution in pp collisions at $\sqrt{s} = 7$ TeV with the ATLAS detector, J. High Energy Phys. 09 (2014) 145.
[87] T. Gleisberg, S. Höche, F. Krauss, M. Schönherr, S. Schumann, F. Siegert, and J. Winter, Event generation with SHERPA 1.1, J. High Energy Phys. 02 (2009) 007.
[88] T. Gleisberg and S. Höche, Comix, a new matrix element generator, J. High Energy Phys. 12 (2008) 039.
[89] S. Schumann and F. Krauss, A parton shower algorithm based on Catani-Seymour dipole factorisation, J. High Energy Phys. 03 (2008) 038.
[90] S. Höche, F. Krauss, M. Schönherr, and F. Siegert, QCD matrix elements + parton showers. The NLO case, J. High Energy Phys. 04 (2013) 027.
[91] S. Catani, L. Cieri, G. Ferrera, D. de Florian, and M. Grazzini, Vector Boson Production at Hadron Colliders: A Fully Exclusive QCD Calculation at Next-to-Next-to-Leading Order, Phys. Rev. Lett. **103**, 082001 (2009).
[92] S. Kallweit, J. M. Lindert, P. Maierhöfer, S. Pozzorini, and M. Schönherr, NLO electroweak automation and precise predictions for $W +$ multijet production at the LHC, J. High Energy Phys. 04 (**2015**) 012.
[93] B. Biedermann, S. Bräuer, A. Denner, M. Pellen, S. Schumann, and J. M. Thompson, Automation of NLO QCD and EW corrections with Sherpa and Recola, Eur. Phys. J. C **77**, 492 (2017).
[94] ATLAS Collaboration, ATLAS Pythia 8 tunes to 7 TeV data, Report No. ATL-PHYS-PUB-2014-021, 2014, https://cds.cern.ch/record/1966419.
[95] M. Czakon and A. Mitov, Top++: A program for the calculation of the top-pair cross-section at hadron colliders, Comput. Phys. Commun. **185**, 2930 (2014).
[96] ATLAS Collaboration, Early inner detector tracking performance in the 2015 Data at $\sqrt{s} = 13$ TeV, Report No. ATL-PHYS-PUB-2015-051, 2015, https://cds.cern.ch/record/2110140.
[97] ATLAS Collaboration, Reconstruction of primary vertices at the ATLAS experiment in Run 1 proton-proton collisions at the LHC, Eur. Phys. J. C **77**, 332 (2017).
[98] M. Cacciari, G. P. Salam, and G. Soyez, FastJet user manual, Eur. Phys. J. C **72**, 1896 (2012).
[99] ATLAS Collaboration, Topological cell clustering in the ATLAS calorimeters and its performance in LHC Run 1, Eur. Phys. J. C **77**, 490 (2017).
[100] ATLAS Collaboration, Selection of jets produced in 13 TeV proton-proton collisions with the ATLAS detector, Report No. ATLAS-CONF-2015-029, 2015, https://cds.cern.ch/record/2037702.
[101] D. Krohn, J. Thaler, and L.-T. Wang, Jet trimming, J. High Energy Phys. 02 (2010) 084.
[102] S. D. Ellis and D. E. Soper, Successive combination jet algorithm for hadron collisions, Phys. Rev. D **48**, 3160 (1993).
[103] ATLAS Collaboration, In situ calibration of large-radius jet energy and mass in 13 TeV proton-proton collisions with the ATLAS detector, Eur. Phys. J. C **79**, 135 (2019).
[104] D. Krohn, J. Thaler, and L.-T. Wang, Jets with variable R, J. High Energy Phys. 06 (2009) 059.
[105] ATLAS Collaboration, Variable radius, exclusive-k_T, and center-of-mass subjet reconstruction for Higgs($\to b\bar{b}$) tagging in ATLAS, Report No. ATL-PHYS-PUB-2017-010, 2017, https://cds.cern.ch/record/2268678.
[106] M. Cacciari, G. P. Salam, and G. Soyez, The catchment area of jets, J. High Energy Phys. 04 (2008) 005.
[107] M. Cacciari and G. P. Salam, Pileup subtraction using jet areas, Phys. Lett. B **659**, 119 (2008).
[108] ATLAS Collaboration, ATLAS b-jet identification performance and efficiency measurement with $t\bar{t}$ events in pp collisions at $\sqrt{s} = 13$ TeV, Eur. Phys. J. C **79**, 970 (2019).
[109] ATLAS Collaboration, Identification of boosted Higgs bosons decaying into b-quark pairs with the ATLAS detector at 13 TeV, Eur. Phys. J. C **79**, 836 (2019).
[110] ATLAS Collaboration, Muon reconstruction and identification efficiency in ATLAS using the full Run 2 pp collision data set at $\sqrt{s} = 13$ TeV, Eur. Phys. J. C **81**, 578 (2021).
[111] ATLAS Collaboration, Muon reconstruction performance of the ATLAS detector in proton-proton collision data at $\sqrt{s} = 13$ TeV, Eur. Phys. J. C **76**, 292 (2016).
[112] ATLAS Collaboration, Jet mass and substructure of inclusive jets in $\sqrt{s} = 7$ TeV pp collisions with the ATLAS experiment, J. High Energy Phys. 05 (2012) 128.
[113] ATLAS Collaboration, Jet mass reconstruction with the ATLAS detector in early Run 2 data, Report No. ATLAS-CONF-2016-035, 2016, https://cds.cern.ch/record/2200211.
[114] ATLAS Collaboration, Measurement of b-tagging efficiency of c-jets in $t\bar{t}$ events using a likelihood approach with the ATLAS detector, Report No. ATLAS-CONF-2018-001, 2018, https://cds.cern.ch/record/2306649.
[115] ATLAS Collaboration, Calibration of light-flavour b-jet mistagging rates using ATLAS proton-proton collision data at $\sqrt{s} = 13$ TeV, Report No. ATLAS-CONF-2018-006, 2018, https://cds.cern.ch/record/2314418.
[116] ATLAS Collaboration, Simulation-based extrapolation of b-tagging calibrations towards high transverse momenta in the ATLAS experiment, Report No. ATL-PHYS-PUB-2021-003, 2021, https://cds.cern.ch/record/2753444.
[117] ATLAS Collaboration, Identification of boosted Higgs bosons decaying into $b\bar{b}$ with neural networks and variable radius subjets in ATLAS, Report No. ATL-PHYS-PUB-2020-019, 2020, https://cds.cern.ch/record/2724739.
[118] ATLAS Collaboration, b-tagging in dense environments, Report No. ATL-PHYS-PUB-2014-014, 2014, https://cds.cern.ch/record/1750682.
[119] J. M. Lindert, K. Kudashkin, K. Melnikov, and C. Wever, Higgs bosons with large transverse momentum at the LHC, Phys. Lett. B **782**, 210 (2018).
[120] J. Lindert *et al.*, Precise predictions for $V +$ jets dark matter backgrounds, Eur. Phys. J. C **77**, 829 (2017).
[121] T. Sjöstrand, Jet fragmentation of multiparton configurations in a string framework, Nucl. Phys. **B248**, 469 (1984).
[122] L. Moneta, K. Belasco, K. S. Cranmer, S. Kreiss, A. Lazzaro *et al.*, The RooStats project, Proc. Sci. ACAT2010 (**2010**) 057.

[123] W. Verkerke and D. Kirkby, The RooFit toolkit for data modeling, arXiv:physics/0306116.
[124] V. V. Gligorov, S. Hageboeck, T. Nanut, A. Sciandra, and D. Y. Tou, Avoiding biases in binned fits, J. Instrum. **16**, T08004 (2021).
[125] T. Junk, Confidence level computation for combining searches with small statistics, Nucl. Instrum. Methods Phys. Res., Sect. A **434**, 435 (1999).
[126] A. L. Read, Presentation of search results: The CL_S technique, J. Phys. G **28**, 2693 (2002).
[127] R. J. Barlow and C. Beeston, Fitting using finite Monte Carlo samples, Comput. Phys. Commun. **77**, 219 (1993).
[128] ATLAS Collaboration, Constraints on Higgs-bosons production with large transverse momentum using the $H \to b\bar{b}$ decay with the ATLAS detector. HEPData. (2021), https://www.hepdata.net/record/102183.
[129] ATLAS Collaboration, Measurements of top-quark pair differential and double-differential cross-sections in the ℓ + jets channel with pp collisions at $\sqrt{s} = 13$ TeV using the ATLAS detector, Eur. Phys. J. C **79**, 1028 (2019); **80**, 1092(E) (2020).
[130] ATLAS Collaboration, ATLAS Computing Acknowledgements, Report No. ATL-SOFT-PUB-2021-003, https://cds.cern.ch/record/2776662.

G. Aad,[98] B. Abbott,[124] D. C. Abbott,[99] A. Abed Abud,[34] K. Abeling,[51] D. K. Abhayasinghe,[91] S. H. Abidi,[27] A. Aboulhorma,[33e] H. Abramowicz,[157] H. Abreu,[156] Y. Abulaiti,[5] A. C. Abusleme Hoffman,[142a] B. S. Acharya,[64a,64b,b] B. Achkar,[51] L. Adam,[96] C. Adam Bourdarios,[4] L. Adamczyk,[81a] L. Adamek,[162] S. V. Addepalli,[24] J. Adelman,[116] A. Adiguzel,[11c,c] S. Adorni,[52] T. Adye,[139] A. A. Affolder,[141] Y. Afik,[34] C. Agapopoulou,[62] M. N. Agaras,[12] J. Agarwala,[68a,68b] A. Aggarwal,[114] C. Agheorghiesei,[25c] J. A. Aguilar-Saavedra,[135f,135a,d] A. Ahmad,[34] F. Ahmadov,[77] W. S. Ahmed,[100] X. Ai,[44] G. Aielli,[71a,71b] I. Aizenberg,[175] S. Akatsuka,[83] M. Akbiyik,[96] T. P. A. Åkesson,[94] A. V. Akimov,[107] K. Al Khoury,[37] G. L. Alberghi,[21b] J. Albert,[171] P. Albicocco,[49] M. J. Alconada Verzini,[86] S. Alderweireldt,[48] M. Aleksa,[34] I. N. Aleksandrov,[77] C. Alexa,[25b] T. Alexopoulos,[9] A. Alfonsi,[115] F. Alfonsi,[21b] M. Alhroob,[124] B. Ali,[137] S. Ali,[154] M. Aliev,[161] G. Alimonti,[66a] C. Allaire,[34] B. M. M. Allbrooke,[152] P. P. Allport,[19] A. Aloisio,[67a,67b] F. Alonso,[86] C. Alpigiani,[144] E. Alunno Camelia,[71a,71b] M. Alvarez Estevez,[95] M. G. Alviggi,[67a,67b] Y. Amaral Coutinho,[78b] A. Ambler,[100] L. Ambroz,[130] C. Amelung,[34] D. Amidei,[102] S. P. Amor Dos Santos,[135a] S. Amoroso,[44] K. R. Amos,[169] C. S. Amrouche,[52] V. Ananiev,[129] C. Anastopoulos,[145] N. Andari,[140] T. Andeen,[10] J. K. Anders,[18] S. Y. Andrean,[43a,43b] A. Andreazza,[66a,66b] S. Angelidakis,[8] A. Angerami,[37] A. V. Anisenkov,[117b,117a] A. Annovi,[69a] C. Antel,[52] M. T. Anthony,[145] E. Antipov,[125] M. Antonelli,[49] D. J. A. Antrim,[16] F. Anulli,[70a] M. Aoki,[79] J. A. Aparisi Pozo,[169] M. A. Aparo,[152] L. Aperio Bella,[44] N. Aranzabal,[34] V. Araujo Ferraz,[78a] C. Arcangeletti,[49] A. T. H. Arce,[47] E. Arena,[88] J-F. Arguin,[106] S. Argyropoulos,[50] J.-H. Arling,[44] A. J. Armbruster,[34] A. Armstrong,[166] O. Arnaez,[162] H. Arnold,[34] Z. P. Arrubarrena Tame,[110] G. Artoni,[130] H. Asada,[112] K. Asai,[122] S. Asai,[159] N. A. Asbah,[57] E. M. Asimakopoulou,[167] L. Asquith,[152] J. Assahsah,[33d] K. Assamagan,[27] R. Astalos,[26a] R. J. Atkin,[31a] M. Atkinson,[168] N. B. Atlay,[17] H. Atmani,[58b] P. A. Atmasiddha,[102] K. Augsten,[137] S. Auricchio,[67a,67b] V. A. Austrup,[177] G. Avner,[156] G. Avolio,[34] M. K. Ayoub,[13c] G. Azuelos,[106,e] D. Babal,[26a] H. Bachacou,[140] K. Bachas,[158] A. Bachiu,[32] F. Backman,[43a,43b] A. Badea,[57] P. Bagnaia,[70a,70b] H. Bahrasemani,[148] A. J. Bailey,[169] V. R. Bailey,[168] J. T. Baines,[139] C. Bakalis,[9] O. K. Baker,[178] P. J. Bakker,[115] E. Bakos,[14] D. Bakshi Gupta,[7] S. Balaji,[153] R. Balasubramanian,[115] E. M. Baldin,[117b,117a] P. Balek,[138] E. Ballabene,[66a,66b] F. Balli,[140] L. M. Baltes,[59a] W. K. Balunas,[130] J. Balz,[96] E. Banas,[82] M. Bandieramonte,[134] A. Bandyopadhyay,[22] S. Bansal,[22] L. Barak,[157] E. L. Barberio,[101] D. Barberis,[53b,53a] M. Barbero,[98] G. Barbour,[92] K. N. Barends,[31a] T. Barillari,[111] M-S. Barisits,[34] J. Barkeloo,[127] T. Barklow,[149] B. M. Barnett,[139] R. M. Barnett,[16] A. Baroncelli,[58a] G. Barone,[27] A. J. Barr,[130] L. Barranco Navarro,[43a,43b] F. Barreiro,[95] J. Barreiro Guimarães da Costa,[13a] U. Barron,[157] S. Barsov,[133] F. Bartels,[59a] R. Bartoldus,[149] G. Bartolini,[98] A. E. Barton,[87] P. Bartos,[26a] A. Basalaev,[44] A. Basan,[96] M. Baselga,[44] I. Bashta,[72a,72b] A. Bassalat,[62,f] M. J. Basso,[162] C. R. Basson,[97] R. L. Bates,[55] S. Batlamous,[33e] J. R. Batley,[30] B. Batool,[147] M. Battaglia,[141] M. Bauce,[70a,70b] F. Bauer,[140,a] P. Bauer,[22] H. S. Bawa,[29] A. Bayirli,[11c] J. B. Beacham,[47] T. Beau,[131] P. H. Beauchemin,[165] F. Becherer,[50] P. Bechtle,[22] H. P. Beck,[18,g] K. Becker,[173] C. Becot,[44] A. J. Beddall,[11c] V. A. Bednyakov,[77] C. P. Bee,[151] T. A. Beermann,[34] M. Begalli,[78b] M. Begel,[27] A. Behera,[151] J. K. Behr,[44] C. Beirao Da Cruz E Silva,[34] J. F. Beirer,[51,34] F. Beisiegel,[22] M. Belfkir,[4] G. Bella,[157] L. Bellagamba,[21b] A. Bellerive,[32] P. Bellos,[19] K. Beloborodov,[117b,117a] K. Belotskiy,[108] N. L. Belyaev,[108] D. Benchekroun,[33a] Y. Benhammou,[157] D. P. Benjamin,[27] M. Benoit,[27] J. R. Bensinger,[24] S. Bentvelsen,[115] L. Beresford,[34] M. Beretta,[49] D. Berge,[17] E. Bergeaas Kuutmann,[167] N. Berger,[4] B. Bergmann,[137] L. J. Bergsten,[24] J. Beringer,[16] S. Berlendis,[6] G. Bernardi,[131] C. Bernius,[149] F. U. Bernlochner,[22] T. Berry,[91] P. Berta,[138] A. Berthold,[46] I. A. Bertram,[87] O. Bessidskaia Bylund,[177] S. Bethke,[111] A. Betti,[40] A. J. Bevan,[90] S. Bhatta,[151]

D. S. Bhattacharya,[172] P. Bhattarai,[24] V. S. Bhopatkar,[5] R. Bi,[134] R. Bi,[27] R. M. Bianchi,[134] O. Biebel,[110] R. Bielski,[127] N. V. Biesuz,[69a,69b] M. Biglietti,[72a] T. R. V. Billoud,[137] M. Bindi,[51] A. Bingul,[11d] C. Bini,[70a,70b] S. Biondi,[21b,21a] A. Biondini,[88] C. J. Birch-sykes,[97] G. A. Bird,[19,139] M. Birman,[175] T. Bisanz,[34] J. P. Biswal,[2] D. Biswas,[176,h] A. Bitadze,[97] C. Bittrich,[46] K. Bjørke,[129] I. Bloch,[44] C. Blocker,[24] A. Blue,[55] U. Blumenschein,[90] J. Blumenthal,[96] G. J. Bobbink,[115] V. S. Bobrovnikov,[117b,117a] M. Boehler,[50] D. Bogavac,[12] A. G. Bogdanchikov,[117b,117a] C. Bohm,[43a] V. Boisvert,[91] P. Bokan,[44] T. Bold,[81a] M. Bomben,[131] M. Bona,[90] M. Boonekamp,[140] C. D. Booth,[91] A. G. Borbély,[55] H. M. Borecka-Bielska,[106] L. S. Borgna,[92] G. Borissov,[87] D. Bortoletto,[130] D. Boscherini,[21b] M. Bosman,[12] J. D. Bossio Sola,[34] K. Bouaouda,[33a] J. Boudreau,[134] E. V. Bouhova-Thacker,[87] D. Boumediene,[36] R. Bouquet,[131] A. Boveia,[123] J. Boyd,[34] D. Boye,[27] I. R. Boyko,[77] A. J. Bozson,[91] J. Bracinik,[19] N. Brahimi,[58d,58c] G. Brandt,[177] O. Brandt,[30] F. Braren,[44] B. Brau,[99] J. E. Brau,[127] W. D. Breaden Madden,[55] K. Brendlinger,[44] R. Brener,[175] L. Brenner,[34] R. Brenner,[167] S. Bressler,[175] B. Brickwedde,[96] D. Britton,[55] D. Britzger,[111] I. Brock,[22] R. Brock,[103] G. Brooijmans,[37] W. K. Brooks,[142e] E. Brost,[27] P. A. Bruckman de Renstrom,[82] B. Brüers,[44] D. Bruncko,[26b] A. Bruni,[21b] G. Bruni,[21b] M. Bruschi,[21b] N. Bruscino,[70a,70b] L. Bryngemark,[149] T. Buanes,[15] Q. Buat,[151] P. Buchholz,[147] A. G. Buckley,[55] I. A. Budagov,[77] M. K. Bugge,[129] O. Bulekov,[108] B. A. Bullard,[57] S. Burdin,[88] C. D. Burgard,[44] A. M. Burger,[125] B. Burghgrave,[7] J. T. P. Burr,[30] C. D. Burton,[10] J. C. Burzynski,[148] E. L. Busch,[37] V. Büscher,[96] P. J. Bussey,[55] J. M. Butler,[23] C. M. Buttar,[55] J. M. Butterworth,[92] W. Buttinger,[139] C. J. Buxo Vazquez,[103] A. R. Buzykaev,[117b,117a] G. Cabras,[21b] S. Cabrera Urbán,[169] D. Caforio,[54] H. Cai,[134] V. M. M. Cairo,[149] O. Cakir,[3a] N. Calace,[34] P. Calafiura,[16] G. Calderini,[131] P. Calfayan,[63] G. Callea,[55] L. P. Caloba,[78b] D. Calvet,[36] S. Calvet,[36] T. P. Calvet,[98] M. Calvetti,[69a,69b] R. Camacho Toro,[131] S. Camarda,[34] D. Camarero Munoz,[95] P. Camarri,[71a,71b] M. T. Camerlingo,[72a,72b] D. Cameron,[129] C. Camincher,[171] M. Campanelli,[92] A. Camplani,[38] V. Canale,[67a,67b] A. Canesse,[100] M. Cano Bret,[75] J. Cantero,[125] Y. Cao,[168] F. Capocasa,[24] M. Capua,[39b,39a] A. Carbone,[66a,66b] R. Cardarelli,[71a] J. C. J. Cardenas,[7] F. Cardillo,[169] G. Carducci,[39b,39a] T. Carli,[34] G. Carlino,[67a] B. T. Carlson,[134] E. M. Carlson,[171,163a] L. Carminati,[66a,66b] M. Carnesale,[70a,70b] R. M. D. Carney,[149] S. Caron,[114] E. Carquin,[142e] S. Carrá,[44] G. Carratta,[21b,21a] J. W. S. Carter,[162] T. M. Carter,[48] D. Casadei,[31c] M. P. Casado,[12,i] A. F. Casha,[162] E. G. Castiglia,[178] F. L. Castillo,[59a] L. Castillo Garcia,[12] V. Castillo Gimenez,[169] N. F. Castro,[135a,135e] A. Catinaccio,[34] J. R. Catmore,[129] A. Cattai,[34] V. Cavaliere,[27] N. Cavalli,[21b,21a] V. Cavasinni,[69a,69b] E. Celebi,[11c] F. Celli,[130] M. S. Centonze,[65a,65b] K. Cerny,[126] A. S. Cerqueira,[78a] A. Cerri,[152] L. Cerrito,[71a,71b] F. Cerutti,[16] A. Cervelli,[21b] S. A. Cetin,[11b,j] Z. Chadi,[33a] D. Chakraborty,[116] M. Chala,[135f] J. Chan,[176] W. S. Chan,[115] W. Y. Chan,[88] J. D. Chapman,[30] B. Chargeishvili,[155b] D. G. Charlton,[19] T. P. Charman,[90] M. Chatterjee,[18] S. Chekanov,[5] S. V. Chekulaev,[163a] G. A. Chelkov,[77,k] A. Chen,[102] B. Chen,[157] B. Chen,[171] C. Chen,[58a] C. H. Chen,[76] H. Chen,[13c] H. Chen,[27] J. Chen,[58c] J. Chen,[24] S. Chen,[132] S. J. Chen,[13c] X. Chen,[58c] X. Chen,[13b] Y. Chen,[58a] Y-H. Chen,[44] C. L. Cheng,[176] H. C. Cheng,[60a] A. Cheplakov,[77] E. Cheremushkina,[44] E. Cherepanova,[77] R. Cherkaoui El Moursli,[33e] E. Cheu,[6] K. Cheung,[61] L. Chevalier,[140] V. Chiarella,[49] G. Chiarelli,[69a] G. Chiodini,[65a] A. S. Chisholm,[19] A. Chitan,[25b] Y. H. Chiu,[171] M. V. Chizhov,[77] K. Choi,[10] A. R. Chomont,[70a,70b] Y. Chou,[99] Y. S. Chow,[115] T. Chowdhury,[31f] L. D. Christopher,[31f] M. C. Chu,[60a] X. Chu,[13a,13d] J. Chudoba,[136] J. J. Chwastowski,[82] D. Cieri,[111] K. M. Ciesla,[82] V. Cindro,[89] I. A. Cioară,[25b] A. Ciocio,[16] F. Cirotto,[67a,67b] Z. H. Citron,[175,l] M. Citterio,[66a] D. A. Ciubotaru,[25b] B. M. Ciungu,[162] A. Clark,[52] P. J. Clark,[48] J. M. Clavijo Columbie,[44] S. E. Clawson,[97] C. Clement,[43a,43b] L. Clissa,[21b,21a] Y. Coadou,[98] M. Cobal,[64a,64c] A. Coccaro,[53b] J. Cochran,[76] R. F. Coelho Barrue,[135a] R. Coelho Lopes De Sa,[99] S. Coelli,[66a] H. Cohen,[157] A. E. C. Coimbra,[34] B. Cole,[37] J. Collot,[56] P. Conde Muiño,[135a,135g] S. H. Connell,[31c] I. A. Connelly,[55] E. I. Conroy,[130] F. Conventi,[67a,m] H. G. Cooke,[19] A. M. Cooper-Sarkar,[130] F. Cormier,[170] L. D. Corpe,[34] M. Corradi,[70a,70b] E. E. Corrigan,[94] F. Corriveau,[100,n] M. J. Costa,[169] F. Costanza,[4] D. Costanzo,[145] B. M. Cote,[123] G. Cowan,[91] J. W. Cowley,[30] K. Cranmer,[121] S. Crépé-Renaudin,[56] F. Crescioli,[131] M. Cristinziani,[147] M. Cristoforetti,[73a,73b,o] V. Croft,[165] G. Crosetti,[39b,39a] A. Cueto,[34] T. Cuhadar Donszelmann,[166] H. Cui,[13a,13d] Z. Cui,[6] A. R. Cukierman,[149] W. R. Cunningham,[55] F. Curcio,[39b,39a] P. Czodrowski,[34] M. M. Czurylo,[59b] M. J. Da Cunha Sargedas De Sousa,[58a] J. V. Da Fonseca Pinto,[78b] C. Da Via,[97] W. Dabrowski,[81a] T. Dado,[45] S. Dahbi,[31f] T. Dai,[102] C. Dallapiccola,[99] M. Dam,[38] G. D'amen,[27] V. D'Amico,[72a,72b] J. Damp,[96] J. R. Dandoy,[132] M. F. Daneri,[28] M. Danninger,[148] V. Dao,[34] G. Darbo,[53b] S. Darmora,[5] A. Dattagupta,[127] S. D'Auria,[66a,66b] C. David,[163b] T. Davidek,[138] D. R. Davis,[47] B. Davis-Purcell,[32] I. Dawson,[90] K. De,[7] R. De Asmundis,[67a] M. De Beurs,[115] S. De Castro,[21b,21a] N. De Groot,[114] P. de Jong,[115] H. De la Torre,[103] A. De Maria,[13c] D. De Pedis,[70a] A. De Salvo,[70a] U. De Sanctis,[71a,71b] M. De Santis,[71a,71b] A. De Santo,[152] J. B. De Vivie De Regie,[56] D. V. Dedovich,[77] J. Degens,[115] A. M. Deiana,[40] J. Del Peso,[95] Y. Delabat Diaz,[44] F. Deliot,[140] C. M. Delitzsch,[6] M. Della Pietra,[67a,67b]

D. Della Volpe,[52] A. Dell'Acqua,[34] L. Dell'Asta,[66a,66b] M. Delmastro,[4] P. A. Delsart,[56] S. Demers,[178] M. Demichev,[77] S. P. Denisov,[118] L. D'Eramo,[116] D. Derendarz,[82] J. E. Derkaoui,[33d] F. Derue,[131] P. Dervan,[88] K. Desch,[22] K. Dette,[162] C. Deutsch,[22] P. O. Deviveiros,[34] F. A. Di Bello,[70a,70b] A. Di Ciaccio,[71a,71b] L. Di Ciaccio,[4] A. Di Domenico,[70a,70b] C. Di Donato,[67a,67b] A. Di Girolamo,[34] G. Di Gregorio,[69a,69b] A. Di Luca,[73a,73b,o] B. Di Micco,[72a,72b] R. Di Nardo,[72a,72b] C. Diaconu,[98] F. A. Dias,[115] T. Dias Do Vale,[135a] M. A. Diaz,[142a] F. G. Diaz Capriles,[22] J. Dickinson,[16] M. Didenko,[169] E. B. Diehl,[102] J. Dietrich,[17] S. Díez Cornell,[44] C. Diez Pardos,[147] C. Dimitriadi,[167,22] A. Dimitrievska,[16] W. Ding,[13b] J. Dingfelder,[22] I-M. Dinu,[25b] S. J. Dittmeier,[59b] F. Dittus,[34] F. Djama,[98] T. Djobava,[155b] J. I. Djuvsland,[15] M. A. B. Do Vale,[143] D. Dodsworth,[24] C. Doglioni,[94] J. Dolejsi,[138] Z. Dolezal,[138] M. Donadelli,[78c] B. Dong,[58c] J. Donini,[36] A. D'onofrio,[13c] M. D'Onofrio,[88] J. Dopke,[139] A. Doria,[67a] M. T. Dova,[86] A. T. Doyle,[55] E. Drechsler,[148] E. Dreyer,[175] T. Dreyer,[51] A. S. Drobac,[165] D. Du,[58a] T. A. du Pree,[115] F. Dubinin,[107] M. Dubovsky,[26a] A. Dubreuil,[52] E. Duchovni,[175] G. Duckeck,[110] O. A. Ducu,[34,25b] D. Duda,[111] A. Dudarev,[34] M. D'uffizi,[97] L. Duflot,[62] M. Dührssen,[34] C. Dülsen,[177] A. E. Dumitriu,[25b] M. Dunford,[59a] S. Dungs,[45] K. Dunne,[43a,43b] A. Duperrin,[98] H. Duran Yildiz,[3a] M. Düren,[54] A. Durglishvili,[155b] B. Dutta,[44] B. L. Dwyer,[116] G. I. Dyckes,[16] M. Dyndal,[81a] S. Dysch,[97] B. S. Dziedzic,[82] B. Eckerova,[26a] M. G. Eggleston,[47] E. Egidio Purcino De Souza,[78b] L. F. Ehrke,[52] G. Eigen,[15] K. Einsweiler,[16] T. Ekelof,[167] Y. El Ghazali,[33b] H. El Jarrari,[33e] A. El Moussaouy,[33a] V. Ellajosyula,[167] M. Ellert,[167] F. Ellinghaus,[177] A. A. Elliot,[90] N. Ellis,[34] J. Elmsheuser,[27] M. Elsing,[34] D. Emeliyanov,[139] A. Emerman,[37] Y. Enari,[159] J. Erdmann,[45] A. Ereditato,[18] P. A. Erland,[82] M. Errenst,[177] M. Escalier,[62] C. Escobar,[169] O. Estrada Pastor,[169] E. Etzion,[157] G. Evans,[135a] H. Evans,[63] M. O. Evans,[152] A. Ezhilov,[133] S. Ezzarqtouni,[33a] F. Fabbri,[55] L. Fabbri,[21b,21a] G. Facini,[173] V. Fadeyev,[141] R. M. Fakhrutdinov,[118] S. Falciano,[70a] P. J. Falke,[22] S. Falke,[34] J. Faltova,[138] Y. Fan,[13a] Y. Fang,[13a] G. Fanourakis,[42] M. Fanti,[66a,66b] M. Faraj,[58c] A. Farbin,[7] A. Farilla,[72a] E. M. Farina,[68a,68b] T. Farooque,[103] S. M. Farrington,[48] P. Farthouat,[34] F. Fassi,[33e] D. Fassouliotis,[8] M. Faucci Giannelli,[71a,71b] W. J. Fawcett,[30] L. Fayard,[62] O. L. Fedin,[133,p] G. Fedotov,[133] M. Feickert,[168] L. Feligioni,[98] A. Fell,[145] C. Feng,[58b] M. Feng,[13b] M. J. Fenton,[166] A. B. Fenyuk,[118] S. W. Ferguson,[41] J. Ferrando,[44] A. Ferrari,[167] P. Ferrari,[115] R. Ferrari,[68a] D. Ferrere,[52] C. Ferretti,[102] F. Fiedler,[96] A. Filipčič,[89] F. Filthaut,[114] M. C. N. Fiolhais,[135a,135c,q] L. Fiorini,[169] F. Fischer,[147] W. C. Fisher,[103] T. Fitschen,[19] I. Fleck,[147] P. Fleischmann,[102] T. Flick,[177] B. M. Flierl,[110] L. Flores,[132] M. Flores,[31d] L. R. Flores Castillo,[60a] F. M. Follega,[73a,73b] N. Fomin,[15] J. H. Foo,[162] B. C. Forland,[63] A. Formica,[140] F. A. Förster,[12] A. C. Forti,[97] E. Fortin,[98] M. G. Foti,[130] L. Fountas,[8] D. Fournier,[62] H. Fox,[87] P. Francavilla,[69a,69b] S. Francescato,[57] M. Franchini,[21b,21a] S. Franchino,[59a] D. Francis,[34] L. Franco,[4] L. Franconi,[18] M. Franklin,[57] G. Frattari,[70a,70b] A. C. Freegard,[90] P. M. Freeman,[19] W. S. Freund,[78b] E. M. Freundlich,[45] D. Froidevaux,[34] J. A. Frost,[130] Y. Fu,[58a] M. Fujimoto,[122] E. Fullana Torregrosa,[169] J. Fuster,[169] A. Gabrielli,[21b,21a] A. Gabrielli,[34] P. Gadow,[44] G. Gagliardi,[53b,53a] L. G. Gagnon,[16] G. E. Gallardo,[130] E. J. Gallas,[130] B. J. Gallop,[139] R. Gamboa Goni,[90] K. K. Gan,[123] S. Ganguly,[159] J. Gao,[58a] Y. Gao,[48] Y. S. Gao,[29,r] F. M. Garay Walls,[142a] C. García,[169] J. E. García Navarro,[169] J. A. García Pascual,[13a] M. Garcia-Sciveres,[16] R. W. Gardner,[35] D. Garg,[75] R. B. Garg,[149] S. Gargiulo,[50] C. A. Garner,[162] V. Garonne,[27] S. J. Gasiorowski,[144] P. Gaspar,[78b] G. Gaudio,[68a] P. Gauzzi,[70a,70b] I. L. Gavrilenko,[107] A. Gavrilyuk,[119] C. Gay,[170] G. Gaycken,[44] E. N. Gazis,[9] A. A. Geanta,[25b] C. M. Gee,[141] C. N. P. Gee,[139] J. Geisen,[94] M. Geisen,[96] C. Gemme,[53b] M. H. Genest,[56] S. Gentile,[70a,70b] S. George,[91] W. F. George,[19] T. Geralis,[42] L. O. Gerlach,[51] P. Gessinger-Befurt,[34] M. Ghasemi Bostanabad,[171] A. Ghosh,[166] A. Ghosh,[6] B. Giacobbe,[21b] S. Giagu,[70a,70b] N. Giangiacomi,[162] P. Giannetti,[69a] A. Giannini,[67a,67b] S. M. Gibson,[91] M. Gignac,[141] D. T. Gil,[81b] B. J. Gilbert,[37] D. Gillberg,[32] G. Gilles,[115] N. E. K. Gillwald,[44] D. M. Gingrich,[2,e] M. P. Giordani,[64a,64c] P. F. Giraud,[140] G. Giugliarelli,[64a,64c] D. Giugni,[66a] F. Giuli,[71a,71b] I. Gkialas,[8,s] P. Gkountoumis,[9] L. K. Gladilin,[109] C. Glasman,[95] G. R. Gledhill,[127] M. Glisic,[127] I. Gnesi,[39b,t] Y. Go,[27] M. Goblirsch-Kolb,[24] D. Godin,[106] S. Goldfarb,[101] T. Golling,[52] D. Golubkov,[118] J. P. Gombas,[103] A. Gomes,[135a,135b] R. Goncalves Gama,[51] R. Gonçalo,[135a,135c] G. Gonella,[127] L. Gonella,[19] A. Gongadze,[77] F. Gonnella,[19] J. L. Gonski,[37] S. González de la Hoz,[169] S. Gonzalez Fernandez,[12] R. Gonzalez Lopez,[88] C. Gonzalez Renteria,[16] R. Gonzalez Suarez,[167] S. Gonzalez-Sevilla,[52] G. R. Gonzalvo Rodriguez,[169] R. Y. González Andana,[142a] L. Goossens,[34] N. A. Gorasia,[19] P. A. Gorbounov,[119] H. A. Gordon,[27] B. Gorini,[34] E. Gorini,[65a,65b] A. Gorišek,[89] A. T. Goshaw,[47] M. I. Gostkin,[77] C. A. Gottardo,[114] M. Gouighri,[33b] V. Goumarre,[44] A. G. Goussiou,[144] N. Govender,[31c] C. Goy,[4] I. Grabowska-Bold,[81a] K. Graham,[32] E. Gramstad,[129] S. Grancagnolo,[17] M. Grandi,[152] V. Gratchev,[133] P. M. Gravila,[25f] F. G. Gravili,[65a,65b] H. M. Gray,[16] C. Grefe,[22] I. M. Gregor,[44] P. Grenier,[149] K. Grevtsov,[44] C. Grieco,[12] N. A. Grieser,[124] A. A. Grillo,[141] K. Grimm,[29,u] S. Grinstein,[12,v] J.-F. Grivaz,[62] S. Groh,[96] E. Gross,[175] J. Grosse-Knetter,[51] C. Grud,[102] A. Grummer,[113] J. C. Grundy,[130] L. Guan,[102] W. Guan,[176] C. Gubbels,[170] J. G. R. Guerrero Rojas,[169] F. Guescini,[111]

D. Guest,[17] R. Gugel,[96] A. Guida,[44] T. Guillemin,[4] S. Guindon,[34] F. Guo,[13a] J. Guo,[58c] L. Guo,[62] Y. Guo,[102] R. Gupta,[44] S. Gurbuz,[22] G. Gustavino,[124] M. Guth,[52] P. Gutierrez,[124] L. F. Gutierrez Zagazeta,[132] C. Gutschow,[92] C. Guyot,[140] C. Gwenlan,[130] C. B. Gwilliam,[88] E. S. Haaland,[129] A. Haas,[121] M. Habedank,[44] C. Haber,[16] H. K. Hadavand,[7] A. Hadef,[96] S. Hadzic,[111] M. Haleem,[172] J. Haley,[125] J. J. Hall,[145] G. Halladjian,[103] G. D. Hallewell,[98] L. Halser,[18] K. Hamano,[171] H. Hamdaoui,[33e] M. Hamer,[22] G. N. Hamity,[48] K. Han,[58a] L. Han,[13c] L. Han,[58a] S. Han,[16] Y. F. Han,[162] K. Hanagaki,[79,w] M. Hance,[141] M. D. Hank,[35] R. Hankache,[97] E. Hansen,[94] J. B. Hansen,[38] J. D. Hansen,[38] M. C. Hansen,[22] P. H. Hansen,[38] K. Hara,[164] T. Harenberg,[177] S. Harkusha,[104] Y. T. Harris,[130] P. F. Harrison,[173] N. M. Hartman,[149] N. M. Hartmann,[110] Y. Hasegawa,[146] A. Hasib,[48] S. Hassani,[140] S. Haug,[18] R. Hauser,[103] M. Havranek,[137] C. M. Hawkes,[19] R. J. Hawkings,[34] S. Hayashida,[112] D. Hayden,[103] C. Hayes,[102] R. L. Hayes,[170] C. P. Hays,[130] J. M. Hays,[90] H. S. Hayward,[88] S. J. Haywood,[139] F. He,[58a] Y. He,[160] Y. He,[131] M. P. Heath,[48] V. Hedberg,[94] A. L. Heggelund,[129] N. D. Hehir,[90] C. Heidegger,[50] K. K. Heidegger,[50] W. D. Heidorn,[76] J. Heilman,[32] S. Heim,[44] T. Heim,[16] B. Heinemann,[44,x] J. G. Heinlein,[132] J. J. Heinrich,[127] L. Heinrich,[34] J. Hejbal,[136] L. Helary,[44] A. Held,[121] C. M. Helling,[141] S. Hellman,[43a,43b] C. Helsens,[34] R. C. W. Henderson,[87] L. Henkelmann,[30] A. M. Henriques Correia,[34] H. Herde,[149] Y. Hernández Jiménez,[151] H. Herr,[96] M. G. Herrmann,[110] T. Herrmann,[46] G. Herten,[50] R. Hertenberger,[110] L. Hervas,[34] N. P. Hessey,[163a] H. Hibi,[80] S. Higashino,[79] E. Higón-Rodriguez,[169] K. H. Hiller,[44] S. J. Hillier,[19] M. Hils,[46] I. Hinchliffe,[16] F. Hinterkeuser,[22] M. Hirose,[128] S. Hirose,[164] D. Hirschbuehl,[177] B. Hiti,[89] O. Hladik,[136] J. Hobbs,[151] R. Hobincu,[25e] N. Hod,[175] M. C. Hodgkinson,[145] B. H. Hodkinson,[30] A. Hoecker,[34] J. Hofer,[44] D. Hohn,[50] T. Holm,[22] M. Holzbock,[111] L. B. A. H. Hommels,[30] B. P. Honan,[97] J. Hong,[58c] T. M. Hong,[134] Y. Hong,[51] J. C. Honig,[50] A. Hönle,[111] B. H. Hooberman,[168] W. H. Hopkins,[5] Y. Horii,[112] L. A. Horyn,[35] S. Hou,[154] J. Howarth,[55] J. Hoya,[86] M. Hrabovsky,[126] A. Hrynevich,[105] T. Hryn'ova,[4] P. J. Hsu,[61] S.-C. Hsu,[144] Q. Hu,[37] S. Hu,[58c] Y. F. Hu,[13a,13d,y] D. P. Huang,[92] X. Huang,[13c] Y. Huang,[58a] Y. Huang,[13a] Z. Hubacek,[137] F. Hubaut,[98] M. Huebner,[22] F. Huegging,[22] T. B. Huffman,[130] M. Huhtinen,[34] S. K. Huiberts,[15] R. Hulsken,[56] N. Huseynov,[77,z] J. Huston,[103] J. Huth,[57] R. Hyneman,[149] S. Hyrych,[26a] G. Iacobucci,[52] G. Iakovidis,[27] I. Ibragimov,[147] L. Iconomidou-Fayard,[62] P. Iengo,[34] R. Iguchi,[159] T. Iizawa,[52] Y. Ikegami,[79] A. Ilg,[18] N. Ilic,[162] H. Imam,[33a] T. Ingebretsen Carlson,[43a,43b] G. Introzzi,[68a,68b] M. Iodice,[72a] V. Ippolito,[70a,70b] M. Ishino,[159] W. Islam,[176] C. Issever,[17,44] S. Istin,[11c,aa] J. M. Iturbe Ponce,[60a] R. Iuppa,[73a,73b] A. Ivina,[175] J. M. Izen,[41] V. Izzo,[67a] P. Jacka,[136] P. Jackson,[1] R. M. Jacobs,[44] B. P. Jaeger,[148] C. S. Jagfeld,[110] G. Jäkel,[177] K. Jakobs,[50] T. Jakoubek,[175] J. Jamieson,[55] K. W. Janas,[81a] G. Jarlskog,[94] A. E. Jaspan,[88] T. Javůrek,[34] M. Javurkova,[99] F. Jeanneau,[140] L. Jeanty,[127] J. Jejelava,[155a,bb] P. Jenni,[50,cc] S. Jézéquel,[4] J. Jia,[151] Z. Jia,[13c] Y. Jiang,[58a] S. Jiggins,[48] J. Jimenez Pena,[111] S. Jin,[13c] A. Jinaru,[25b] O. Jinnouchi,[160] H. Jivan,[31f] P. Johansson,[145] K. A. Johns,[6] C. A. Johnson,[63] D. M. Jones,[30] E. Jones,[173] R. W. L. Jones,[87] T. J. Jones,[88] J. Jovicevic,[14] X. Ju,[16] J. J. Junggeburth,[34] A. Juste Rozas,[12,v] S. Kabana,[142d] A. Kaczmarska,[82] M. Kado,[70a,70b] H. Kagan,[123] M. Kagan,[149] A. Kahn,[37] A. Kahn,[132] C. Kahra,[96] T. Kaji,[174] E. Kajomovitz,[156] C. W. Kalderon,[27] A. Kamenshchikov,[118] M. Kaneda,[159] N. J. Kang,[141] Y. Kano,[112] D. Kar,[31f] K. Karava,[130] M. J. Kareem,[163b] I. Karkanias,[158] S. N. Karpov,[77] Z. M. Karpova,[77] V. Kartvelishvili,[87] A. N. Karyukhin,[118] E. Kasimi,[158] C. Kato,[58d] J. Katzy,[44] S. Kaur,[32] K. Kawade,[146] K. Kawagoe,[85] T. Kawaguchi,[112] T. Kawamoto,[140] G. Kawamura,[51] E. F. Kay,[171] F. I. Kaya,[165] S. Kazakos,[12] V. F. Kazanin,[117b,117a] Y. Ke,[151] J. M. Keaveney,[31a] R. Keeler,[171] J. S. Keller,[32] A. S. Kelly,[92] D. Kelsey,[152] J. J. Kempster,[19] J. Kendrick,[19] K. E. Kennedy,[37] O. Kepka,[136] S. Kersten,[177] B. P. Kerševan,[89] S. Ketabchi Haghighat,[162] M. Khandoga,[131] A. Khanov,[125] A. G. Kharlamov,[117b,117a] T. Kharlamova,[117b,117a] E. E. Khoda,[144] T. J. Khoo,[17] G. Khoriauli,[172] E. Khramov,[77] J. Khubua,[155b] S. Kido,[80] M. Kiehn,[34] A. Kilgallon,[127] E. Kim,[160] Y. K. Kim,[35] N. Kimura,[92] A. Kirchhoff,[51] D. Kirchmeier,[46] C. Kirfel,[22] J. Kirk,[139] A. E. Kiryunin,[111] T. Kishimoto,[159] D. P. Kisliuk,[162] C. Kitsaki,[9] O. Kivernyk,[22] T. Klapdor-Kleingrothaus,[50] M. Klassen,[59a] C. Klein,[32] L. Klein,[172] M. H. Klein,[102] M. Klein,[88] U. Klein,[88] P. Klimek,[34] A. Klimentov,[27] F. Klimpel,[111] T. Klingl,[22] T. Klioutchnikova,[34] F. F. Klitzner,[110] P. Kluit,[115] S. Kluth,[111] E. Kneringer,[74] T. M. Knight,[162] A. Knue,[50] D. Kobayashi,[85] R. Kobayashi,[83] M. Kocian,[149] T. Kodama,[159] P. Kodys,[138] D. M. Koeck,[152] P. T. Koenig,[22] T. Koffas,[32] N. M. Köhler,[34] M. Kolb,[140] I. Koletsou,[4] T. Komarek,[126] K. Köneke,[50] A. X. Y. Kong,[1] T. Kono,[122] V. Konstantinides,[92] N. Konstantinidis,[92] B. Konya,[94] R. Kopeliansky,[63] S. Koperny,[81a] K. Korcyl,[82] K. Kordas,[158] G. Koren,[157] A. Korn,[92] S. Korn,[51] I. Korolkov,[12] E. V. Korolkova,[145] N. Korotkova,[109] B. Kortman,[115] O. Kortner,[111] S. Kortner,[111] W. H. Kostecka,[116] V. V. Kostyukhin,[147,161] A. Kotsokechagia,[62] A. Kotwal,[47] A. Koulouris,[34] A. Kourkoumeli-Charalampidi,[68a,68b] C. Kourkoumelis,[8] E. Kourlitis,[5] O. Kovanda,[152] R. Kowalewski,[171] W. Kozanecki,[140] A. S. Kozhin,[118] V. A. Kramarenko,[109] G. Kramberger,[89] P. Kramer,[96] D. Krasnopevtsev,[58a] M. W. Krasny,[131] A. Krasznahorkay,[34] J. A. Kremer,[96] J. Kretzschmar,[88] K. Kreul,[17] P. Krieger,[162] F. Krieter,[110] S. Krishnamurthy,[99] A. Krishnan,[59b] M. Krivos,[138] K. Krizka,[16] K. Kroeninger,[45]

H. Kroha,[111] J. Kroll,[136] J. Kroll,[132] K. S. Krowpman,[103] U. Kruchonak,[77] H. Krüger,[22] N. Krumnack,[76] M. C. Kruse,[47] J. A. Krzysiak,[82] A. Kubota,[160] O. Kuchinskaia,[161] S. Kuday,[3a] D. Kuechler,[44] J. T. Kuechler,[44] S. Kuehn,[34] T. Kuhl,[44] V. Kukhtin,[77] Y. Kulchitsky,[104,dd] S. Kuleshov,[142c] M. Kumar,[31f] N. Kumari,[98] M. Kuna,[56] A. Kupco,[136] T. Kupfer,[45] O. Kuprash,[50] H. Kurashige,[80] L. L. Kurchaninov,[163a] Y. A. Kurochkin,[104] A. Kurova,[108] M. G. Kurth,[13a,13d] E. S. Kuwertz,[34] M. Kuze,[160] A. K. Kvam,[144] J. Kvita,[126] T. Kwan,[100] K. W. Kwok,[60a] C. Lacasta,[169] F. Lacava,[70a,70b] H. Lacker,[17] D. Lacour,[131] N. N. Lad,[92] E. Ladygin,[77] R. Lafaye,[4] B. Laforge,[131] T. Lagouri,[142d] S. Lai,[51] I. K. Lakomiec,[81a] N. Lalloue,[56] J. E. Lambert,[124] S. Lammers,[63] W. Lampl,[6] C. Lampoudis,[158] E. Lançon,[27] U. Landgraf,[50] M. P. J. Landon,[90] V. S. Lang,[50] J. C. Lange,[51] R. J. Langenberg,[99] A. J. Lankford,[166] F. Lanni,[27] K. Lantzsch,[22] A. Lanza,[68a] A. Lapertosa,[53b,53a] J. F. Laporte,[140] T. Lari,[66a] F. Lasagni Manghi,[21b] M. Lassnig,[34] V. Latonova,[136] T. S. Lau,[60a] A. Laudrain,[96] A. Laurier,[32] M. Lavorgna,[67a,67b] S. D. Lawlor,[91] Z. Lawrence,[97] M. Lazzaroni,[66a,66b] B. Le,[97] B. Leban,[89] A. Lebedev,[76] M. LeBlanc,[34] T. LeCompte,[5] F. Ledroit-Guillon,[56] A. C. A. Lee,[92] G. R. Lee,[15] L. Lee,[57] S. C. Lee,[154] S. Lee,[76] L. L. Leeuw,[31c] B. Lefebvre,[163a] H. P. Lefebvre,[91] M. Lefebvre,[171] C. Leggett,[16] K. Lehmann,[148] N. Lehmann,[18] G. Lehmann Miotto,[34] W. A. Leight,[44] A. Leisos,[158,ee] M. A. L. Leite,[78c] C. E. Leitgeb,[44] R. Leitner,[138] K. J. C. Leney,[40] T. Lenz,[22] S. Leone,[69a] C. Leonidopoulos,[48] A. Leopold,[150] C. Leroy,[106] R. Les,[103] C. G. Lester,[30] M. Levchenko,[133] J. Levêque,[4] D. Levin,[102] L. J. Levinson,[175] D. J. Lewis,[19] B. Li,[13b] B. Li,[58b] C. Li,[58a] C-Q. Li,[58c,58d] H. Li,[58a] H. Li,[58b] H. Li,[58b] J. Li,[58c] K. Li,[144] L. Li,[58c] M. Li,[13a,13d] Q. Y. Li,[58a] S. Li,[58d,58c,ff] T. Li,[58b] X. Li,[44] Y. Li,[44] Z. Li,[58b] Z. Li,[130] Z. Li,[100] Z. Li,[88] Z. Liang,[13a] M. Liberatore,[44] B. Liberti,[71a] K. Lie,[60c] J. Lieber Marin,[78b] K. Lin,[103] R. A. Linck,[63] R. E. Lindley,[6] J. H. Lindon,[2] A. Linss,[44] E. Lipeles,[132] A. Lipniacka,[15] T. M. Liss,[168,gg] A. Lister,[170] J. D. Little,[7] B. Liu,[13a] B. X. Liu,[148] D. Liu,[58d,58c] J. B. Liu,[58a] J. K. K. Liu,[35] K. Liu,[58d,58c] M. Liu,[58a] M. Y. Liu,[58a] P. Liu,[13a] Q. Liu,[58d,144,58c] X. Liu,[58a] Y. Liu,[44] Y. Liu,[13c,13d] Y. L. Liu,[102] Y. W. Liu,[58a] M. Livan,[68a,68b] J. Llorente Merino,[148] S. L. Lloyd,[90] E. M. Lobodzinska,[44] P. Loch,[6] S. Loffredo,[71a,71b] T. Lohse,[17] K. Lohwasser,[145] M. Lokajicek,[136] J. D. Long,[168] I. Longarini,[70a,70b] L. Longo,[34] R. Longo,[168] I. Lopez Paz,[34] A. Lopez Solis,[44] J. Lorenz,[110] N. Lorenzo Martinez,[4] A. M. Lory,[110] A. Lösle,[50] X. Lou,[43a,43b] X. Lou,[13a] A. Lounis,[62] J. Love,[5] P. A. Love,[87] J. J. Lozano Bahilo,[169] G. Lu,[13a] M. Lu,[58a] S. Lu,[132] Y. J. Lu,[61] H. J. Lubatti,[144] C. Luci,[70a,70b] F. L. Lucio Alves,[13c] A. Lucotte,[56] F. Luehring,[63] I. Luise,[151] L. Luminari,[70a] O. Lundberg,[150] B. Lund-Jensen,[150] N. A. Luongo,[127] M. S. Lutz,[157] D. Lynn,[27] H. Lyons,[88] R. Lysak,[136] E. Lytken,[94] F. Lyu,[13a] V. Lyubushkin,[77] T. Lyubushkina,[77] H. Ma,[27] L. L. Ma,[58b] Y. Ma,[92] D. M. Mac Donell,[171] G. Maccarrone,[49] C. M. Macdonald,[145] J. C. MacDonald,[145] R. Madar,[36] W. F. Mader,[46] M. Madugoda Ralalage Don,[125] N. Madysa,[46] J. Maeda,[80] T. Maeno,[27] M. Maerker,[46] V. Magerl,[50] J. Magro,[64a,64c] D. J. Mahon,[37] C. Maidantchik,[78b] A. Maio,[135a,135b,135d] K. Maj,[81a] O. Majersky,[26a] S. Majewski,[127] N. Makovec,[62] V. Maksimovic,[14] B. Malaescu,[131] Pa. Malecki,[82] V. P. Maleev,[133] F. Malek,[56] D. Malito,[39b,39a] U. Mallik,[75] C. Malone,[30] S. Maltezos,[9] S. Malyukov,[77] J. Mamuzic,[169] G. Mancini,[49] J. P. Mandalia,[90] I. Mandić,[89] L. Manhaes de Andrade Filho,[78a] I. M. Maniatis,[158] M. Manisha,[140] J. Manjarres Ramos,[46] K. H. Mankinen,[94] A. Mann,[110] A. Manousos,[74] B. Mansoulie,[140] I. Manthos,[158] S. Manzoni,[115] A. Marantis,[158,ee] G. Marchiori,[131] M. Marcisovsky,[136] L. Marcoccia,[71a,71b] C. Marcon,[94] M. Marjanovic,[124] Z. Marshall,[16] S. Marti-Garcia,[169] T. A. Martin,[173] V. J. Martin,[48] B. Martin dit Latour,[15] L. Martinelli,[70a,70b] M. Martinez,[12,v] P. Martinez Agullo,[169] V. I. Martinez Outschoorn,[99] S. Martin-Haugh,[139] V. S. Martoiu,[25b] A. C. Martyniuk,[92] A. Marzin,[34] S. R. Maschek,[111] L. Masetti,[96] T. Mashimo,[159] J. Masik,[97] A. L. Maslennikov,[117b,117a] L. Massa,[21b] P. Massarotti,[67a,67b] P. Mastrandrea,[69a,69b] A. Mastroberardino,[39b,39a] T. Masubuchi,[159] D. Matakias,[27] T. Mathisen,[167] A. Matic,[110] N. Matsuzawa,[159] J. Maurer,[25b] B. Maček,[89] D. A. Maximov,[117b,117a] R. Mazini,[154] I. Maznas,[158] S. M. Mazza,[141] C. Mc Ginn,[27] J. P. Mc Gowan,[100] S. P. Mc Kee,[102] T. G. McCarthy,[111] W. P. McCormack,[16] E. F. McDonald,[101] A. E. McDougall,[115] J. A. Mcfayden,[152] G. Mchedlidze,[155b] M. A. McKay,[40] D. J. Mclaughlin,[92] K. D. McLean,[171] S. J. McMahon,[139] P. C. McNamara,[101] R. A. McPherson,[171,n] J. E. Mdhluli,[31f] Z. A. Meadows,[99] S. Meehan,[34] T. Megy,[36] S. Mehlhase,[110] A. Mehta,[88] B. Meirose,[41] D. Melini,[156] B. R. Mellado Garcia,[31f] A. H. Melo,[51] F. Meloni,[44] A. Melzer,[22] E. D. Mendes Gouveia,[135a] A. M. Mendes Jacques Da Costa,[19] H. Y. Meng,[162] L. Meng,[34] S. Menke,[111] M. Mentink,[34] E. Meoni,[39b,39a] C. Merlassino,[130] P. Mermod,[52,a] L. Merola,[67a,67b] C. Meroni,[66a] G. Merz,[102] O. Meshkov,[107,109] J. K. R. Meshreki,[147] J. Metcalfe,[5] A. S. Mete,[5] C. Meyer,[63] J-P. Meyer,[140] M. Michetti,[17] R. P. Middleton,[139] L. Mijović,[48] G. Mikenberg,[175] M. Mikestikova,[136] M. Mikuž,[89] H. Mildner,[145] A. Milic,[162] C. D. Milke,[40] D. W. Miller,[35] L. S. Miller,[32] A. Milov,[175] D. A. Milstead,[43a,43b] T. Min,[13c] A. A. Minaenko,[118] I. A. Minashvili,[155b] L. Mince,[55] A. I. Mincer,[121] B. Mindur,[81a] M. Mineev,[77] Y. Minegishi,[159] Y. Mino,[83] L. M. Mir,[12] M. Miralles Lopez,[169] M. Mironova,[130] T. Mitani,[174] V. A. Mitsou,[169] M. Mittal,[58c] O. Miu,[162] P. S. Miyagawa,[90] Y. Miyazaki,[85] A. Mizukami,[79] J. U. Mjörnmark,[94] T. Mkrtchyan,[59a] M. Mlynarikova,[116] T. Moa,[43a,43b]

S. Mobius,[51] K. Mochizuki,[106] P. Moder,[44] P. Mogg,[110] A. F. Mohammed,[13a] S. Mohapatra,[37] G. Mokgatitswane,[31f] B. Mondal,[147] S. Mondal,[137] K. Mönig,[44] E. Monnier,[98] L. Monsonis Romero,[169] A. Montalbano,[148] J. Montejo Berlingen,[34] M. Montella,[123] F. Monticelli,[86] N. Morange,[62] A. L. Moreira De Carvalho,[135a] M. Moreno Llácer,[169] C. Moreno Martinez,[12] P. Morettini,[53b] S. Morgenstern,[173] D. Mori,[148] M. Morii,[57] M. Morinaga,[159] V. Morisbak,[129] A. K. Morley,[34] A. P. Morris,[92] L. Morvaj,[34] P. Moschovakos,[34] B. Moser,[115] M. Mosidze,[155b] T. Moskalets,[50] P. Moskvitina,[114] J. Moss,[29,hh] E. J. W. Moyse,[99] S. Muanza,[98] J. Mueller,[134] R. Mueller,[18] D. Muenstermann,[87] G. A. Mullier,[94] J. J. Mullin,[132] D. P. Mungo,[66a,66b] J. L. Munoz Martinez,[12] F. J. Munoz Sanchez,[97] M. Murin,[97] P. Murin,[26b] W. J. Murray,[173,139] A. Murrone,[66a,66b] J. M. Muse,[124] M. Muškinja,[16] C. Mwewa,[27] A. G. Myagkov,[118,k] A. J. Myers,[7] A. A. Myers,[134] G. Myers,[63] M. Myska,[137] B. P. Nachman,[16] O. Nackenhorst,[45] A. Nag Nag,[46] K. Nagai,[130] K. Nagano,[79] J. L. Nagle,[27] E. Nagy,[98] A. M. Nairz,[34] Y. Nakahama,[79] K. Nakamura,[79] H. Nanjo,[128] F. Napolitano,[59a] R. Narayan,[40] E. A. Narayanan,[113] I. Naryshkin,[133] M. Naseri,[32] C. Nass,[22] T. Naumann,[44] G. Navarro,[20a] J. Navarro-Gonzalez,[169] R. Nayak,[157] P. Y. Nechaeva,[107] F. Nechansky,[44] T. J. Neep,[19] A. Negri,[68a,68b] M. Negrini,[21b] C. Nellist,[114] C. Nelson,[100] K. Nelson,[102] S. Nemecek,[136] M. Nessi,[34,ii] M. S. Neubauer,[168] F. Neuhaus,[96] J. Neundorf,[44] R. Newhouse,[170] P. R. Newman,[19] C. W. Ng,[134] Y. S. Ng,[17] Y. W. Y. Ng,[166] B. Ngair,[33e] H. D. N. Nguyen,[106] R. B. Nickerson,[130] R. Nicolaidou,[140] D. S. Nielsen,[38] J. Nielsen,[141] M. Niemeyer,[51] N. Nikiforou,[10] V. Nikolaenko,[118,k] I. Nikolic-Audit,[131] K. Nikolopoulos,[19] P. Nilsson,[27] H. R. Nindhito,[52] A. Nisati,[70a] N. Nishu,[2] R. Nisius,[111] T. Nitta,[174] T. Nobe,[159] D. L. Noel,[30] Y. Noguchi,[83] I. Nomidis,[131] M. A. Nomura,[27] M. B. Norfolk,[145] R. R. B. Norisam,[92] J. Novak,[89] T. Novak,[44] O. Novgorodova,[46] L. Novotny,[137] R. Novotny,[113] L. Nozka,[126] K. Ntekas,[166] E. Nurse,[92] F. G. Oakham,[32,e] J. Ocariz,[131] A. Ochi,[80] I. Ochoa,[135a] J. P. Ochoa-Ricoux,[142a] S. Oda,[85] S. Odaka,[79] S. Oerdek,[167] A. Ogrodnik,[81a] A. Oh,[97] C. C. Ohm,[150] H. Oide,[160] R. Oishi,[159] M. L. Ojeda,[44] Y. Okazaki,[83] M. W. O'Keefe,[88] Y. Okumura,[159] A. Olariu,[25b] L. F. Oleiro Seabra,[135a] S. A. Olivares Pino,[142d] D. Oliveira Damazio,[27] D. Oliveira Goncalves,[78a] J. L. Oliver,[166] M. J. R. Olsson,[166] A. Olszewski,[82] J. Olszowska,[82] Ö. O. Öncel,[22] D. C. O'Neil,[148] A. P. O'neill,[18] A. Onofre,[135a,135e] P. U. E. Onyisi,[10] R. G. Oreamuno Madriz,[116] M. J. Oreglia,[35] G. E. Orellana,[86] D. Orestano,[72a,72b] N. Orlando,[12] R. S. Orr,[162] V. O'Shea,[55] R. Ospanov,[58a] G. Otero y Garzon,[28] H. Otono,[85] P. S. Ott,[59a] G. J. Ottino,[16] M. Ouchrif,[33d] J. Ouellette,[27] F. Ould-Saada,[129] A. Ouraou,[140,a] Q. Ouyang,[13a] M. Owen,[55] R. E. Owen,[139] K. Y. Oyulmaz,[11c] V. E. Ozcan,[11c] N. Ozturk,[7] S. Ozturk,[11c,j] J. Pacalt,[126] H. A. Pacey,[30] K. Pachal,[47] A. Pacheco Pages,[12] C. Padilla Aranda,[12] S. Pagan Griso,[16] G. Palacino,[63] S. Palazzo,[48] S. Palestini,[34] M. Palka,[81b] P. Palni,[81a] D. K. Panchal,[10] C. E. Pandini,[52] J. G. Panduro Vazquez,[91] P. Pani,[44] G. Panizzo,[64a,64c] L. Paolozzi,[52] C. Papadatos,[106] S. Parajuli,[40] A. Paramonov,[5] C. Paraskevopoulos,[9] D. Paredes Hernandez,[60b] B. Parida,[175] T. H. Park,[162] A. J. Parker,[29] M. A. Parker,[30] F. Parodi,[53b,53a] E. W. Parrish,[116] V. A. Parrish,[48] J. A. Parsons,[37] U. Parzefall,[50] L. Pascual Dominguez,[157] V. R. Pascuzzi,[16] F. Pasquali,[115] E. Pasqualucci,[70a] S. Passaggio,[53b] F. Pastore,[91] P. Pasuwan,[43a,43b] J. R. Pater,[97] A. Pathak,[176] J. Patton,[88] T. Pauly,[34] J. Pearkes,[149] M. Pedersen,[129] L. Pedraza Diaz,[114] R. Pedro,[135a] T. Peiffer,[51] S. V. Peleganchuk,[117b,117a] O. Penc,[136] C. Peng,[60b] H. Peng,[58a] M. Penzin,[161] B. S. Peralva,[78a] A. P. Pereira Peixoto,[135a] L. Pereira Sanchez,[43a,43b] D. V. Perepelitsa,[27] E. Perez Codina,[163a] M. Perganti,[9] L. Perini,[66a,66b] H. Pernegger,[34] S. Perrella,[34] A. Perrevoort,[115] K. Peters,[44] R. F. Y. Peters,[97] B. A. Petersen,[34] T. C. Petersen,[38] E. Petit,[98] V. Petousis,[137] C. Petridou,[158] P. Petroff,[62] F. Petrucci,[72a,72b] A. Petrukhin,[147] M. Pettee,[178] N. E. Pettersson,[34] K. Petukhova,[138] A. Peyaud,[140] R. Pezoa,[142e] L. Pezzotti,[34] G. Pezzullo,[178] T. Pham,[101] P. W. Phillips,[139] M. W. Phipps,[168] G. Piacquadio,[151] E. Pianori,[16] F. Piazza,[66a,66b] A. Picazio,[99] R. Piegaia,[28] D. Pietreanu,[25b] J. E. Pilcher,[35] A. D. Pilkington,[97] M. Pinamonti,[64a,64c] J. L. Pinfold,[2] C. Pitman Donaldson,[92] D. A. Pizzi,[32] L. Pizzimento,[71a,71b] A. Pizzini,[115] M.-A. Pleier,[27] V. Plesanovs,[50] V. Pleskot,[138] E. Plotnikova,[77] R. Poettgen,[94] R. Poggi,[52] L. Poggioli,[131] I. Pogrebnyak,[103] D. Pohl,[22] I. Pokharel,[51] G. Polesello,[68a] A. Poley,[148,163a] A. Policicchio,[70a,70b] R. Polifka,[137] A. Polini,[21b] C. S. Pollard,[130] Z. B. Pollock,[123] V. Polychronakos,[27] D. Ponomarenko,[108] L. Pontecorvo,[34] S. Popa,[25a] G. A. Popeneciu,[25d] L. Portales,[4] D. M. Portillo Quintero,[163a] S. Pospisil,[137] P. Postolache,[25c] K. Potamianos,[130] I. N. Potrap,[77] C. J. Potter,[30] H. Potti,[1] T. Poulsen,[44] J. Poveda,[169] T. D. Powell,[145] G. Pownall,[44] M. E. Pozo Astigarraga,[34] A. Prades Ibanez,[169] P. Pralavorio,[98] M. M. Prapa,[42] S. Prell,[76] D. Price,[97] M. Primavera,[65a] M. A. Principe Martin,[95] M. L. Proffitt,[144] N. Proklova,[108] K. Prokofiev,[60c] F. Prokoshin,[77] G. Proto,[71a,71b] S. Protopopescu,[27] J. Proudfoot,[5] M. Przybycien,[81a] D. Pudzha,[133] P. Puzo,[62] D. Pyatiizbyantseva,[108] J. Qian,[102] Y. Qin,[97] T. Qiu,[90] A. Quadt,[51] M. Queitsch-Maitland,[34] G. Rabanal Bolanos,[57] F. Ragusa,[66a,66b] J. A. Raine,[52] S. Rajagopalan,[27] K. Ran,[13a,13d] D. F. Rassloff,[59a] D. M. Rauch,[44] S. Rave,[96] B. Ravina,[55] I. Ravinovich,[175] M. Raymond,[34] A. L. Read,[129] N. P. Readioff,[145] D. M. Rebuzzi,[68a,68b] G. Redlinger,[27] K. Reeves,[41] D. Reikher,[157] A. Reiss,[96] A. Rej,[147] C. Rembser,[34] A. Renardi,[44] M. Renda,[25b] M. B. Rendel,[111] A. G. Rennie,[55] S. Resconi,[66a] M. Ressegotti,[53b,53a]

E. D. Resseguie,[16] S. Rettie,[92] B. Reynolds,[123] E. Reynolds,[19] M. Rezaei Estabragh,[177] O. L. Rezanova,[117b,117a] P. Reznicek,[138] E. Ricci,[73a,73b] R. Richter,[111] S. Richter,[44] E. Richter-Was,[81b] M. Ridel,[131] P. Rieck,[111] P. Riedler,[34] O. Rifki,[44] M. Rijssenbeek,[151] A. Rimoldi,[68a,68b] M. Rimoldi,[44] L. Rinaldi,[21b,21a] T. T. Rinn,[168] M. P. Rinnagel,[110] G. Ripellino,[150] I. Riu,[12] P. Rivadeneira,[44] J. C. Rivera Vergara,[171] F. Rizatdinova,[125] E. Rizvi,[90] C. Rizzi,[52] B. A. Roberts,[173] B. R. Roberts,[16] S. H. Robertson,[100,n] M. Robin,[44] D. Robinson,[30] C. M. Robles Gajardo,[142e] M. Robles Manzano,[96] A. Robson,[55] A. Rocchi,[71a,71b] C. Roda,[69a,69b] S. Rodriguez Bosca,[59a] Y. Rodriguez Garcia,[20a] A. Rodriguez Rodriguez,[50] A. M. Rodríguez Vera,[163b] S. Roe,[34] A. R. Roepe,[124] J. Roggel,[177] O. Røhne,[129] R. A. Rojas,[171] B. Roland,[50] C. P. A. Roland,[63] J. Roloff,[27] A. Romaniouk,[108] M. Romano,[21b] A. C. Romero Hernandez,[168] N. Rompotis,[88] M. Ronzani,[121] L. Roos,[131] S. Rosati,[70a] B. J. Rosser,[132] E. Rossi,[162] E. Rossi,[4] E. Rossi,[67a,67b] L. P. Rossi,[53b] L. Rossini,[44] R. Rosten,[123] M. Rotaru,[25b] B. Rottler,[50] D. Rousseau,[62] D. Rousso,[30] G. Rovelli,[68a,68b] A. Roy,[10] A. Rozanov,[98] Y. Rozen,[156] X. Ruan,[31f] A. J. Ruby,[88] T. A. Ruggeri,[1] F. Rühr,[50] A. Ruiz-Martinez,[169] A. Rummler,[34] Z. Rurikova,[50] N. A. Rusakovich,[77] H. L. Russell,[34] L. Rustige,[36] J. P. Rutherfoord,[6] E. M. Rüttinger,[145] K. Rybacki,[87] M. Rybar,[138] E. B. Rye,[129] A. Ryzhov,[118] J. A. Sabater Iglesias,[52] P. Sabatini,[169] L. Sabetta,[70a,70b] H. F-W. Sadrozinski,[141] R. Sadykov,[77] F. Safai Tehrani,[70a] B. Safarzadeh Samani,[152] M. Safdari,[149] S. Saha,[100] M. Sahinsoy,[111] A. Sahu,[177] M. Saimpert,[140] M. Saito,[159] T. Saito,[159] D. Salamani,[34] G. Salamanna,[72a,72b] A. Salnikov,[149] J. Salt,[169] A. Salvador Salas,[12] D. Salvatore,[39b,39a] F. Salvatore,[152] A. Salzburger,[34] D. Sammel,[50] D. Sampsonidis,[158] D. Sampsonidou,[58d,58c] J. Sánchez,[169] A. Sanchez Pineda,[4] V. Sanchez Sebastian,[169] H. Sandaker,[129] C. O. Sander,[44] I. G. Sanderswood,[87] J. A. Sandesara,[99] M. Sandhoff,[177] C. Sandoval,[20b] D. P. C. Sankey,[139] M. Sannino,[53b,53a] A. Sansoni,[49] C. Santoni,[36] H. Santos,[135a,135b] S. N. Santpur,[16] A. Santra,[175] K. A. Saoucha,[145] A. Sapronov,[77] J. G. Saraiva,[135a,135d] J. Sardain,[98] O. Sasaki,[79] K. Sato,[164] C. Sauer,[59b] F. Sauerburger,[50] E. Sauvan,[4] P. Savard,[162,e] R. Sawada,[159] C. Sawyer,[139] L. Sawyer,[93] I. Sayago Galvan,[169] C. Sbarra,[21b] A. Sbrizzi,[21b,21a] T. Scanlon,[92] J. Schaarschmidt,[144] P. Schacht,[111] D. Schaefer,[35] U. Schäfer,[96] A. C. Schaffer,[62] D. Schaile,[110] R. D. Schamberger,[151] E. Schanet,[110] C. Scharf,[17] N. Scharmberg,[97] V. A. Schegelsky,[133] D. Scheirich,[138] F. Schenck,[17] M. Schernau,[166] C. Schiavi,[53b,53a] L. K. Schildgen,[22] Z. M. Schillaci,[24] E. J. Schioppa,[65a,65b] M. Schioppa,[39b,39a] B. Schlag,[96] K. E. Schleicher,[50] S. Schlenker,[34] K. Schmieden,[96] C. Schmitt,[96] S. Schmitt,[44] L. Schoeffel,[140] A. Schoening,[59b] P. G. Scholer,[50] E. Schopf,[130] M. Schott,[96] J. Schovancova,[34] S. Schramm,[52] F. Schroeder,[177] H-C. Schultz-Coulon,[59a] M. Schumacher,[50] B. A. Schumm,[141] Ph. Schune,[140] A. Schwartzman,[149] T. A. Schwarz,[102] Ph. Schwemling,[140] R. Schwienhorst,[103] A. Sciandra,[141] G. Sciolla,[24] F. Scuri,[69a] F. Scutti,[101] C. D. Sebastiani,[88] K. Sedlaczek,[45] P. Seema,[17] S. C. Seidel,[113] A. Seiden,[141] B. D. Seidlitz,[27] T. Seiss,[35] C. Seitz,[44] J. M. Seixas,[78b] G. Sekhniaidze,[67a] S. J. Sekula,[40] L. P. Selem,[4] N. Semprini-Cesari,[21b,21a] S. Sen,[47] C. Serfon,[27] L. Serin,[62] L. Serkin,[64a,64b] M. Sessa,[72a,72b] H. Severini,[124] S. Sevova,[149] F. Sforza,[53b,53a] A. Sfyrla,[52] E. Shabalina,[51] R. Shaheen,[150] J. D. Shahinian,[132] N. W. Shaikh,[43a,43b] D. Shaked Renous,[175] L. Y. Shan,[13a] M. Shapiro,[16] A. Sharma,[34] A. S. Sharma,[1] S. Sharma,[44] P. B. Shatalov,[119] K. Shaw,[152] S. M. Shaw,[97] P. Sherwood,[92] L. Shi,[92] C. O. Shimmin,[178] Y. Shimogama,[174] J. D. Shinner,[91] I. P. J. Shipsey,[130] S. Shirabe,[52] M. Shiyakova,[77] J. Shlomi,[175] M. J. Shochet,[35] J. Shojaii,[101] D. R. Shope,[150] S. Shrestha,[123] E. M. Shrif,[31f] M. J. Shroff,[171] E. Shulga,[175] P. Sicho,[136] A. M. Sickles,[168] E. Sideras Haddad,[31f] O. Sidiropoulou,[34] A. Sidoti,[21b] F. Siegert,[46] Dj. Sijacki,[14] J. M. Silva,[19] M. V. Silva Oliveira,[34] S. B. Silverstein,[43a] S. Simion,[62] R. Simoniello,[34] N. D. Simpson,[94] S. Simsek,[11c] S. Sindhu,[51] P. Sinervo,[162] V. Sinetckii,[109] S. Singh,[148] S. Singh,[162] S. Sinha,[44] S. Sinha,[31f] M. Sioli,[21b,21a] I. Siral,[127] S. Yu. Sivoklokov,[109] J. Sjölin,[43a,43b] A. Skaf,[51] E. Skorda,[94] P. Skubic,[124] M. Slawinska,[82] K. Sliwa,[165] V. Smakhtin,[175] B. H. Smart,[139] J. Smiesko,[138] S. Yu. Smirnov,[108] Y. Smirnov,[108] L. N. Smirnova,[109,jj] O. Smirnova,[94] E. A. Smith,[35] H. A. Smith,[130] M. Smizanska,[87] K. Smolek,[137] A. Smykiewicz,[82] A. A. Snesarev,[107] H. L. Snoek,[115] S. Snyder,[27] R. Sobie,[171,n] A. Soffer,[157] C. A. Solans Sanchez,[34] E. Yu. Soldatov,[108] U. Soldevila,[169] A. A. Solodkov,[118] S. Solomon,[50] A. Soloshenko,[77] O. V. Solovyanov,[118] V. Solovyev,[133] P. Sommer,[145] H. Son,[165] A. Sonay,[12] W. Y. Song,[163b] A. Sopczak,[137] A. L. Sopio,[92] F. Sopkova,[26b] S. Sottocornola,[68a,68b] R. Soualah,[120c] A. M. Soukharev,[117b,117a] Z. Soumaimi,[33e] D. South,[44] S. Spagnolo,[65a,65b] M. Spalla,[111] M. Spangenberg,[173] F. Spanò,[91] D. Sperlich,[50] G. Spigo,[34] M. Spina,[152] S. Spinali,[87] D. P. Spiteri,[55] M. Spousta,[138] A. Stabile,[66a,66b] R. Stamen,[59a] M. Stamenkovic,[115] A. Stampekis,[19] M. Standke,[22] E. Stanecka,[82] B. Stanislaus,[34] M. M. Stanitzki,[44] M. Stankaityte,[130] B. Stapf,[44] E. A. Starchenko,[118] G. H. Stark,[141] J. Stark,[98] D. M. Starko,[163b] P. Staroba,[136] P. Starovoitov,[59a] S. Stärz,[100] R. Staszewski,[82] G. Stavropoulos,[42] P. Steinberg,[27] A. L. Steinhebel,[127] B. Stelzer,[148,163a] H. J. Stelzer,[134] O. Stelzer-Chilton,[163a] H. Stenzel,[54] T. J. Stevenson,[152] G. A. Stewart,[34] M. C. Stockton,[34] G. Stoicea,[25b] M. Stolarski,[135a] S. Stonjek,[111] A. Straessner,[46] J. Strandberg,[150] S. Strandberg,[43a,43b] M. Strauss,[124] T. Strebler,[98] P. Strizenec,[26b]

R. Ströhmer,[172] D. M. Strom,[127] L. R. Strom,[44] R. Stroynowski,[40] A. Strubig,[43a,43b] S. A. Stucci,[27] B. Stugu,[15] J. Stupak,[124] N. A. Styles,[44] D. Su,[149] S. Su,[58a] W. Su,[58d,144,58c] X. Su,[58a] K. Sugizaki,[159] V. V. Sulin,[107] M. J. Sullivan,[88] D. M. S. Sultan,[73a,73b] L. Sultanaliyeva,[107] S. Sultansoy,[3c] T. Sumida,[83] S. Sun,[102] S. Sun,[176] X. Sun,[97] O. Sunneborn Gudnadottir,[167] C. J. E. Suster,[153] M. R. Sutton,[152] M. Svatos,[136] M. Swiatlowski,[163a] T. Swirski,[172] I. Sykora,[26a] M. Sykora,[138] T. Sykora,[138] D. Ta,[96] K. Tackmann,[44,kk] A. Taffard,[166] R. Tafirout,[163a] R. H. M. Taibah,[131] R. Takashima,[84] K. Takeda,[80] T. Takeshita,[146] E. P. Takeva,[48] Y. Takubo,[79] M. Talby,[98] A. A. Talyshev,[117b,117a] K. C. Tam,[60b] N. M. Tamir,[157] A. Tanaka,[159] J. Tanaka,[159] R. Tanaka,[62] J. Tang,[58c] Z. Tao,[170] S. Tapia Araya,[76] S. Tapprogge,[96] A. Tarek Abouelfadl Mohamed,[103] S. Tarem,[156] K. Tariq,[58b] G. Tarna,[25b] G. F. Tartarelli,[66a] P. Tas,[138] M. Tasevsky,[136] E. Tassi,[39b,39a] G. Tateno,[159] Y. Tayalati,[33e] G. N. Taylor,[101] W. Taylor,[163b] H. Teagle,[88] A. S. Tee,[176] R. Teixeira De Lima,[149] P. Teixeira-Dias,[91] H. Ten Kate,[34] J. J. Teoh,[115] K. Terashi,[159] J. Terron,[95] S. Terzo,[12] M. Testa,[49] R. J. Teuscher,[162,n] N. Themistokleous,[48] T. Theveneaux-Pelzer,[17] O. Thielmann,[177] D. W. Thomas,[91] J. P. Thomas,[19] E. A. Thompson,[44] P. D. Thompson,[19] E. Thomson,[132] E. J. Thorpe,[90] Y. Tian,[51] V. O. Tikhomirov,[107,ll] Yu. A. Tikhonov,[117b,117a] S. Timoshenko,[108] E. X. L. Ting,[1] P. Tipton,[178] S. Tisserant,[98] S. H. Tlou,[31f] A. Tnourji,[36] K. Todome,[21b,21a] S. Todorova-Nova,[138] S. Todt,[46] M. Togawa,[79] J. Tojo,[85] S. Tokár,[26a] K. Tokushuku,[79] E. Tolley,[123] R. Tombs,[30] M. Tomoto,[79,112] L. Tompkins,[149] P. Tornambe,[99] E. Torrence,[127] H. Torres,[46] E. Torró Pastor,[169] M. Toscani,[28] C. Tosciri,[35] J. Toth,[98,mm] D. R. Tovey,[145] A. Traeet,[15] C. J. Treado,[121] T. Trefzger,[172] A. Tricoli,[27] I. M. Trigger,[163a] S. Trincaz-Duvoid,[131] D. A. Trischuk,[170] W. Trischuk,[162] B. Trocmé,[56] A. Trofymov,[62] C. Troncon,[66a] F. Trovato,[152] L. Truong,[31c] M. Trzebinski,[82] A. Trzupek,[82] F. Tsai,[151] M. Tsai,[102] A. Tsiamis,[158] P. V. Tsiareshka,[104] A. Tsirigotis,[158,ee] V. Tsiskaridze,[151] E. G. Tskhadadze,[155a] M. Tsopoulou,[158] Y. Tsujikawa,[83] I. I. Tsukerman,[119] V. Tsulaia,[16] S. Tsuno,[79] O. Tsur,[156] D. Tsybychev,[151] Y. Tu,[60b] A. Tudorache,[25b] V. Tudorache,[25b] A. N. Tuna,[34] S. Turchikhin,[77] I. Turk Cakir,[3a] R. J. Turner,[19] R. Turra,[66a] P. M. Tuts,[37] S. Tzamarias,[158] P. Tzanis,[9] E. Tzovara,[96] K. Uchida,[159] F. Ukegawa,[164] P. A. Ulloa Poblete,[142b] G. Unal,[34] M. Unal,[10] A. Undrus,[27] G. Unel,[166] K. Uno,[159] J. Urban,[26b] P. Urquijo,[101] G. Usai,[7] R. Ushioda,[160] M. Usman,[106] Z. Uysal,[11d] V. Vacek,[137] B. Vachon,[100] K. O. H. Vadla,[129] T. Vafeiadis,[34] C. Valderanis,[110] E. Valdes Santurio,[43a,43b] M. Valente,[163a] S. Valentinetti,[21b,21a] A. Valero,[169] R. A. Vallance,[19] A. Vallier,[98] J. A. Valls Ferrer,[169] T. R. Van Daalen,[144] P. Van Gemmeren,[5] S. Van Stroud,[92] I. Van Vulpen,[115] M. Vanadia,[71a,71b] W. Vandelli,[34] M. Vandenbroucke,[140] E. R. Vandewall,[125] D. Vannicola,[157] L. Vannoli,[53b,53a] R. Vari,[70a] E. W. Varnes,[6] C. Varni,[16] T. Varol,[154] D. Varouchas,[62] K. E. Varvell,[153] M. E. Vasile,[25b] L. Vaslin,[36] G. A. Vasquez,[171] F. Vazeille,[36] D. Vazquez Furelos,[12] T. Vazquez Schroeder,[34] J. Veatch,[51] V. Vecchio,[97] M. J. Veen,[115] I. Veliscek,[130] L. M. Veloce,[162] F. Veloso,[135a,135c] S. Veneziano,[70a] A. Ventura,[65a,65b] A. Verbytskyi,[111] M. Verducci,[69a,69b] C. Vergis,[22] M. Verissimo De Araujo,[78b] W. Verkerke,[115] A. T. Vermeulen,[115] J. C. Vermeulen,[115] C. Vernieri,[149] P. J. Verschuuren,[91] M. Vessella,[99] M. L. Vesterbacka,[121] M. C. Vetterli,[148,e] A. Vgenopoulos,[158] N. Viaux Maira,[142e] T. Vickey,[145] O. E. Vickey Boeriu,[145] G. H. A. Viehhauser,[130] L. Vigani,[59b] M. Villa,[21b,21a] M. Villaplana Perez,[169] E. M. Villhauer,[48] E. Vilucchi,[49] M. G. Vincter,[32] G. S. Virdee,[19] A. Vishwakarma,[48] C. Vittori,[21b,21a] I. Vivarelli,[152] V. Vladimirov,[173] E. Voevodina,[111] M. Vogel,[177] P. Vokac,[137] J. Von Ahnen,[44] E. Von Toerne,[22] B. Vormwald,[34] V. Vorobel,[138] K. Vorobev,[108] M. Vos,[169] J. H. Vossebeld,[88] M. Vozak,[97] L. Vozdecky,[90] N. Vranjes,[14] M. Vranjes Milosavljevic,[14] V. Vrba,[137,a] M. Vreeswijk,[115] N. K. Vu,[98] R. Vuillermet,[34] O. V. Vujinovic,[96] I. Vukotic,[35] S. Wada,[164] C. Wagner,[99] W. Wagner,[177] S. Wahdan,[177] H. Wahlberg,[86] R. Wakasa,[164] M. Wakida,[112] V. M. Walbrecht,[111] J. Walder,[139] R. Walker,[110] S. D. Walker,[91] W. Walkowiak,[147] A. M. Wang,[57] A. Z. Wang,[176] C. Wang,[58a] C. Wang,[58c] H. Wang,[16] J. Wang,[60a] P. Wang,[40] R.-J. Wang,[96] R. Wang,[57] R. Wang,[116] S. M. Wang,[154] S. Wang,[58b] T. Wang,[58a] W. T. Wang,[75] W. X. Wang,[58a] X. Wang,[13c] X. Wang,[168] X. Wang,[58c] Y. Wang,[58a] Z. Wang,[102] Z. Wang,[58d,47,58c] Z. Wang,[102] C. Wanotayaroj,[34] A. Warburton,[100] C. P. Ward,[30] R. J. Ward,[19] N. Warrack,[55] A. T. Watson,[19] M. F. Watson,[19] G. Watts,[144] B. M. Waugh,[92] A. F. Webb,[10] C. Weber,[27] M. S. Weber,[18] S. A. Weber,[32] S. M. Weber,[59a] C. Wei,[58a] Y. Wei,[130] A. R. Weidberg,[130] J. Weingarten,[45] M. Weirich,[96] C. Weiser,[50] T. Wenaus,[27] B. Wendland,[45] T. Wengler,[34] S. Wenig,[34] N. Wermes,[22] M. Wessels,[59a] K. Whalen,[127] A. M. Wharton,[87] A. S. White,[57] A. White,[7] M. J. White,[1] D. Whiteson,[166] L. Wickremasinghe,[128] W. Wiedenmann,[176] C. Wiel,[46] M. Wielers,[139] N. Wieseotte,[96] C. Wiglesworth,[38] L. A. M. Wiik-Fuchs,[50] D. J. Wilbern,[124] H. G. Wilkens,[34] L. J. Wilkins,[91] D. M. Williams,[37] H. H. Williams,[132] S. Williams,[30] S. Willocq,[99] P. J. Windischhofer,[130] I. Wingerter-Seez,[4] F. Winklmeier,[127] B. T. Winter,[50] M. Wittgen,[149] M. Wobisch,[93] A. Wolf,[96] R. Wölker,[130] J. Wollrath,[166] M. W. Wolter,[82] H. Wolters,[135a,135c] V. W. S. Wong,[170] A. F. Wongel,[44] S. D. Worm,[44] B. K. Wosiek,[82] K. W. Woźniak,[82] K. Wraight,[55] J. Wu,[13a,13d] S. L. Wu,[176] X. Wu,[52] Y. Wu,[58a] Z. Wu,[140,58a] J. Wuerzinger,[130] T. R. Wyatt,[97] B. M. Wynne,[48] S. Xella,[38] L. Xia,[13c] M. Xia,[13b] J. Xiang,[60c] X. Xiao,[102]

M. Xie,[58a] X. Xie,[58a] I. Xiotidis,[152] D. Xu,[13a] H. Xu,[58a] H. Xu,[58a] L. Xu,[58a] R. Xu,[132] T. Xu,[58a] W. Xu,[102] Y. Xu,[13b] Z. Xu,[58b] Z. Xu,[149] B. Yabsley,[153] S. Yacoob,[31a] N. Yamaguchi,[85] Y. Yamaguchi,[160] M. Yamatani,[159] H. Yamauchi,[164] T. Yamazaki,[16] Y. Yamazaki,[80] J. Yan,[58c] S. Yan,[130] Z. Yan,[23] H. J. Yang,[58c,58d] H. T. Yang,[16] S. Yang,[58a] T. Yang,[60c] X. Yang,[58a] X. Yang,[13a] Y. Yang,[159] Z. Yang,[102,58a] W-M. Yao,[16] Y. C. Yap,[44] H. Ye,[13c] J. Ye,[40] S. Ye,[27] I. Yeletskikh,[77] M. R. Yexley,[87] P. Yin,[37] K. Yorita,[174] K. Yoshihara,[76] C. J. S. Young,[50] C. Young,[149] M. Yuan,[102] R. Yuan,[58b,nn] X. Yue,[59a] M. Zaazoua,[33e] B. Zabinski,[82] G. Zacharis,[9] E. Zaid,[48] A. M. Zaitsev,[118,k] T. Zakareishvili,[155b] N. Zakharchuk,[32] S. Zambito,[34] D. Zanzi,[50] O. Zaplatilek,[137] S. V. Zeißner,[45] C. Zeitnitz,[177] J. C. Zeng,[168] D. T. Zenger Jr.,[24] O. Zenin,[118] T. Ženiš,[26a] S. Zenz,[90] S. Zerradi,[33a] D. Zerwas,[62] B. Zhang,[13c] D. F. Zhang,[145] G. Zhang,[13b] J. Zhang,[5] K. Zhang,[13a] L. Zhang,[13c] M. Zhang,[168] R. Zhang,[176] S. Zhang,[102] X. Zhang,[58c] X. Zhang,[58b] Z. Zhang,[62] P. Zhao,[47] T. Zhao,[58b] Y. Zhao,[141] Z. Zhao,[58a] A. Zhemchugov,[77] Z. Zheng,[149] D. Zhong,[168] B. Zhou,[102] C. Zhou,[176] H. Zhou,[6] N. Zhou,[58c] Y. Zhou,[6] C. G. Zhu,[58b] C. Zhu,[13a,13d] H. L. Zhu,[58a] H. Zhu,[13a] J. Zhu,[102] Y. Zhu,[58a] X. Zhuang,[13a] K. Zhukov,[107] V. Zhulanov,[117b,117a] D. Zieminska,[63] N. I. Zimine,[77] S. Zimmermann,[50,a] J. Zinsser,[59b] M. Ziolkowski,[147] L. Živković,[14] A. Zoccoli,[21b,21a] K. Zoch,[52] T. G. Zorbas,[145] O. Zormpa,[42] W. Zou,[37] and L. Zwalinski[34]

(ATLAS Collaboration)

[1]*Department of Physics, University of Adelaide, Adelaide, Australia*
[2]*Department of Physics, University of Alberta, Edmonton, Alberta, Canada*
[3a]*Department of Physics, Ankara University, Ankara, Turkey*
[3b]*Istanbul Aydin University, Application and Research Center for Advanced Studies, Istanbul, Turkey*
[3c]*Division of Physics, TOBB University of Economics and Technology, Ankara, Turkey*
[4]*LAPP, Univ. Savoie Mont Blanc, CNRS/IN2P3, Annecy, France*
[5]*High Energy Physics Division, Argonne National Laboratory, Argonne, Illinois, USA*
[6]*Department of Physics, University of Arizona, Tucson, Arizona, USA*
[7]*Department of Physics, University of Texas at Arlington, Arlington Texas, USA*
[8]*Physics Department, National and Kapodistrian University of Athens, Athens, Greece*
[9]*Physics Department, National Technical University of Athens, Zografou, Greece*
[10]*Department of Physics, University of Texas at Austin, Austin Texas, USA*
[11a]*Bahcesehir University, Faculty of Engineering and Natural Sciences, Istanbul, Turkey*
[11b]*Istanbul Bilgi University, Faculty of Engineering and Natural Sciences, Istanbul, Turkey*
[11c]*Department of Physics, Bogazici University, Istanbul, Turkey*
[11d]*Department of Physics Engineering, Gaziantep University, Gaziantep, Turkey*
[12]*Institut de Física d'Altes Energies (IFAE), Barcelona Institute of Science and Technology, Barcelona, Spain*
[13a]*Institute of High Energy Physics, Chinese Academy of Sciences, Beijing, China*
[13b]*Physics Department, Tsinghua University, Beijing, China*
[13c]*Department of Physics, Nanjing University, Nanjing, China*
[13d]*University of Chinese Academy of Science (UCAS), Beijing, China*
[14]*Institute of Physics, University of Belgrade, Belgrade, Serbia*
[15]*Department for Physics and Technology, University of Bergen, Bergen, Norway*
[16]*Physics Division, Lawrence Berkeley National Laboratory and University of California, Berkeley, California, USA*
[17]*Institut für Physik, Humboldt Universität zu Berlin, Berlin, Germany*
[18]*Albert Einstein Center for Fundamental Physics and Laboratory for High Energy Physics, University of Bern, Bern, Switzerland*
[19]*School of Physics and Astronomy, University of Birmingham, Birmingham, United Kingdom*
[20a]*Facultad de Ciencias y Centro de Investigaciónes, Universidad Antonio Nariño, Bogotá, Colombia*
[20b]*Departamento de Física, Universidad Nacional de Colombia, Bogotá, Colombia*
[21a]*Dipartimento di Fisica e Astronomia A. Righi, Università di Bologna, Bologna, Italy*
[21b]*INFN Sezione di Bologna, Bologna, Italy*
[22]*Physikalisches Institut, Universität Bonn, Bonn, Germany*
[23]*Department of Physics, Boston University, Boston, Massachusetts, USA*
[24]*Department of Physics, Brandeis University, Waltham, Massachusetts, USA*
[25a]*Transilvania University of Brasov, Brasov, Romania*
[25b]*Horia Hulubei National Institute of Physics and Nuclear Engineering, Bucharest, Romania*
[25c]*Department of Physics, Alexandru Ioan Cuza University of Iasi, Iasi, Romania*

[25d]National Institute for Research and Development of Isotopic and Molecular Technologies, Physics Department, Cluj-Napoca, Romania
[25e]University Politehnica Bucharest, Bucharest, Romania
[25f]West University in Timisoara, Timisoara, Romania
[26a]Faculty of Mathematics, Physics and Informatics, Comenius University, Bratislava, Slovak Republic
[26b]Department of Subnuclear Physics, Institute of Experimental Physics of the Slovak Academy of Sciences, Kosice, Slovak Republic
[27]Physics Department, Brookhaven National Laboratory, Upton, New York, USA
[28]Departamento de Física (FCEN) and IFIBA, Universidad de Buenos Aires and CONICET, Buenos Aires, Argentina
[29]California State University, Long Beach, California, USA
[30]Cavendish Laboratory, University of Cambridge, Cambridge, United Kingdom
[31a]Department of Physics, University of Cape Town, Cape Town, South Africa
[31b]iThemba Labs, Western Cape, South Africa
[31c]Department of Mechanical Engineering Science, University of Johannesburg, Johannesburg, South Africa
[31d]National Institute of Physics, University of the Philippines Diliman (Philippines), Diliman, Philippines
[31e]University of South Africa, Department of Physics, Pretoria, South Africa
[31f]School of Physics, University of the Witwatersrand, Johannesburg, South Africa
[32]Department of Physics, Carleton University, Ottawa, Ontario, Canada
[33a]Faculté des Sciences Ain Chock, Réseau Universitaire de Physique des Hautes Energies—Université Hassan II, Casablanca, Morocco
[33b]Faculté des Sciences, Université Ibn-Tofail, Kénitra, Morocco
[33c]Faculté des Sciences Semlalia, Université Cadi Ayyad, LPHEA-Marrakech, Morocco
[33d]LPMR, Faculté des Sciences, Université Mohamed Premier, Oujda, Morocco
[33e]Faculté des sciences, Université Mohammed V, Rabat, Morocco
[33f]Mohammed VI Polytechnic University, Ben Guerir, Morocco
[34]CERN, Geneva, Switzerland
[35]Enrico Fermi Institute, University of Chicago, Chicago, Illinois, USA
[36]LPC, Université Clermont Auvergne, CNRS/IN2P3, Clermont-Ferrand, France
[37]Nevis Laboratory, Columbia University, Irvington, New York, USA
[38]Niels Bohr Institute, University of Copenhagen, Copenhagen, Denmark
[39a]Dipartimento di Fisica, Università della Calabria, Rende, Italy
[39b]INFN Gruppo Collegato di Cosenza, Laboratori Nazionali di Frascati, Italy
[40]Physics Department, Southern Methodist University, Dallas, Texas, USA
[41]Physics Department, University of Texas at Dallas, Richardson Texas, USA
[42]National Centre for Scientific Research "Demokritos", Agia Paraskevi, Greece
[43a]Department of Physics, Stockholm University, Stockholm, Sweden
[43b]Oskar Klein Centre, Stockholm, Sweden
[44]Deutsches Elektronen-Synchrotron DESY, Hamburg and Zeuthen, Germany
[45]Fakultät Physik, Technische Universität Dortmund, Dortmund, Germany
[46]Institut für Kern- und Teilchenphysik, Technische Universität Dresden, Dresden, Germany
[47]Department of Physics, Duke University, Durham, North Carolina, USA
[48]SUPA—School of Physics and Astronomy, University of Edinburgh, Edinburgh, United Kingdom
[49]INFN e Laboratori Nazionali di Frascati, Frascati, Italy
[50]Physikalisches Institut, Albert-Ludwigs-Universität Freiburg, Freiburg, Germany
[51]II. Physikalisches Institut, Georg-August-Universität Göttingen, Göttingen, Germany
[52]Département de Physique Nucléaire et Corpusculaire, Université de Genève, Genève, Switzerland
[53a]Dipartimento di Fisica, Università di Genova, Genova, Italy
[53b]INFN Sezione di Genova, Italy
[54]II. Physikalisches Institut, Justus-Liebig-Universität Giessen, Giessen, Germany
[55]SUPA—School of Physics and Astronomy, University of Glasgow, Glasgow, United Kingdom
[56]LPSC, Université Grenoble Alpes, CNRS/IN2P3, Grenoble INP, Grenoble, France
[57]Laboratory for Particle Physics and Cosmology, Harvard University, Cambridge, Massachusetts, USA
[58a]Department of Modern Physics and State Key Laboratory of Particle Detection and Electronics, University of Science and Technology of China, Hefei, China
[58b]Institute of Frontier and Interdisciplinary Science and Key Laboratory of Particle Physics and Particle Irradiation (MOE), Shandong University, Qingdao, China
[58c]School of Physics and Astronomy, Shanghai Jiao Tong University, Key Laboratory for Particle Astrophysics and Cosmology (MOE), SKLPPC, Shanghai, China

[58d]*Tsung-Dao Lee Institute, Shanghai, China*
[59a]*Kirchhoff-Institut für Physik, Ruprecht-Karls-Universität Heidelberg, Heidelberg, Germany*
[59b]*Physikalisches Institut, Ruprecht-Karls-Universität Heidelberg, Heidelberg, Germany*
[60a]*Department of Physics, Chinese University of Hong Kong, Shatin, N.T., Hong Kong, China*
[60b]*Department of Physics, University of Hong Kong, Hong Kong, China*
[60c]*Department of Physics and Institute for Advanced Study, Hong Kong University of Science and Technology, Clear Water Bay, Kowloon, Hong Kong, China*
[61]*Department of Physics, National Tsing Hua University, Hsinchu, Taiwan*
[62]*IJCLab, Université Paris-Saclay, CNRS/IN2P3, 91405, Orsay, France*
[63]*Department of Physics, Indiana University, Bloomington, Indiana, USA*
[64a]*INFN Gruppo Collegato di Udine, Sezione di Trieste, Udine, Italy*
[64b]*ICTP, Trieste, Italy*
[64c]*Dipartimento Politecnico di Ingegneria e Architettura, Università di Udine, Udine, Italy*
[65a]*INFN Sezione di Lecce, Italy*
[65b]*Dipartimento di Matematica e Fisica, Università del Salento, Lecce, Italy*
[66a]*INFN Sezione di Milano, Milano, Italy*
[66b]*Dipartimento di Fisica, Università di Milano, Milano, Italy*
[67a]*INFN Sezione di Napoli, Napoli, Italy*
[67b]*Dipartimento di Fisica, Università di Napoli, Napoli, Italy*
[68a]*INFN Sezione di Pavia, Italy*
[68b]*Dipartimento di Fisica, Università di Pavia, Pavia, Italy*
[69a]*INFN Sezione di Pisa, Pisa, Italy*
[69b]*Dipartimento di Fisica E.Fermi, Università di Pisa, Pisa, Italy*
[70a]*INFN Sezione di Roma, Roma, Italy*
[70b]*Dipartimento di Fisica, Sapienza Università di Roma, Roma, Italy*
[71a]*INFN Sezione di Roma Tor Vergata, Italy*
[71b]*Dipartimento di Fisica, Università di Roma Tor Vergata, Roma, Italy*
[72a]*INFN Sezione di Roma Tre, Roma, Italy*
[72b]*Dipartimento di Matematica e Fisica, Università Roma Tre, Roma, Italy*
[73a]*INFN-TIFPA, Trento, Italy*
[73b]*Università degli Studi di Trento, Trento, Italy*
[74]*Institut für Astro- und Teilchenphysik, Leopold-Franzens-Universität, Innsbruck, Austria*
[75]*University of Iowa, Iowa City, Iowa, USA*
[76]*Department of Physics and Astronomy, Iowa State University, Ames, Iowa, USA*
[77]*Joint Institute for Nuclear Research, Dubna, Russia*
[78a]*Departamento de Engenharia Elétrica, Universidade Federal de Juiz de Fora (UFJF), Juiz de Fora, Brazil*
[78b]*Universidade Federal do Rio De Janeiro COPPE/EE/IF, Rio de Janeiro, Brazil*
[78c]*Instituto de Física, Universidade de São Paulo, São Paulo, Brazil*
[79]*KEK, High Energy Accelerator Research Organization, Tsukuba, Japan*
[80]*Graduate School of Science, Kobe University, Kobe, Japan*
[81a]*AGH University of Science and Technology, Faculty of Physics and Applied Computer Science, Krakow, Poland*
[81b]*Marian Smoluchowski Institute of Physics, Jagiellonian University, Krakow, Poland*
[82]*Institute of Nuclear Physics Polish Academy of Sciences, Krakow, Poland*
[83]*Faculty of Science, Kyoto University, Kyoto, Japan*
[84]*Kyoto University of Education, Kyoto, Japan*
[85]*Research Center for Advanced Particle Physics and Department of Physics, Kyushu University, Fukuoka, Japan*
[86]*Instituto de Física La Plata, Universidad Nacional de La Plata and CONICET, La Plata, Argentina*
[87]*Physics Department, Lancaster University, Lancaster, United Kingdom*
[88]*Oliver Lodge Laboratory, University of Liverpool, Liverpool, United Kingdom*
[89]*Department of Experimental Particle Physics, Jožef Stefan Institute and Department of Physics, University of Ljubljana, Ljubljana, Slovenia*
[90]*School of Physics and Astronomy, Queen Mary University of London, London, United Kingdom*
[91]*Department of Physics, Royal Holloway University of London, Egham, United Kingdom*
[92]*Department of Physics and Astronomy, University College London, London, United Kingdom*
[93]*Louisiana Tech University, Ruston, Louisiana, USA*
[94]*Fysiska institutionen, Lunds universitet, Lund, Sweden*
[95]*Departamento de Física Teorica C-15 and CIAFF, Universidad Autónoma de Madrid, Madrid, Spain*

[96]Institut für Physik, Universität Mainz, Mainz, Germany
[97]School of Physics and Astronomy, University of Manchester, Manchester, United Kingdom
[98]CPPM, Aix-Marseille Université, CNRS/IN2P3, Marseille, France
[99]Department of Physics, University of Massachusetts, Amherst, Massachusetts, USA
[100]Department of Physics, McGill University, Montreal, Quebec City, Canada
[101]School of Physics, University of Melbourne, Victoria, Australia
[102]Department of Physics, University of Michigan, Ann Arbor, Michigan, USA
[103]Department of Physics and Astronomy, Michigan State University, East Lansing, Michigan, USA
[104]B.I. Stepanov Institute of Physics, National Academy of Sciences of Belarus, Minsk, Belarus
[105]Research Institute for Nuclear Problems of Byelorussian State University, Minsk, Belarus
[106]Group of Particle Physics, University of Montreal, Montreal, Quebec City, Canada
[107]P.N. Lebedev Physical Institute of the Russian Academy of Sciences, Moscow, Russia
[108]National Research Nuclear University MEPhI, Moscow, Russia
[109]D.V. Skobeltsyn Institute of Nuclear Physics, M.V. Lomonosov Moscow State University, Moscow, Russia
[110]Fakultät für Physik, Ludwig-Maximilians-Universität München, München, Germany
[111]Max-Planck-Institut für Physik (Werner-Heisenberg-Institut), München, Germany
[112]Graduate School of Science and Kobayashi-Maskawa Institute, Nagoya University, Nagoya, Japan
[113]Department of Physics and Astronomy, University of New Mexico, Albuquerque, New Mexico, USA
[114]Institute for Mathematics, Astrophysics and Particle Physics, Radboud University/Nikhef, Nijmegen, Netherlands
[115]Nikhef National Institute for Subatomic Physics and University of Amsterdam, Amsterdam, Netherlands
[116]Department of Physics, Northern Illinois University, DeKalb, Illinois, USA
[117a]Budker Institute of Nuclear Physics and NSU, SB RAS, Novosibirsk, Russia
[117b]Novosibirsk State University Novosibirsk, Novosibirsk, Russia
[118]Institute for High Energy Physics of the National Research Centre Kurchatov Institute, Protvino, Russia
[119]Institute for Theoretical and Experimental Physics named by A.I. Alikhanov of National Research Centre "Kurchatov Institute", Moscow, Russia
[120a]New York University Abu Dhabi, Abu Dhabi, United Arab Emirates
[120b]United Arab Emirates University, Al Ain, United Arab Emirates
[120c]University of Sharjah, Sharjah, United Arab Emirates
[121]Department of Physics, New York University, New York, New York, USA
[122]Ochanomizu University, Otsuka, Bunkyo-ku, Tokyo, Japan
[123]Ohio State University, Columbus, Ohio, USA
[124]Homer L. Dodge Department of Physics and Astronomy, University of Oklahoma, Norman, Oklahoma, USA
[125]Department of Physics, Oklahoma State University, Stillwater, Oklahoma, USA
[126]Palacký University, Joint Laboratory of Optics, Olomouc, Czech Republic
[127]Institute for Fundamental Science, University of Oregon, Eugene, Oregon, USA
[128]Graduate School of Science, Osaka University, Osaka, Japan
[129]Department of Physics, University of Oslo, Oslo, Norway
[130]Department of Physics, Oxford University, Oxford, United Kingdom
[131]LPNHE, Sorbonne Université, Université de Paris, CNRS/IN2P3, Paris, France
[132]Department of Physics, University of Pennsylvania, Philadelphia, Pennsylvania, USA
[133]Konstantinov Nuclear Physics Institute of National Research Centre "Kurchatov Institute", PNPI, St. Petersburg, Russia
[134]Department of Physics and Astronomy, University of Pittsburgh, Pittsburgh, Pennsylvania, USA
[135a]Laboratório de Instrumentação e Física Experimental de Partículas—LIP, Lisboa, Portugal
[135b]Departamento de Física, Faculdade de Ciências, Universidade de Lisboa, Lisboa, Portugal
[135c]Departamento de Física, Universidade de Coimbra, Coimbra, Portugal
[135d]Centro de Física Nuclear da Universidade de Lisboa, Lisboa, Portugal
[135e]Departamento de Física, Universidade do Minho, Braga, Portugal
[135f]Departamento de Física Teórica y del Cosmos, Universidad de Granada, Granada (Spain), Spain
[135g]Instituto Superior Técnico, Universidade de Lisboa, Lisboa, Portugal
[136]Institute of Physics of the Czech Academy of Sciences, Prague, Czech Republic
[137]Czech Technical University in Prague, Prague, Czech Republic
[138]Charles University, Faculty of Mathematics and Physics, Prague, Czech Republic
[139]Particle Physics Department, Rutherford Appleton Laboratory, Didcot, United Kingdom
[140]IRFU, CEA, Université Paris-Saclay, Gif-sur-Yvette, France

[141]*Santa Cruz Institute for Particle Physics, University of California Santa Cruz, Santa Cruz, California, USA*
[142a]*Departamento de Física, Pontificia Universidad Católica de Chile, Santiago, Chile*
[142b]*Instituto de Investigación Multidisciplinario en Ciencia y Tecnología, y Departamento de Física, Universidad de La Serena, Santiago, Chile*
[142c]*Universidad Andres Bello, Department of Physics, Santiago, Chile*
[142d]*Instituto de Alta Investigación, Universidad de Tarapacá, Arica, Chile*
[142e]*Departamento de Física, Universidad Técnica Federico Santa María, Valparaíso, Chile*
[143]*Universidade Federal de São João del Rei (UFSJ), São João del Rei, Brazil*
[144]*Department of Physics, University of Washington, Seattle, Washington, USA*
[145]*Department of Physics and Astronomy, University of Sheffield, Sheffield, United Kingdom*
[146]*Department of Physics, Shinshu University, Nagano, Japan*
[147]*Department Physik, Universität Siegen, Siegen, Germany*
[148]*Department of Physics, Simon Fraser University, Burnaby British Columbia, Canada*
[149]*SLAC National Accelerator Laboratory, Stanford, California, USA*
[150]*Department of Physics, Royal Institute of Technology, Stockholm, Sweden*
[151]*Departments of Physics and Astronomy, Stony Brook University, Stony Brook, New York, USA*
[152]*Department of Physics and Astronomy, University of Sussex, Brighton, United Kingdom*
[153]*School of Physics, University of Sydney, Sydney, Australia*
[154]*Institute of Physics, Academia Sinica, Taipei, Taiwan*
[155a]*E. Andronikashvili Institute of Physics, Iv. Javakhishvili Tbilisi State University, Tbilisi, Georgia*
[155b]*High Energy Physics Institute, Tbilisi State University, Tbilisi, Georgia*
[156]*Department of Physics, Technion, Israel Institute of Technology, Haifa, Israel*
[157]*Raymond and Beverly Sackler School of Physics and Astronomy, Tel Aviv University, Tel Aviv, Israel*
[158]*Department of Physics, Aristotle University of Thessaloniki, Thessaloniki, Greece*
[159]*International Center for Elementary Particle Physics and Department of Physics, University of Tokyo, Tokyo, Japan*
[160]*Department of Physics, Tokyo Institute of Technology, Tokyo, Japan*
[161]*Tomsk State University, Tomsk, Russia*
[162]*Department of Physics, University of Toronto, Toronto, Ontario, Canada*
[163a]*TRIUMF, Vancouver, British Columbia, Canada*
[163b]*Department of Physics and Astronomy, York University, Toronto, Ontario, Canada*
[164]*Division of Physics and Tomonaga Center for the History of the Universe, Faculty of Pure and Applied Sciences, University of Tsukuba, Tsukuba, Japan*
[165]*Department of Physics and Astronomy, Tufts University, Medford, Massachusetts, USA*
[166]*Department of Physics and Astronomy, University of California Irvine, Irvine, California, USA*
[167]*Department of Physics and Astronomy, University of Uppsala, Uppsala, Sweden*
[168]*Department of Physics, University of Illinois, Urbana, Illinois, USA*
[169]*Instituto de Física Corpuscular (IFIC), Centro Mixto Universidad de Valencia—CSIC, Valencia, Spain*
[170]*Department of Physics, University of British Columbia, Vancouver, British Columbia, Canada*
[171]*Department of Physics and Astronomy, University of Victoria, Victoria, British Columbia, Canada*
[172]*Fakultät für Physik und Astronomie, Julius-Maximilians-Universität Würzburg, Würzburg, Germany*
[173]*Department of Physics, University of Warwick, Coventry, United Kingdom*
[174]*Waseda University, Tokyo, Japan*
[175]*Department of Particle Physics and Astrophysics, Weizmann Institute of Science, Rehovot, Israel*
[176]*Department of Physics, University of Wisconsin, Madison, Wisconsin, USA*
[177]*Fakultät für Mathematik und Naturwissenschaften, Fachgruppe Physik, Bergische Universität Wuppertal, Wuppertal, Germany*
[178]*Department of Physics, Yale University, New Haven, Connecticut, USA*

[a]Deceased.
[b]Also at Department of Physics, King's College London, London, United Kingdom.
[c]Also at Istanbul University, Department of Physics, Istanbul, Turkey.
[d]Also at Instituto de Fisica Teorica, IFT-UAM/CSIC, Madrid, Spain.
[e]Also at TRIUMF, Vancouver, British Columbia, Canada.
[f]Also at Physics Department, An-Najah National University, Nablus, Palestinian Authority.
[g]Also at Department of Physics, University of Fribourg, Fribourg, Switzerland.
[h]Also at Department of Physics and Astronomy, University of Louisville, Louisville, Kentucky, USA.
[i]Also at Departament de Fisica de la Universitat Autonoma de Barcelona, Barcelona, Spain.
[j]Also at Istinye University, Istanbul, Turkey.

[k]Also at Moscow Institute of Physics and Technology State University, Dolgoprudny, Russia.
[l]Also at Department of Physics, Ben Gurion University of the Negev, Beer Sheva, Israel.
[m]Also at Università di Napoli Parthenope, Napoli, Italy.
[n]Also at Institute of Particle Physics (IPP), Canada.
[o]Also at Bruno Kessler Foundation, Trento, Italy.
[p]Also at Department of Physics, St. Petersburg State Polytechnical University, St. Petersburg, Russia.
[q]Also at Borough of Manhattan Community College, City University of New York, New York, New York, USA.
[r]Also at Department of Physics, California State University, Fresno, USA.
[s]Also at Department of Financial and Management Engineering, University of the Aegean, Chios, Greece.
[t]Also at Centro Studi e Ricerche Enrico Fermi, Italy.
[u]Also at Department of Physics, California State University, East Bay, Hayward, USA.
[v]Also at Institucio Catalana de Recerca i Estudis Avancats, ICREA, Barcelona, Spain.
[w]Also at Graduate School of Science, Osaka University, Osaka, Japan.
[x]Also at Physikalisches Institut, Albert-Ludwigs-Universität Freiburg, Freiburg, Germany.
[y]Also at University of Chinese Academy of Sciences (UCAS), Beijing, China.
[z]Also at Institute of Physics, Azerbaijan Academy of Sciences, Baku, Azerbaijan.
[aa]Also at Yeditepe University, Physics Department, Istanbul, Turkey.
[bb]Also at Institute of Theoretical Physics, Ilia State University, Tbilisi, Georgia.
[cc]Also at CERN, Geneva, Switzerland.
[dd]Also at Joint Institute for Nuclear Research, Dubna, Russia.
[ee]Also at Hellenic Open University, Patras, Greece.
[ff]Also at Center for High Energy Physics, Peking University, China.
[gg]Also at The City College of New York, New York, New York, USA.
[hh]Also at Department of Physics, California State University, Sacramento, Sacramento, USA.
[ii]Also at Département de Physique Nucléaire et Corpusculaire, Université de Genève, Genève, Switzerland.
[jj]Also at Faculty of Physics, M.V. Lomonosov Moscow State University, Moscow, Russia.
[kk]Also at Institut für Experimentalphysik, Universität Hamburg, Hamburg, Germany.
[ll]Also at National Research Nuclear University MEPhI, Moscow, Russia.
[mm]Also at Institute for Particle and Nuclear Physics, Wigner Research Centre for Physics, Budapest, Hungary.
[nn]Also at Department of Physics and Astronomy, Michigan State University, East Lansing, Michigan, USA.